A NOVEL SWARMING BACTERIAL STRAIN EXHIBITS UNIQUE BIOPHYSICAL AND PROBIOTIC PROPERTIES

By

Weijie Chen

B.S., Purdue University, 2013

M.Sc., Brown University, 2017

A dissertation submitted in partial fulfilment of the
requirements for the degree of Doctor of Philosophy
in the Department of Physics at Brown University

PROVIDENCE, RHODE ISLAND

May 2021

This dissertation by Weijie Chen is accepted in its present form
by the Department of Physics as satisfying the
dissertation requirement for the degree of Doctor of Philosophy

Date_____ _____
Prof. Jay X. Tang, Advisor

Recommended to the Graduate Council

Date_____ _____
Prof. Sridhar Mani, Reader

Date_____ _____
Prof. Robert A. Pelcovits, Reader

Approved by the Graduate Council

Date_____ _____
Andrew G. Campbell,
Dean of the Graduate School

Curriculum Vitae

Education

- Ph.D. (Physics), 2021, Brown University
- M. Sc. (Physics), 2017, Brown University
- B. Sc. (Physics), 2013, Purdue University

Publications

- W. Chen, N. Mani, H. Karani, H. Li, S. Mani, J. X. Tang. Confinement Discerns Swarmers from Planktonic Bacteria. *Under revision, elife.*

- A. De*, W. Chen*, H. Li*, J. X. Tang, S. Mani. Bacterial Swarmers Enriched during Intestinal Stress Ameliorates Damage. *Provisionally Accepted, Journal of Gastroenterology.*

- H. Ma, J. Bell, W. Chen, S. Mani, J. X. Tang. An expanding bacterial colony forms a depletion zone with growing droplets. *Soft matter*, 2021.

- W. Chen, J. X. Tang, S. Mani. An Inexpensive Way to Record and Quantify Bacterial Swarming. *Nature Protocol Exchange*, 2019.

- G. Araujo, W. Chen, S. Mani, J. X. Tang. Orbiting of Flagellated Bacteria within a Thin Fluid Film around Micrometer-Sized Particles. *Biophysical Journal*, 2019.

- A. Byju*, D. Patel*, W. Chen, S. Mani. A Protocol for Assessing Bacterial Swarming from Human Fecal Matter. *Accepted, Bio-protocol*, 2019.

Teaching

- Teaching Assistant, Physics 0030: Basic Physics, Brown University, Fall 2017

Presentations

- Identifying bacterial swarming characteristics via confined motion. Cold Spring Harbor Laboratory Conference (Microbiome). Virtual, 2020.
- Confinement discerns swarmers from planktonic bacteria. American Physical Society March Meeting. Virtual, 2021.

Preface and Acknowledgments

I still remember the Spring Festival of 2016 when I decided to quit my job and pursue a PhD degree at Brown University. The outcome has proved to me that the decision I made was right. It has really been a fruitful PhD study for me. A lot of work has been done and my knowledge has grown exponentially. The most important thing I have learned from my PhD experience is the way to think and solve problems. I will face new challenges in the future, but I will not be defeated by difficulties. The years spent on hard work gave me a strong heart and I am ready to tackle tougher problems in future life, no matter what problems they will be.

I would like to thank Prof. Tang and Prof. Mani for being great co-advisors. I learned a lot from the countless discussions with you, scientific ones, and others. I could not achieve what I have now without your careful supervision. Besides, I want to thank Prof. Pelcovits for agreeing to be my thesis committee member. I enjoyed the courses you taught and appreciated your patient, detailed explanation on problems during the office hours you offered.

I thank my colleagues and friends from both Brown University and Albert Einstein College of Medicine for the help. I thank Arpan De, Hao Li, Subho Ghosh, Arjun Byju, Deeti Patel, Adam Hines, Peng Guo, and Xiaoping Luo from Einstein. I thank Hamid Karani, George Araujo, Hui Ma, Jordan Bell, Haobei Wang, Neha Mani, Zhiyu Zhang, Guanyang He, Yiming Xing, Yiou Zhang, Zekun Zhuang, Shenming Fu, Yangrui Hu, Mary Ellen Woycik, Ida Alarcon, and Morgan Latus from Brown and countless others who are etched in my memory but too extensive to list down.

I especially want to thank my parents and uncle for taking care of the family and encouraging every step of my education. Finally, I want to thank Dean Hudek, my physics lab instructional lab staff. I will not forget that every time when you saw me, you asked “Are you happy?”. You taught me the spirit that rather than lab techniques, intrinsic happiness is the driving force for doing science or doing anything great.

TABLE OF CONTENTS

List of Tables

List of Figures

CHAPTER 1

INTRODUCTION

This thesis consists of two main projects, presented in Chapter 3 and Chapter 4, respectively. The first project describes a novel biophysical property of bacterial swarming: based on the motion pattern difference, bacterial swarmers can be discerned from their motile planktonic counterparts under circular confinement. The second project reports a novel probiotic property on swarming bacteria: during intestinal inflammation, there is enhanced presence of fecal bacteria with swarming properties; however, surprisingly, these bacteria are shown to play a protective role when present in sufficiently abundant quantities. Also, several biophysical features of swarming patterns of bacteria from a polymicrobial mix are shown in this report.

Following an outline in this first chapter, Chapter 2 introduces the common background for both projects, such as the basic concepts of bacterial motility, and the motility types: swarming, swimming, etc. Then, bacterial swarming is introduced in more detail in the vintage point of biophysical properties and biomedical relevance. Additionally, inflammatory bowel disease is described, as its corresponding animal model is used in the course of this thesis study.

In Chapter 3, I described how swarming cells could be distinguished from the planktonic cells for the same bacterial strain under confinement on a soft-agar surface. By "planktonic", we mean freely swimming cells in liquid media. When the novel bacteria *Enterobacter sp.* SM3 is constrained within a circular microwell, the global motion pattern of the confined cells changes from "single-swirl" to "multi-swirl" as the well size increases.

Interestingly, swarming SM3 could hold single-swirl motion patterns in a much larger well size than the planktonic SM3. After excluding the factor of cell length, speed, and density, I attribute this phenomenon to the unique cell-cell alignment among the swarmers, which was revealed by the dynamic clustering phenomenon of swarmers in a dilution experiment. This theory was further verified through numerical simulation based on a Zonal Model in active matter.

In Chapter 4, I investigate the probiotic effect of SM3 on mammalian health. "Probiotic" means that the bacteria have beneficial effects on the host health. We derived genetically identical bacteria strains *Enterobacter sp.* SM1 and *Enterobacter sp.* SM3 from conventional mice without and with intestinal inflammation, respectively. The only difference between SM1 and SM3 is that SM3 swarms much faster than SM1. When mice with intestinal inflammation are administered SM strains, SM3 acts to prevent severe intestinal inflammation, whereas SM1 and two swarming deficient isogenic mutant strains of SM3 do not. Hence, I propose that the probiotic effect of SM3 is correlated with its swarming phenotype. Further investigation reveals that SM bacteria may enrich the abundance of S24-7, which is a family of bacteria associated with maintaining intestinal immune balance[2]. However, only SM3, with its strong swarming phenotype, has advantage in moving on an inflamed tissue surface, ensuring a good chance for contact with S24-7. This contact within the intestines is thought to enhance S24-7 levels and abrogate intestinal inflammation.

Chapter 5 states concluding remarks and offers perspectives based on the projects discussed in Chapters 3 and 4. Some additional information is provided in the appendices. Appendix A describes in detail the numeric modelling work in Chapter 3. Appendix B

provides supplementary information for Chapter 4. As a separate piece of work, Appendix C describes protocols on how to engineer a photographing incubator particularly suitable for the study of bacterial swarming.

CHAPTER 2

BACKGROUND

2.1 Bacterial Motility

Bacteria are one of the earliest life forms that appeared on Earth. They are unicellular microorganisms of a few microns in length. They inhabit almost everywhere such as water, soil, hot springs, and even in the radioactive waste. Bacteria are also found in human body, especially in the mouth, gut, and on the skin. Some bacteria are non-motile, whereas other species can propel themselves through their environment, necessitating an area of inquiry known as "bacterial motility". There are different types of bacterial motility such as swimming, swarming, twitching, gliding, sliding, and surfing[3-5] depending on the mechanisms of motion and on the cellular organelles employed (Fig. 2.1). For example, bacteria use pili to twitch, flagella to swim and swarm, and focal adhesion complexes to glide[5].

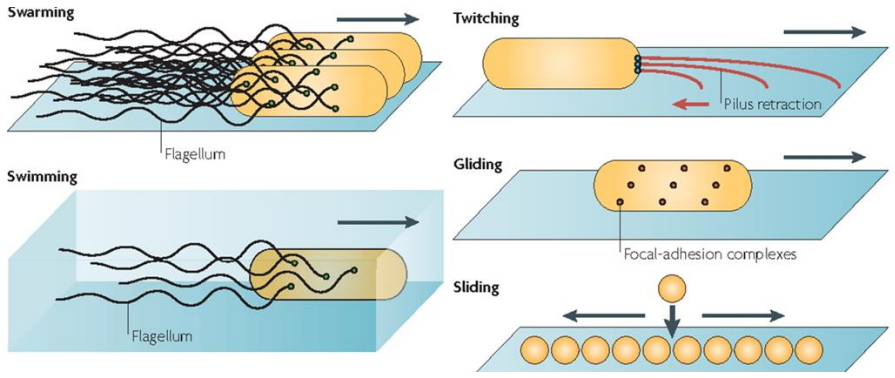

Figure 2.1 | Different bacterial motility types. Swarming is coordinated translocation of bacteria on a semi-solid surface. **Swimming** is individual movement in liquid powered by rotating flagella. **Twitching** is surface movement powered by the extension and retraction of pili. **Gliding** is active surface movement that does not require flagella or pili and involves focal adhesion complexes. **Sliding** is passive surface translocation powered by growth and facilitated by a surfactant.

2.1.1 Swimming

One of the most common motility types of bacteria is swimming. In this form of motility, the cells are propelled by the rotating whip-like flagella in liquid medium. Flagella are helical filaments each connected through a flexible hook to a rotary motor rooted in the cell wall. The length of bacterial cells ranges from 1 to 100 microns and the velocity is typically a few body lengths per second. This allows the bacteria to live in the world of low Reynolds numbers, where the effects of inertia are negligible and the fluid motion is dominated by viscous forces[6, 7]. The nonreciprocal motion of flagella in the form of helical rotations enables bacterial cells to swim freely in the medium which breaks the restriction of reversibility imposed by the Stokes equations. The thrust imparted by the flagella balances the drag on the cell body, resulting in a net unidirectional motion at speed v_0[6].

Swimming enables the bacterial cells to run away from danger and hunt food through the mechanism called chemotaxis[8]. Bacteria like *Escherichia coli* swim towards certain direction for seconds, and then pause and change the swimming direction for a fraction of a second before they continue to swim, known as "run and tumble". Strategically, as bacteria swim along certain direction, they sense the concentration gradients of chemo-attractants or repellents. If the direction is appealing (increasing concentration of an attractant or decreasing concentration of a repellent), the cells will spend more time swimming in this direction. Conversely, if the environment ahead is not favorable, they will tumble more frequently[9] to explore other directions and, over iterations of trial and error, migrate to a more favorable place.

Swimming motility of pathogenic bacteria is associated with the host health. For example, *Salmonella enterica serovar typhimurium* relies on flagella and chemotaxis to induce colitis in streptomycin-pretreated mice[10] and motility allows them to grow and benefit from the mucosal defense[11]. Swimming motility is key to pathobiont activity[12, 13]. Besides, research shows that the flagellin, protein subunit comprising flagellum, plays an important role in causing inflammation[14-16]. Emphasizing the importance of suppressing the pathogenic potential of swimming bacteria, studies in mice highlighted mechanisms by which hosts detect and quench flagellar motility to maintain intestinal homeostasis[15, 17, 18].

2.1.2 Swarming

Swarming, or swarm behavior, refers to the collective motion of a large number of self-propelled entities[19]. These entities can be a school of fish, a flock of birds, or a group of insects like bees and ants. First reported in 1972 by Jorgen Henrichsen, bacterial swarming is defined as flagellum-driven bacterial group motility on a surface[3]. The rapid multicellular movement was originally observed on the surface of media solidified with agar in Petri dishes, and the agar gel remains the most popular surface for studying this form of motility. Usually, the agar concentration is in the range of 0.3% - 1%. Below the lower boundary, the agar become porous enough to allow bacteria enter the gel and move about individually. At concentrations above 1%, swarming motility of many bacterial species become suppressed, likely due to insufficient flow of the liquid medium to sustain swarm expansion.

Indeed, migrating on a semi-solid surface seems to be more challenging compared with swimming in liquid medium. To swarm smoothly on the agar surface, bacterial swarmers

need to first draw sufficient water from the gel to immerse the cells. Besides, they must overcome the frictional force and the surface tension. In reality, bacteria tend to secret osmolytes, polysaccharides, lipopolysaccharide (LPS) and extracellular matrix (ECM) to attract water towards the cells while swarming[20]. In addition, some swarming bacteria produce biosurfactants which also serve as lubricants to reduce the frictional force and surface tension (e.g., rhamnolipids and their derivatives for *Pseudomonas*, lipopeptides for *Serratia* and *Bacillus* bacterial species[21]).

Swarming motility is associated with a number of unique phenotypes, such as swarming lag, cell elongation, cell hyper flagellation, rafting among the cells, and diverse colony pattern formation[5] and it is often oppositely regulated and antagonistic to biofilm formation[22]. Not as well studied as swimming motility or biofilm formation, bacterial swarming is a relatively young field of research. Thus, there are mysteries and controversies in the field. Mysteries include the role of chemotaxis in swarming, the mechanism of surface sensing, and the mechanism of force generation. A persistent question is "why swarming is not simply swimming motility constrained in two-dimensions?"[5].

2.1.3 Other motility types

Most of the other motility types of bacteria deal with the locomotion on a surface. Twitching is a flagella-independent motility that takes place on organic and inorganic surfaces such as agar gels, epithelial cells, plastics, glass, and metals where the motion is realized through the extension, tethering, and extraction of type IV pili[23]. Gliding is another active surface motility but without the aid of either flagella or pili. The motion typically occurs along the long axis of the cell and bacteria move via focal adhesion

complexes that bind to the substrate[24]. In contrast, the sliding motility is a passive form of surface spreading that requires no active motor[3], and the driving force is the outward pressure of the cell growth accompanied with the surfactant to reduce surface tension.

Recently, researchers defined several new types of bacterial motility. Surfing motility, for instance, refers to the surface motility of bacterial cells on a mucin added medium where mucin would largely promote the expansion rate of the colony[25]. In porous media, bacteria do not perform "swim-reverse-flick" motility as in open space but get trapped regularly. Once the cell is trapped, it reorients its body constantly until it can escape and move in a new path through the space until it is trapped again. This type of motion is called hopping motility[26]. Screwing motility serves as an alternative escaping strategy where the bacteria wind the flagellar bundle around the cell body to release trapped cells from narrow passages[27].

2.2 Bacterial Swarming Properties

Bacterial swarming is an interdisciplinary field of study that connects the fields of biophysics and microbiology. To better understand the contents and the significance of the projects described in the following chapters, I will briefly introduce presently known properties of bacterial swarming in this section, covering both physical movement characteristics and a few biomedical implications.

2.2.1 Collective motion and beyond

From a physical point of view, the collective motion of self-propelled bacteria in a swarming colony serves as a biological example of active matter[28] where particles take in and use energy to generate motion. Macroscopically, the swarming colony expands at

the rate of up to several centimeters per hour and form a variety of patterns such as circular, dendritic, and Bull's-eye[5]. Based on the thickness of the swarm, swarming bacteria can be categorized into monolayer swarms and multilayer swarms[29]. In monolayer colonies (e.g., *B. subtilis*), bacteria secrete large amounts of surfactant so that the cells in the advancing colonial edge may become sparse. For multilayer swarms (e.g., *S. marcescens*), the advancing edge is much more crowded, usually with 2-10 layers of densely packed yet actively moving cells. In both cases, the swarm colony is typically thicker behind the advancing edge as the bacterial population continues to growth over time.

Zooming in to the mesoscopic level and look at the swarming colony on the scale of 100 μm, we see coherent swirling and dynamic clusters billowing in the swarm. The collective motion is typically analyzed using particle image velocimetry (PIV) where image sequences are taken under the microscope and the velocity field calculated via computer software. Based on the flow field, several derivatives can be derived such as the vorticity field, the distribution of velocities and vortices, spatiotemporal correlation functions that indicate the characteristic length λ (typical size of the vortices) and characteristic time τ (typical lifetime of a vortex) scales of the dynamic flow (e.g., for *S. marcescens*, $\lambda \sim 20$ μm, $\tau \sim 0.1$ s)[29, 30]. One emergent property resulted from the collective motion of the bacteria within a swarm is that swarms can carry materials such as small beads. The transportation shows super-diffusive behavior that is not seen on a drop of bacterial suspension, supernatant, or non-swarming but surfactant-producing colonies[31].

Besides the environmental conditions, the properties of the collective motion mainly depend on the characteristics of the individual swarmers. Microscopically, when diluted in liquid medium, bacterial swarmers move at comparable speed or slightly faster than that of

their planktonic counterpart (~ 20 – 30 μm/s) and for certain bacterial swarmers (e.g., *Bacillus, Pseudomonas, Serratia*) tumble is suppressed[32]. By tracking the motion of fluorescently labelled individuals on agar surface, bacterial swarmers show super-diffusion trajectories that are consistent with Lévy walks[33]. Bacterial swarmers tend to move in side-by-side groups called rafts unlike planktonic bacteria that swim as dispersed individuals[5, 29]. While the rafting of *Proteus mirabilis* swarm is through intercellular bundling of flagella[34], the mechanism of rafting formation for other swarming bacteria remains unclear at present.

As Avraham described in his recent review paper[29], swarming is not just swimming at high density despite many similarities between these two motilities. His view is that swarming is a natural state, i.e., cells "decide" to transition into the swarming state compared to dense swimming in artificially concentrated suspensions[35]. This decision brings more advantages to swarmers in their natural habitat (e.g., swarmer cells elongated to the aspect ratio that maximizes the collective speed and vorticity[36]).

2.2.2 Biomedical Viewpoint

Swarming phenotype may bring advantages to the bacteria. For example, the surfactants secreted during swarming are potent antimicrobials that can prevent colonization and growth of other microorganisms[37]. In effect, surfactants can enhance bioavailability by increasing the solubility of hydrocarbons and aid bacterial nutrition[38-40]. From the biomedical perspective, bacterial swarming is often associated with pathogenesis. The rapid surface movement may enable the bacteria to migrate over, adhere to, and disperse from sites of infection[34, 41-43] (e.g., swarming is essential for *Proteus mirabilis* to migrate over hydrogel-coated latex catheters and cause the urinary tract infection

(UTI)[34]). Swarming protects pathogens from macrophages[44] and toxin secretion is often co-regulated with swarming motility[43, 45]. Furthermore, many species of bacteria show enhanced antibiotic resistance when swarming[46, 47], owing to rapid spreading of cells at high density[47-49]. Unlike biofilm formation, the association between bacterial swarming and host health is not studied nearly as extensively. Whereas correlation between swarming and virulence has been shown for certain species of bacteria, such as *E. coli[50]* and *P. aeruginosa[51]*, the probiotic properties of swarming bacteria (e.g., whether swarming as a phenotype can benefit the host health) has not been established in the literature.

2.3 Inflammatory Bowel Disease (IBD)

In the following chapters, I will show the evidence of bacterial swarming on IBD tissue surfaces and discuss the pharmacological implication of swarming motility in the context of mouse IBD models. Thus, I will briefly introduce the clinical facts of IBD and the animal models in this section. A general background knowledge of IBD here may help to better understand the contents and significance of the projects to be presented in the subsequent chapters.

2.3.1 Clinical facts

Inflammatory bowel disease (IBD) is a term for two conditions: Crohn's disease (CD) and ulcerative colitis (UC). The disease is characterized by chronic inflammation of the gastrointestinal (GI) tract[52]. Crohn's disease affects a wide range of the GI tract, mouth, esophagus, stomach, small intestine, large intestine, and the rectum. Ulcerative colitis is limited to the large intestine (colon) and the rectum. For Crohn's disease, the damaged

areas appear in patches next to the areas of healthy tissues, and the inflammation may penetrate multiple layers of the GI tract wall. For Ulcerative colitis, the inflammation is present only in the innermost layer of the colon and damaged areas are continuous, starting at the rectum and spreading further into the colon. In both conditions, the symptoms include abdominal pain, persistent diarrhea, rectal bleeding/bloody stools, fatigue, and sometimes internal cramps/muscle spasms in the region of pelvis[53]. The diagnosis of IBD is generally by assessment of inflammatory markers in stool followed by colonoscopy with biopsy of pathological lesions. Despite similar symptoms, IBD should not be confused with irritable bowel syndrome (IBS) or Celiac disease. IBS is not caused by inflammation and the tissues of bowel are not damaged the way they are in IBD. Celiac disease is an inflammatory response to gluten and symptoms will go away after starting a gluten-free diet.

According to the Crohn's & Colitis Foundation of America (CCFA), approximately 1.6 million Americans currently have IBD with an average growth rate of 70,000 new cases diagnosed in the US every year. IBD is the result of a defective immune system whose duty is to attack foreign organisms (e.g., viruses and bacteria). However, in IBD, the immune system responds incorrectly to environmental triggers and causes inflammation of the GI tract. IBD is a complex disease whose exact cause is still unknown but the dietary patterns, microbiota, genetic factors all seem to associate with the disease. For example, people with a healthier diet could lower the risk of ulcerative colitis by 79%[54] while an unhealthy diet high in animal protein associates with increased risk of IBD[55]. Alteration of the gut microbiome may contribute to IBD[56] since the IBD patients are found to have 30-50% reduced biodiversity of commensal bacteria and they are more likely to have been

prescribed antibiotics in the 2-5 year period before their diagnosis compared with normal individuals[57]. Furthermore, 5% to 20% of affected individuals have a first-degree relative (parent, child, or sibling) with IBD[58] and children of parents with IBD are at greater risk than the general population for developing IBD[59], which shows a genetic factor of the disease.

Although IBD itself is not fatal, it may increase the risk of getting other diseases such as colon cancer, blood clots and liver diseases[60, 61], resulting in slightly higher mortality than the general healthy population. There is no standard treatment for all people with IBD, and the treatment approach is tailored to individuals based on the disease severity, anatomic location, previous response and side effects to medication, and comorbidities. Main categories of medication used to treat IBD include aminosalicylates, corticosteroids, immunomodulators, and antibiotics. Around half of the IBD patients will be in remission over the next 5 years, but when medication cannot adequately control symptoms, patients that develop complications may require surgery.

2.3.2 Mouse models

To study the complex interactions among immunologic, environmental, and genetic components in IBD, researchers have established mouse experimental models to simulate human IBD. Although no animal model exactly reproduces human IBD, the *in vivo* models allow us to approach the complex mechanism of intestinal inflammation while each component are well controlled and defined.

Currently, there are many dozens of preclinical IBD models of different types and subtypes, each with their own pros and cons. Main types of the mouse models include chemically

induced, microbiome induced, genetically engineered, and those involving adoptive T cell transfer or spontaneous mutation[62]. Dextran sulfate sodium (DSS), trinitrobenzene sulfonic acid (TNBS), and oxazolone are common chemicals used in induction of colitis. The chemically induced IBD models are relatively cheap, quick, and easy to develop while researchers need to closely monitor the chemical batch and supplier, mouse strain, gender and source, dosing level and frequency to ensure the reproducibility of the study. A spontaneous mutation mouse model such as Samp1/YitFc colitis provides a well-defined time course of the disease progression, but it also results in a long and costly study timeline (~30 weeks for full disease penetrance)[63]. The most well-known genetically engineered mouse model of IBD should be the interleukin-10-deficient (IL-10 KO) mouse, which is still in use since its development 27 years ago[64]. IL-$10^{-/-}$ Knockout mouse model is useful for studying different immune mechanisms of IBD, but substantial variability in colitis development is observed between facilities since the model is highly dependent on microbiome differences.

When studying the probiotic properties of bacterial swarming, we chose to use the Dextran Sulfate Sodium (DSS) acute colitis mouse model. Feeding mice with 3% DSS polymers in the drinking water for 10-12 days reproducibly induces an acute intestinal inflammation (colitis) characterized by bloody diarrhea, weight loss, shortening of the colon, mucosal ulceration and neutrophilic infiltration[65]. DSS is directly toxic to gut epithelial cells of the basal crypts and therefore affects the integrity of the mucosal barrier. Indeed, DSS inhibits the proliferation of mouse epithelial cells and early lesions occur mainly in the left colon and over lymphoid aggregates[66]. DSS is a relatively simple method to quickly induce damage in the colon of most strains of mice. It is a very reproducible mouse model,

and the histologic severity can be quantified for statistical analysis in research. Due to these advantages, DSS colitis model is very popular for screening of potential therapeutic agents. In effect, many agents have shown benefit in this model, implying that DSS model is a sensitive system. The model represents a non-specific injury model that does not require either T cells or B cells, thus being limited for addressing immunologic or therapeutic issues involving the adaptive immune system. However, for our purpose to prove the concept of the effect of bacterial swarming on IBD, DSS colitis is deemed a sufficiently good mouse model.

CHAPTER 3

CONFINEMENT DISCERNS SWARMERS FROM PLANKTONIC BACTERIA

3.1 Introduction

Motility is an essential characteristic of bacteria. Although energy-consuming, it provides high returns, enabling cells to uptake nutrients efficiently and escape from noxious environments[67]. In a host environment, bacterial motility is an essential phenotype that intimately relates to virulence through complex regulatory networks[68]. Swimming and swarming are two common motility phenotypes mediated by flagella. Whereas the planktonic phenotype defines individual bacteria's motility, a collective movement powered by rotating flagella[5] on a partially solidified surface defines swarming[20]. In swarming, bacteria utilize their flagella to navigate, two-dimensionally, through a medium and acquire necessary molecules to maintain homeostasis and overall survival[69]. Morphological changes like cell elongation or hyperflagellation may occur during swarming for some bacterial strains (e.g., *Proteus mirabilis*)[70], but for others, radical cell differentiation is not observed (e.g., *Photorhabdus temperata)*[71]. Thus, concentrated swimming bacteria are often called "a swarm of bacteria" without requiring precise identification of swarming motility, per se. Nevertheless, most microbiologists believe that swarming and swimming are fundamentally different motility types. For instance, studies found that compared with swimming cells, the requirement for flagella torque is higher for swarming *B. subtilis*[72]; swarming *E. coli* remodel their chemotaxis pathway[73]; and in swarming *P. aeruginosa*, both the production of virulence factors and antibiotic resistance increase[48]. Our recent study has demonstrated a medically relevant distinction between swarming and swimming: a particular strain of swarming *Enterobacter sp.* protects against

mice intestinal inflammation while their swimming counterparts does not[74]. The evidence to date that shows swarming is different from swimming comes mostly from biological data[5]. However, reliable characterization and quantitation of these differences are lacking. In this report, using *Enterobacter sp*. SM3, which is a newly isolated strain that possesses both swimming and swarming motilities, we show distinct biophysical characteristics between these two types of motility under confined, circular geometry of a particular confinement size range.

Studies have shown that geometric constraints have a profound influence on patterns of microswimmers' collective motion. For example, these constraints may create mesoscopically or macroscopically coherent structures such as swirls and jets[75-77]. Circular confinement, in particular, could stabilize a suspension of motile bacteria into a spiral vortex[78-81]. Here, we compare the behaviors of bacteria in swarming and planktonic states under quasi-two dimensional (quasi-2D) circular confinement. Many species of bacteria show distinctive motion patterns while confined. This characteristic may lead to new ways to detect bacterial swarmers from a given clinical sample. Such a new method of detection might lead to diagnostic applications since there are established associations between bacterial swarming and virulence pathology[48, 50].

3.2 Results

3.2.1 Swarming *Enterobacter sp*. SM3 forms large single swirls.

A novel bacterial strain *Enterobacter sp*. SM3 (NCBI BioProject PRJNA558971), isolated in 2014 from mice with colitis induced with dextran sulfate sodium (DSS), has been previously studied for motility[82]. SM3 expands rapidly on 0.5% agar with the collective

motion of multilayers of cells at the edge. We mounted a PDMS chip containing circular microwells on the agar so that bacteria in confinement could rotate for more than 3 hours (details with illustration in Methods). Under confinement of circular wells in the diameter range of 31-90 μm, swarming SM3 cells form single swirls. In contrast, SM3 planktonic cells concentrated from the liquid medium form mesoscale vortices (multiple swirls) in the same size range, except for the smallest well diameter of 31 μm. A clear difference is shown at the well diameter of 74 μm (Fig. 3.1A-D). This striking difference persists in several well depths, except that the concentrated cells yield small but non-zero vortex order parameters (VOPs, defined as illustrated in Fig. 3.1E) in deeper wells, instead of nearly zero VOPs in shallow wells (Fig. 3.1F).

The confinement well diameter has a strong influence on the motion pattern in the wells. In smaller wells such as ones of 31 μm in diameter, even concentrated planktonic SM3 forms a single vortex (Fig. 3.2A), whereas in larger wells, such as ones of 112 μm in diameter, swarming SM3 also breaks into mesoscale vortices (Fig. 3.2B). The phase diagram shows a single swirl in small confinement for both phenotypes of SM3. As the confinement size increases, the VOP of planktonic SM3 drops as the motion pattern breaks into multiple vortices. The drop of VOP and occurrence of multiple vortices occur to swarming SM3 at much larger sizes (Fig. 3.2C). To further compare the dynamics of the confined swarming and swimming SM3, the spatial correlation of the velocity field was calculated for d = 90 μm (where the motion patterns differ for swarming and planktonic SM3) and for d = 500 μm (where both motilities show mesoscale vortices) (see Methods). We computed the correlation function for an inscribed square within a well, which shows

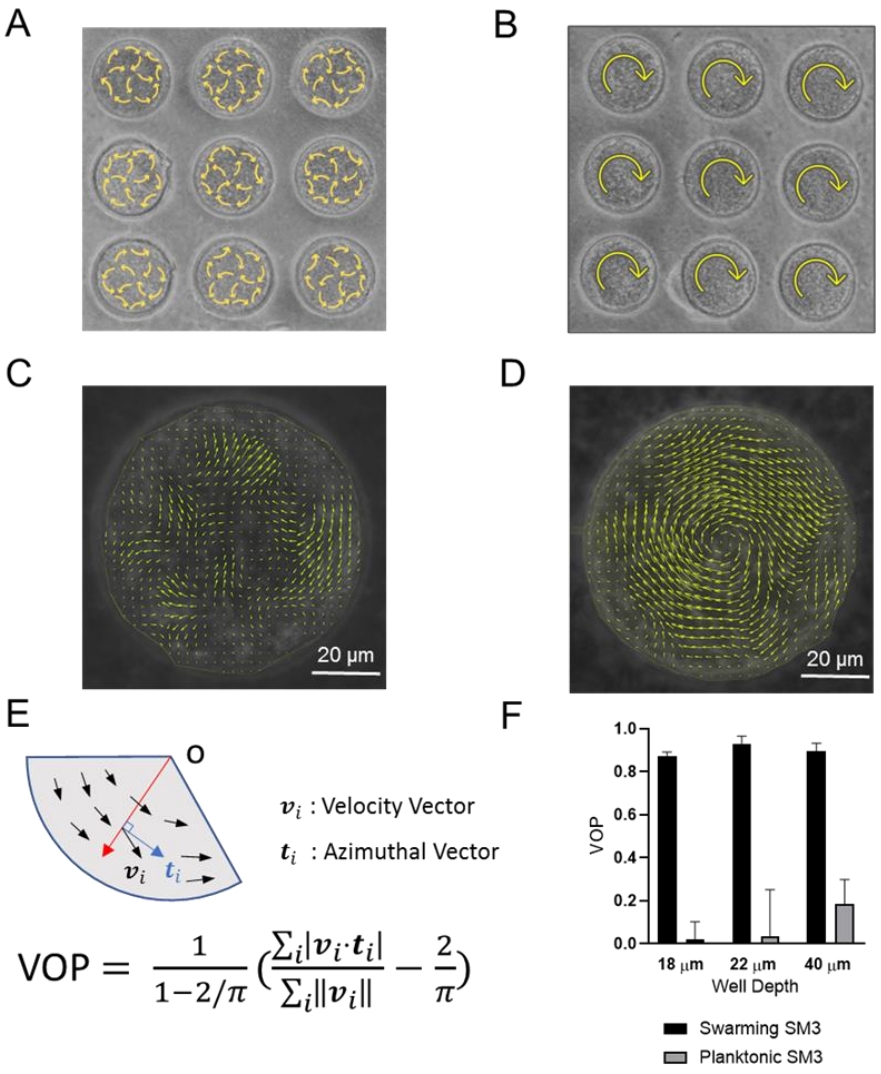

Figure 3.1 | Swirls of *Enterobacter* sp. SM3 under circular confinement. (A-B) Motion pattern of concentrated planktonic (A) and swarming (B) SM3 in the PDMS microwells of 74 μm in diameter. Circular arrows indicate the direction of bacterial collective motion. (C-D) Velocity field of concentrated planktonic (C) and swarming (D) SM3 in a single microwell. (E) Illustration of how vortex order parameter (VOP) is defined. $|\cdot|$ denotes the absolute value while $\|\cdot\|$ denotes the Euclidean norm. (F) VOP of swarming and swimming SM3 in 74 μm microwells of 3 different depths. The sample size n = 5 for each group and data are represented as mean and standard deviation (± SD).

the extent to which the velocity at an arbitrary location correlated with the velocity at a distance Δr away from that location. In 90 μm wells, swarming SM3 velocity correlates positively or negatively throughout the whole well (negative values have resulted from the opposite sides of a single swirl). In contrast, the swimming velocity of planktonic cells of comparable concentration does not correlate once $\Delta r > 25$ μm (Fig. 3.2D). However, in a large open space where both swarming and swimming SM3 break into small vortices, the correlation functions fall into similarly low values. The characteristic length as the curve first crosses $C_r(\Delta r) = 0$, which represents the size of the mesoscale vortices of planktonic and swarming SM3 is 23 μm and 28 μm, respectively (Fig. 3.2E).

3.2.2 The large single swirl behavior indicates strong cell-cell alignment.

We performed several experiments to explore the parameters that might have caused the divergence of motion patterns between swarming and concentrated planktonic cells in confinement. First, we rule out cell density difference as the reason for the difference in the confined motion patterns by concentrating planktonic cells to a comparable density of a naturally expanding swarm on agar (see Methods) before mounting the PDMS chip. Second, we noticed that SM3 tends to get elongated when they swarm[74]. We hypothesize that elongated bacteria may enhance the local alignment of the rod-shaped cells and increase the vortices' size in mesoscale turbulence[83]. Thus, we treated SM3 planktonic cells with cephalexin (CEP) which has been shown to elongate *E. coli* [84] . This treatment indeed caused the cell length of SM3 to reach that of swarming cells on average (Fig. 3.3A). However, we found no significant change following the centrifugation and CEP treatment of the planktonic SM3 (Fig. 3.3B). Although CEP treated planktonic SM3 has similar cell length, cell density, and cell speed as swarming SM3, we could not restore the single swirl

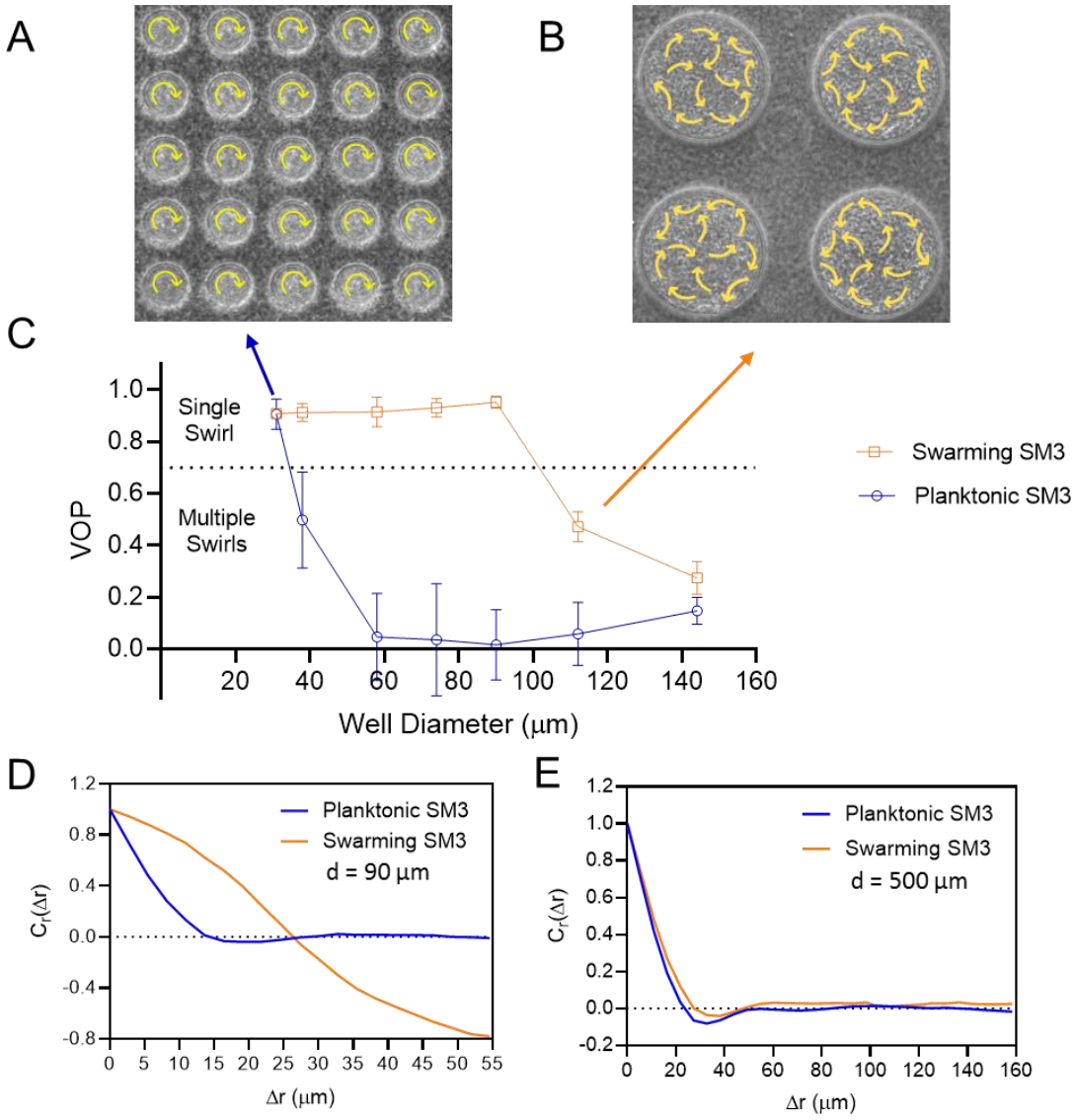

Figure 3.2 | The effect of well diameter on confined *Enterobacter Sp.* SM3 motility patterns. (A-B) Motion pattern of concentrated planktonic SM3 confined in 31 μm (A) and swarming SM3 confined in 112 μm (B) diameter microwells. (C) VOP of swarming and concentrated planktonic SM3 as a function of well diameter. The error bars represent the standard deviations (± SD) for each data point, and the sample size is n = 5. (D-E) Spatial autocorrelations of the bacterial velocity field in the well diameter of 90 μm (D) and 500 μm (E). Unless otherwise noted, the depth of the wells is 22 μm.

pattern in 74 μm confinement wells (Fig. 3.3C). Third, noticing a surfactant rim on the swarming SM3 colony edge, we conjectured that surfactants secreted by swarming SM3 might help align the swarmers in confinement. As a prototypical surface wetting agent, surfactin was added in several concentrations to planktonic SM3 to test whether it could promote a single-swirl motion pattern. However, it did not establish a stable single-swirl pattern. Finally, we found that adding lyophilized swarming supernatant to swimming SM3 did not increase the VOP either (Fig. 3.3C).

Unable to make the concentrated planktonic SM3 form a single swirl in the 74 μm well, we tackled the problem from another angle, by altering the conditions of swarming SM3 in order to break the single swirls. Initially, we tried to physically "disrupt" the swarming colony by rubbing the swarming colony gently with a piece of PDMS offcut. This operation did not break the single swirl pattern in the wells (Fig. 3.3D). Then, 0.2% D-mannose was added to the swarming colony to de-cluster bacteria bundles due to cells' sticking to each other[84]. However, this treatment could not alter the single swirl pattern, either (Fig. 3.3D). Finally, we diluted the swarming cells in Lysogenic Broth (LB) by 20-fold and then reconcentrated the cells in order to test if the single swirl pattern may still form. This was done by centrifugation and removing extra LB to recover the initial cell density, and then these "rinsed" swarming SM3 cells were pipetted back on the agar plate. As shown in Fig. 3.3B, centrifugation at 1,500 g for 10 min did not alter the cell motility significantly. However, the process of centrifugation may wash away some extracellular matrix polymers, including perhaps some weakly adhered on the bacterial surface. After this treatment, we observed multiple swirls under the confinement that previously produced single swirls (Fig. 3.3D), suggesting that these "rinsed" cells behave much like planktonic

cells now. We conclude that the single swirl pattern depends on strong cell-cell alignment interaction mediated by biochemical factor/s removable by matrix dilution.

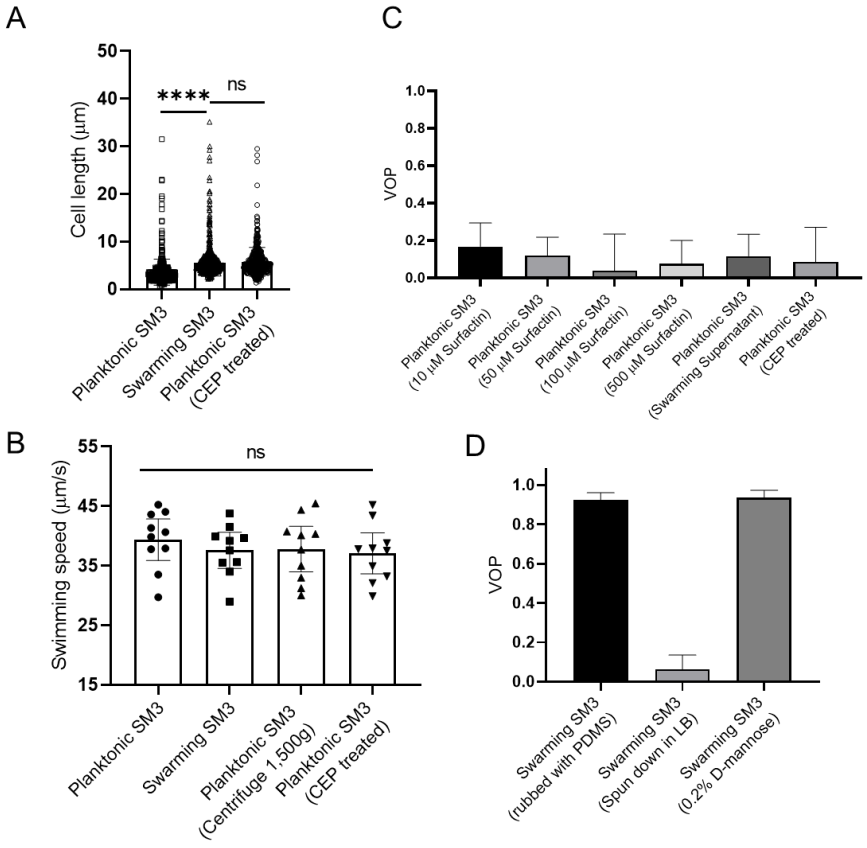

Figure 3.3 | Factors that possibly influence the bacterial motion pattern in the well. (A) Bacterial cell length of planktonic, swarming, and cephalexin (CEP) treated planktonic SM3, n = 500 for each group. Data are represented as median and interquartile range. **** indicates $P < 0.0001$. ns indicates not significant (Kruskal-Wallis test), p = 0.8755. (B) Bacterial cell speed of swimming, swarming, centrifuged, and CEP treated swimming SM3, n = 10 for each group. p = 0.7375; ns, not significant, one-way ANOVA followed by Tukey's post hoc test. (C) VOP of swimming SM3 under 74 μm diameter confinement with different treatments, n = 5 for each group. (D) VOP of swarming SM3 under 74 μm diameter confinement with different treatments, n = 5 for each group. B-D, Data are represented as mean and standard deviation (±SD).

3.2.3 Diluted swarming SM3 show unique dynamic clustering patterns.

We suspected that specific interactions between the neighboring swarming cells were weakened or diminished upon dilution with the LB medium. A fifty (50) μL water droplet was applied to the swarming and the concentrated planktonic SM3 colony edges to

investigate the potential intercellular alignment at a microscopic scale within the bacterial colony. In the diluted swarming colony, groups of cells formed bacterial rafts, a characteristic feature previously associated with gliding motility[5, 29]. Those cells within a polar cluster are moving in the same direction in a cohesive pack at the same speed. In contrast, upon dilution of the concentrated planktonic SM3, the cells disperse uniformly, and their moving directions appear random. Swarming SM3 cells tend to move together near the agar surface, while planktonic SM3 cells swim freely in the bulk fluid (Fig. 3.4A-B). We used the MATLAB PIV toolkit to track the moving bacteria in the image sequences of diluted swarming and planktonic SM3 for comparison. We found that swarming SM3 formed clusters with more than 20 cells on average, while we did not see such clusters of planktonic SM3 cells (Fig. 3.4C-D). The lingering clusters of cells in the swarming phase upon dilution point to a more substantial cell-cell alignment than between planktonic cells.

3.2.4 Numerical simulation reveals cell-cell alignment to be the key player for large swirls.

To further verify that rafting in swarming is a crucially relevant factor to the motion pattern discrepancy, we performed computer simulations using a zonal model for pair-wise interactions. The interactions among the moving particles (short-range repulsion, velocity alignment, and anti-alignment) are considered, all as functions of the particle-particle distance[85, 86]. The particles' speed is fixed for simplicity, but the initial particle positions and initial moving directions are randomized. In the simulations, we interpret the rafting as due to a lower repulsion force and more substantial alignment among the swarmers (see Methods and Appendix A.2). We simulated the situation of confined swarmers and planktonic cells in different sizes of circular confinement, as performed in the experiments. The simulation results mirror the experimental results. Both swarmers and

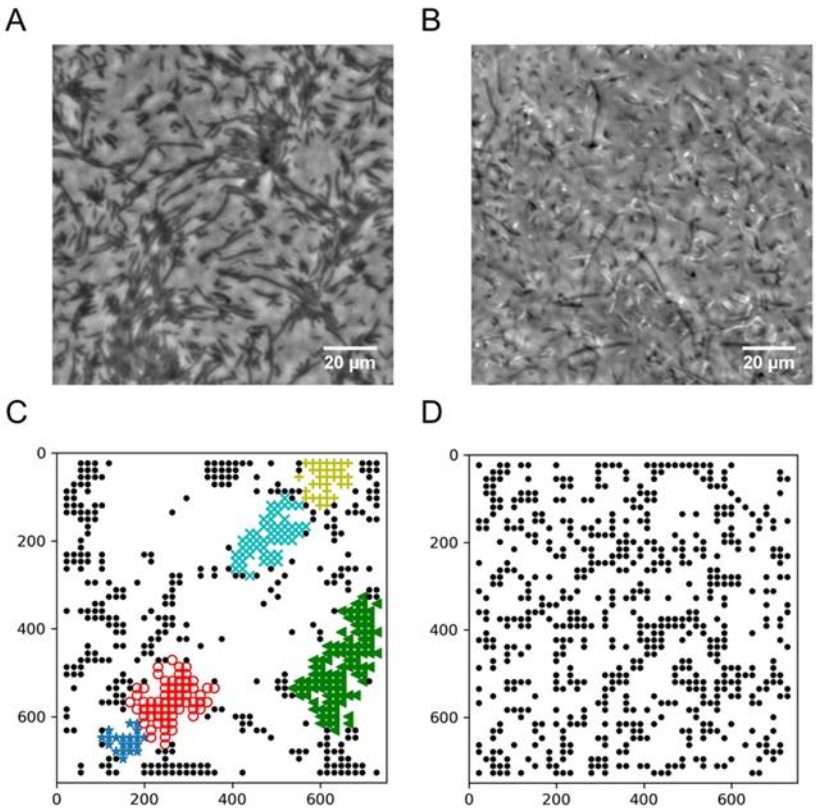

Figure 3.4 | Spatial distribution of swarming and swimming SM3 cells. (A-B) Snapshots showing diluted swarming SM3 (A) and planktonic SM3 (B) on a soft agar surface, respectively. (C-D) DBSCAN clustering analysis of diluted swarming SM3 (C) and planktonic SM3 (D). Black dots represent moving bacterial cells and colored markers show cells in clusters, as determined by the program. The axis represents the dimension of the image in pixels.

planktonic cells start with a single-swirl pattern; as the circle size is increased, the planktonic cells break into a multi-swirl motion pattern earlier than the swarmers. At large enough size, multi-swirl regions occur to samples of both cell types (Fig. 3.5A, compared with Fig. 3.2C; also see Fig. A.3). We then performed the "dilution" simulation for both states, finding that swarming cells form dynamic polar clusters when the cell density is around $\rho = 235$. In contrast, the planktonic cells form a "gas" phase without clustering at all comparable densities (Fig. 3.5B). This result supports the experimental observation in Fig. 3.4A. By assigning a stronger cell-cell alignment interaction among the swarming

cells, our computational model phenocopied the experimental results in both confinement and dilution experiments.

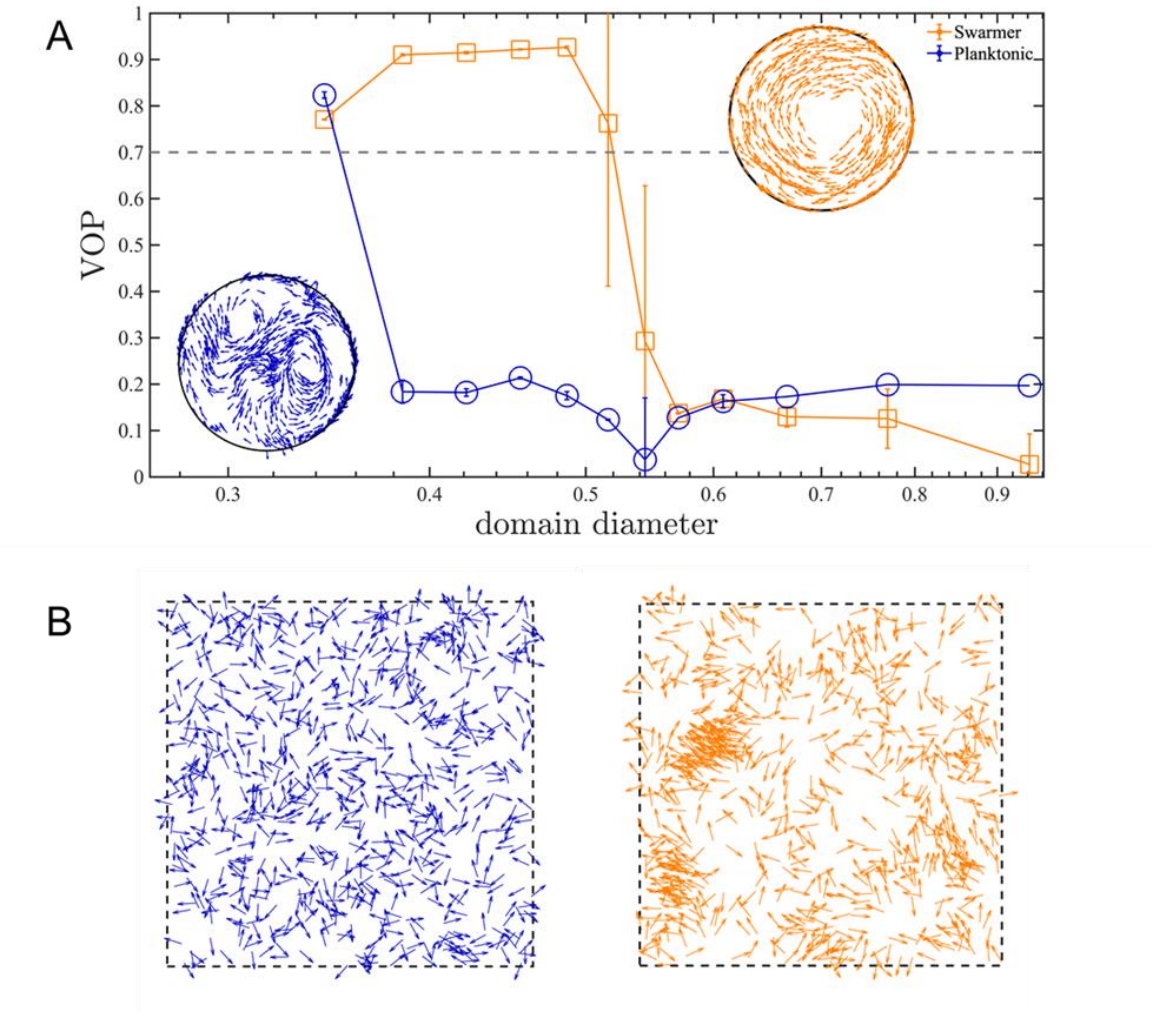

Figure 3.5 | Numerical simulations of planktonic and swarming SM3 in confinement and open space. (A) VOP of swarming and concentrated planktonic SM3 as a function of well diameter. The error bars represent the standard deviations (± SD) for each data point, and the sample size is n = 5. The circles on the upper right corner and the lower left corner show representative motion patterns of swarmers and concentrated planktonic cells in the confinement size between 0.38 and 0.5. (B) Planktonic cells (left) and diluted swarming cells (right) with same cell density in a space of periodic boundary condition. (*Credit to Hamid Karani*)

3.2.5 Identifying SM3 motility type on mice mucosal surface.

The difference in confined motion patterns enables us to detect bacterial swarming on surfaces other than agar, including physiological environments such as on mucosal surfaces. Unlike experiments on an agar surface, there are considerable technical challenges in dealing with uneven or more complex surfaces. The mouse intestinal tissue, for instance, is more than 1 mm thick and non-transparent. Since light cannot penetrate the tissue, observing bacteria directly on the tissue surface is not feasible. Staining or fluorescence labeling may alter the bacterial swarming motility (e.g., we found that SM3 becomes non-swarming once GFP labeled). If the bacterial cells are labeled biochemically, the fluorescence signal weakens when the cells reproduce. As an alternative strategy, using PDMS chips coated with fluorescent beads and then mounted on SM3 inoculated C57BL6 mouse intestine tissue, we detected swarming motility based on the "collective" swirling motion of the beads (see Methods, Fig. 3.6). This experiment on the mouse intestine tissue confirms that bacterial swarming indeed occurs on a non-agar, physiologically relevant surface.

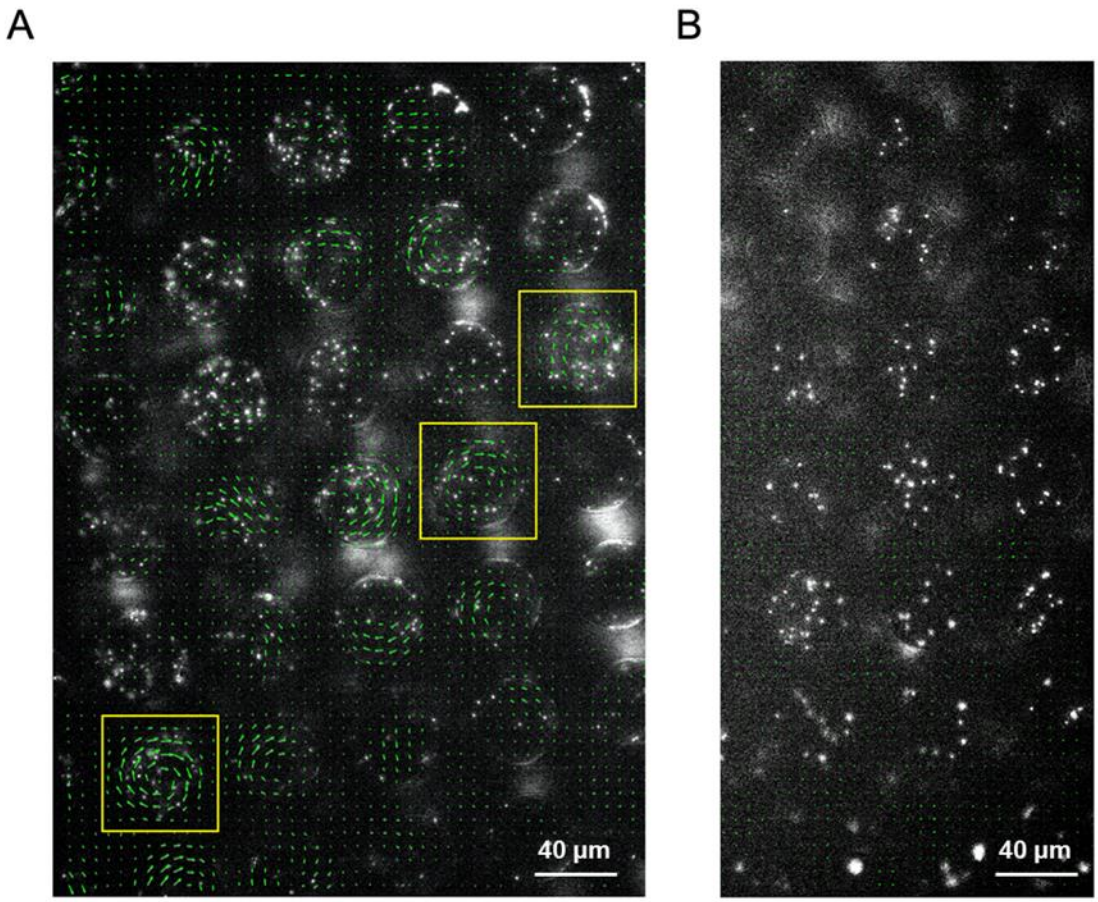

Figure 3.6 | Motion of fluorescent beads in microwells mounted on infected murine tissue. PDMS chips were coated with 0.5 µm fluorescent beads and mounted on SM3 inoculated colitic (A) or non-colitic (B) mice intestine tissue surfaces. The beads motion was measured after 4.5 hr incubation. Average velocity field was calculated by tracing the beads motion using PIV toolkit. (A) On colitic tissue, wells with VOP > 0.7 were found and marked with yellow squares. We conclude that, in these wells, the single swirl motion pattern of the beads was powered by the confined swarming SM3. Since the tissue surface was not as smooth as on agar surface, the motion of the beads in some wells did not form a complete vortex, yet jets indicating partial vortices were discernable. (B) On a normal tissue lacking swarming bacteria, the average velocity of the beads in the wells due to random motion was close to zero, giving rise to uniformly small VOP values. We could infer that the confined SM3 in these wells were predominantly swimming rather than swarming.

3.3 Material and Methods

PDMS confinement sheet fabrication. Polydimethylsiloxane (PDMS) microwell confinement sheets with different combinations of well sizes and depths were fabricated using a soft photolithography technique. Patterns of the confinement were first designed using the software "L-Edit" and then uploaded into a maskless aligner (MLA 150, Heidelberg). On a 3.5-inch silicon wafer (University Wafer Inc.), photoresist gel SQ25 (KemLab, Inc.) was spin-coated at 2,000 rpm (spin speed varies according to the desired coating thickness). After baking, UV exposure, and chemical development, the microwells' designed pattern was shown on the wafer (molding). Then, PDMS (Dow Corning Sylgard 184) base elastomer was mixed with the curing agent at the ratio of 10:1 in weight. The mixture was cast onto the patterned silicon wafer. Two grams of the mixture ended up with a PDMS sheet about 0.5 mm thick. The PDMS solidified at room temperature within 48 hours and it was cut into pieces and peeled off from the silicon wafer before use (demolding).

Bacterial growth and confinement (Fig. 3.7A). *Enterobacter sp*. SM3 is a novel swarming bacterial strain isolated from inflammatory mice[74]. SM3 was transferred from - 80℃ glycerol stock to fresh LB (Lysogeny Broth: water solution with 10 g/L tryptone, 5 g/L yeast, and 5 g/L NaCl) and shaken overnight (~ 16 h) in a 37℃ incubator at 200 rpm. For swarming under confinement assay (Fig. 3.7A, red arrows), 2 μL overnight bacterial culture was inoculated on the center of an LB agar plate (10 g/L tryptone, 5 g/L yeast, 5 g/L NaCl, and 5 g/L Agar; volume = 20 mL/plate) and kept in a 37℃ incubator. After bacteria started swarming for 2.5 hours, a PDMS chip (~ 1 cm^2) was mounted upon the

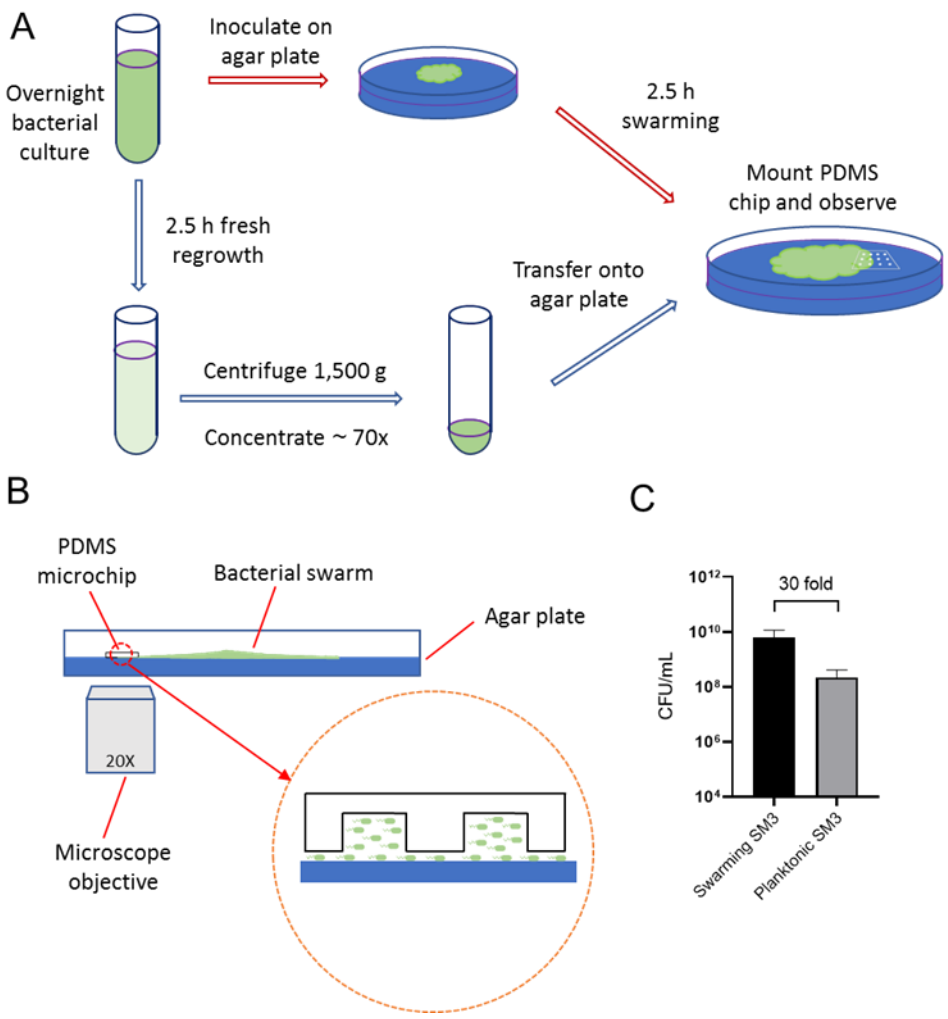

Figure 3.7 | Illustration of experimental procedure. (A) Schematic of sample preparation procedure. Red arrows represent the assay procedure for swarming bacteria. Blue arrows represent the assay procedure for swimming planktonic bacteria. (B) Schematic diagram of the experimental device (side view). The gap of a few microns between the PDMS chip and the agar surface allows the bacteria under the chip to spread. (C) Cell density measured by colony forming unit (CFU/mL) of swarming SM3 and swimming SM3. Swarming SM3 cell density is measured after SM3 swarming on an agar surface for 2.5 h while swimming SM3 cell density is measured for overnight SM3 culture being regrown in fresh Lysogeny Broth (LB) for 2.5 h. Since cell density of swarming SM3 was higher than that of planktonic SM3, the latter was concentrated to acquire comparable cell density before being applied on the agar plate.

edge of the swarming colony and the Petri dish was transferred onto the microscope stage for observation. For swimming under confinement assay (Fig. 3.7A, blue arrows), overnight bacterial culture was resuspended in fresh LB (1:100 in volume) and shaken in the 37℃ incubator at 200 rpm for 2.5 h. The freshly grown culture was centrifuged at 1,500

g for 10 min and ~ 98.6% of the supernatant was removed so that the resultant cell density is about 70 times the freshly grown culture. 10 μL concentrated bacteria culture was inoculated on the LB agar plate, and the PDMS chip was mounted immediately. The plate was then transferred onto the microscope stage for observation. For other bacteria strains, including *Bacillus Subtilis* 3610, the procedure was the same as that of SM3. There are thousands of wells on one PDMS chip, and when mounted on a bacteria spot or colony edge, hundreds of them are occupied by bacteria. The PDMS chip was first brought to contact with the bacteria and then gently mounted onto the agar. By doing so, there was a cell density gradient across an array of wells, with the wells closer to the bacteria spot or colony center having relatively higher cell density. We focused on the area where the confined bacteria showed collective motion, i.e., the cell density was not too high to oversaturate the well, or too low so that each cell was moving independently.

Bacterial cell density measurement (Fig. 3.7B). Two and half hour (2.5 h) freshly grown SM3 was subjected to different factors of dilution in LB, such as 10^2, 10^3, until 10^8. Fifty (50) μL of each diluted culture was inoculated and spread on 1.5 % LB agar plate (10 g/L tryptone, 5 g/L yeast, 5 g/L NaCl, and 15 g/L agar; volume = 20 mL/plate) and was incubated at 37℃ for 16 h. Bacterial colonies appeared on the agar plates and the number of colonies was counted for the dilution that resulted in the colony's number on the order of 100. The colony forming unit per microliter (CFU/mL) was calculated by dividing the colony number by the sampled volume. For swarming SM3, the cell density was measured similarly. On the edge of the swarming colony, a chunk of swarming SM3 (~ 1 mm wide) was picked by an eight (8) mm-wide square spatulate containing a small agar bottom to ensure all the cells in that region were sampled. The 1 mm x 8 mm chunk of swarming

SM3 was then mixed into 1 mL LB for CFU determination. The colony thickness was assumed to be uniform across the sample. It was measured by microscopy focusing on the top of the colony and the top of the agar surface (i.e., at the bottom of the colony), keeping track of the fine adjustment knob readings. Particles of baby powder (~ several micrometers in diameter) were spread on the swarm colony surface and the agar to aid in the microscope focus. The thickness of the swarming colony was calculated based on the calibration of the knob turning tick readings. Then the cell density was estimated by CFU/mL. CFU was calculated for both swarming and swimming SM3 to ensure the cell densities of these two cases were comparable inside the wells. We consider colony-forming unit counting a better way to control the live cell number than merely using the volume fraction because 1), Dead cells that count in the volume fraction will not contribute to the motion in the well, but they will be excluded in CFU calculation; 2), It is challenging to measure the volume of dense bacterial suspension using pipetting method due to high viscosity.

Bacterial cell length and motility. For swimming SM3, 2.5 h freshly grown culture was diluted 100 times in LB and 50 μL of which was transferred on a glass slide and covered with a coverslip. The sample slide was placed under the microscope (Olympus CKX41, 20X), and image sequences were captured. Cell lengths were measured using ImageJ (v1.59e) freehand label tool. Cell speed was calculated as the traveling trajectory length divided by the traveling duration (~ 1s). For swarming SM3, a chunk of swarming bacteria was collected from the swarming colony edge and mixed with 1 mL LB. A glass slide and a cover slip sandwiched a droplet of 50 μL mixed culture, and the rest of the procedure was the same as that for the swimming SM3.

Swimming SM3 with different treatments. i) Cephalexin treatment. Overnight SM3 culture was diluted 100 times in fresh LB and incubated in a 37℃ shaker at 200 rpm for 1.5 h. Cephalexin (CEP) (C4895; Sigma-Aldrich) was added to the culture so that the CEP's resultant concentration was 60 μg/mL. The culture was kept in the shaker for another two hours before use. **ii) Surfactin additions.** After 2.5 h regrown culture was centrifuged, excess supernatant was removed, and surfactin (S3523; Sigma-Aldrich) was added so that the resulting concentrations of surfactin were 10, 50, 100, 500 μM. At the same time, the cell density remained comparable to that of swarming SM3. **iii) Addition of swarming supernatant.** Before swarming SM3 covered the plate, the colony was scratched carefully using a PDMS spatulate (~ 0.5 cm^2) and transferred into 1 mL deionized water. The mixture was sucked into a syringe and filtered with a 0.2 μm filter. The solution was then lyophilized to powder and then dissolved into the concentrated planktonic SM3 of roughly the same volume as the collected swarm fluid. Thus, the concentration of the swarming supernatant was kept the same to subject the concentrated planktonic SM3 to.

Swarming SM3 with different treatments. i) Soft scratching with PDMS. After SM3 swarmed on the agar plate for 2.5 h, a piece of PDMS (~ 0.5 cm^2) was used to softly scratch the edge of the swarming colony so that the swarming cells were disturbed. A PDMS confinement chip was then mounted on the disturbed region for observation. **ii) Spun down in LB.** After swarming for 2.5 h, SM3 cells were collected from the colony's edge using the blotting method[87]. The cells were blotted by a piece of spare PDMS and transferred to 1 mL LB. The swarming cells were centrifuged at 1,500g for 10 min, and LB was removed to restore the initially high cell density. Ten (10) μL of the swarming cells thus treated were inoculated on a new swarm agar and a PDMS confinement chip was mounted

for observation. **iii) D-mannose treatment.** A droplet of 50 μL 0.2% (w/v) D-mannose (Cas No. 3458-28-4; RPI) was pipetted on a swarming SM3 colony edge. After 1-2 minutes, when the cell density became uniform again, a piece of PDMS confinement chip was applied to the D-mannose treated region for observation under the microscope.

VOP measurement and spatial autocorrelation function. Image sequences of swarming or swimming SM3 under confinement were taken by a microscope camera (ThorLabs, Kiralux CS505MU) and then processed using a particle image velocimetry (PIV) package in MATLAB. The velocity field was marked for the confined bacteria and the VOP was calculated using the equation in Fig. 3.1E. Using the velocity field information, we calculated the spatial autocorrelation function through the equation $C_r(\Delta r) = < \frac{\boldsymbol{v}(r_0)\cdot\boldsymbol{v}(r_0+\Delta r)}{|\boldsymbol{v}(r_0)^2|} >$, where r_0 is the local position vector and Δr is the displacement vector[30]. A Python script was written to calculate all the C_r values in the region of interest (ROI) with a label of Δr values. These C_r values were then plotted as a function of Δr.

Clustering analysis. On the swarming SM3 colony edge or concentrated swimming SM3 inoculation, a droplet of 50 μL deionized water was added via a pipette. Once the fluid flow stabilizes, image sequences were captured at the diluted swarming or planktonic SM3 sample locations. In a region of 130 μm x 130 μm, the velocity field was calculated using the PIV toolkit, and the vectors with magnitude below four (4) μm/s were removed. The purpose of the vector validation was to exclude non-motile bacteria. Once the moving cells were identified, a Python script was implemented to perform the clustering analysis using the function of DBSCAN[88] where the parameter ε was set to 50, which specifies how close points should be to each other to be considered a part of a cluster, and the minimum number of points to form a cluster was set to 20.

Numerical Simulations. The numerical simulation consists of a 2D system of *N* particles. The position **r** of each particle is modeled via the following overdamped Langevin equation:

$$\partial_t \boldsymbol{r_i} = v_0 \widehat{p_\iota} - \sum_{j \neq i} G_\theta\left(d_{ex}, r_{ji}\right) + \sqrt{2D_T}\xi_i \tag{1}$$

It is assumed that particles are cruising at a constant speed of v_0 in the direction of $\widehat{p_\iota} = [\cos(\theta_i), \sin(\theta_i)]$. The second term includes the exclusion forcing term from all neighboring particles residing at a distance r_{ji} closer than the exclusion range d_{ex}. The last term is the thermal fluctuation term with the translational diffusivity D_T and a zero-mean and delta-correlated noise term ξ. The direction of motion θ_i of each particle is updated by the interaction terms F_θ , which includes alignment, anti-alignment and repulsion effects with all neighboring particles and the rotational diffusion term with diffusivity of D_r and noise term ζ:

$$\partial_t \theta_i = \sum_{j \neq i} F_\theta(\boldsymbol{r_{ji}}, \widehat{p_\iota}, \widehat{p_j}) + \sqrt{2D_r}\zeta_i \tag{2}$$

The details of the binary interaction terms G_θ and F_θ are provided in the Appendix A.

The simulation starts with random initial position and orientations, followed by numerical integration of equations (1) and (2) using a first-order Euler method. The integration time step Δt is chosen small enough to ensure numerical stability and independence of long-term dynamics from the time step increment. The interaction of particles with a circular bounded domain is modeled through a reflective boundary condition. The particles are reflected off the boundary with an angle equal to their incident angle. In all diluted cases,

the reflecting solid boundary is replaced with a periodic boundary condition to ensure that boundary scattering does not affect the dynamics in bulk.

Detecting bacterial motility on mouse intestinal mucosal tissue using PDMS chips. Six-week-old female C57BL/6 mice (Jackson Laboratories, Bar Harbor, ME; #000664) were administered 3%(w/v) DSS (Dextran Sulfate Sodium) (MPI; # 160110) in animal facility drinking water daily to induce acute colitis[74]. After 9-12 days, when the mice's weight loss reached 20%, mice were euthanized using isoflurane anesthesia and large intestines were harvested. For controls, conventional six-week-old female C57BL/6 mice exposed to drinking water with DSS-vehicle added were also sacrificed and the intestines were collected. This study was approved by the Institute of Animal Studies at the Albert Einstein College of Medicine, Inc (IACUC # 20160706 & 00001172). Intestinal tissue was surgically exposed, cleansed with 35% (v/v) ethanol, and rinsed with PBS twice. The mucosal surface of the tissue was cultured (on gar streaks) for any residual bacteria and only used when there were no bacterial colonies on aerobic or anaerobic culture. Prior to experiments, a portion of the mucosal tissue was also harvested after ethanol cleansing for histology and to validate its histologic integrity with respect to non-cleansed DSS-exposed tissue. Tissues were spread on a 1% agar plate with the inner side facing up, and overnight SM3 bacterial culture was inoculated on one end of the tissue. The agar plate was incubated under 37°C for 4.5 hours to allow SM3 bacteria to duplicate and move on the tissue surface. PDMS chips (d = 38 μm) were coated with 0.5 μm fluorescent beads (Dragon green; Bangs Laboratory, IN) and cut into strips to fit the tissue's size. The PDMS strip was mounted on and covered the tissue surface. Bead motion was observed under the fluorescence microscope (Olympus CKX41) with 20X objectives.

3.4 Discussion

We have shown the motion pattern differences between PDMS chip confined planktonic and swarming *Enterobacter sp*. SM3 in the size range of 40 μm ≤ d ≤ 90 μm. Compared with previous work, our experimental setup has the advantage of ensuring stable and sustainable patterns. First, PDMS material does not harm living bacteria and is permeable to oxygen[89], thus ensuring continued oxygen exposure required for swarming[74]. Second, we mounted the microchip on a soft agar containing over 97% water, which automatically fills the wells via permeability and capillary flow. Finally, the LB agar also provides the necessary nutrients to fuel the bacterial movement in the wells. Therefore, bacterial cells confined in the microwells remain motile for hours, much longer than in droplets surrounded by mineral oil[78, 84] or in microfluidic chambers with glass surfaces[75, 80], where bacterial movement typically lasted no more than 10 minutes.

One interesting observation is that the rotation direction of the single swirls in our system is clockwise biased (85%, 84 out of 99). We interpret this bias of swirl direction as a consequence of flagellar handedness. When confined between the agar and PDMS surfaces, bacteria tend to swim closer to the porous agar surface[90]. For bacteria swimming near the agar surface, there is a side way component of drag force experienced by the rotating cell body, which results in a net torque on the bacteria to turn right[82, 90]. In our case, the agar surface is the bottom surface, and the bacteria tend to follow a clockwise curved trajectory near the bottom (when viewed from the top). This effect on individual swimmers may act to break the symmetry of the motion pattern in a swarm. It is the most likely cause for the single swirls to appear as clockwise more often than counterclockwise. This effect is notably weak, in view of the exceptions occurring in nearly

15% cases. The effect is also overridden in cases of multiple swirls, or when other dynamic effect becomes dominant.

Prior studies have proposed different models to explain the circularly confined motion of rod-shaped swimmers[79, 84, 91]. In our case, we adopt the Zonal model[85] in order to explain the motion pattern difference observed for confined swarming and planktonic SM3. Noticing that swarming SM3 washed in LB lost the single swirl pattern, we hypothesize that other than cell length or cell speed, the strong cell-cell interaction may be a key factor responsible for the persistence of single swirls in the wells. The mechanism of the rafting phenomenon of swarming cells has not been fully deciphered yet[5]. It might be due to cohesive interaction among neighboring cells and hydrodynamic effects among 2D-confined peritrichous flagellated bacteria[92]. The cell-cell interaction may further result from biochemical change of cell envelope during swarming (e.g., more long sidechain lipopolysaccharides) or secretions[93]. Once these surrounding matrix or polymers are washed away by ~ 100-fold dilution, the alignment may diminish, resulting in a loss of dynamic clusters in the dilution experiment. Upon concentrated back to comparable cell density and subjected to the same confinement, multi-swirl motion patterns occur as opposed to the more coherent single swirls. We confirm that lower repulsion and higher alignment are the key factors that differentiate swarmers and planktonic cells by reproducing the experimental results via numerical simulation. Future work is called upon to explore the swarmer rafting phenomenon further and investigate the molecular basis for cell-cell alignment interaction among the swarming cells.

Our experiments on SM3 confirm the prediction made by Beppu *et al.* that single vortex occurs when the confinement diameter d is smaller than a critical length l^*[80]. Here, from

Fig. 3.2C, we found that the critical length for swarming SM3 is ~ 98 μm, whereas, for concentrated planktonic SM3, it is ~ 34 μm. Interestingly, the same bacterial strain in different motility states has two distinct critical lengths. Thus, we were able to use this property to identify the motility types on mouse mucosal surfaces. The beads' motion is not a perfect swirl in every well on the colitic tissue because the mucosal surface is not as smooth as the agar surface. There are sags and crests on the inflamed mucosal surface due to the disrupted mucin layer[74]. We conjectured that this unevenness hindered the swirl formation to a certain extent. Indeed, intact swirl patterns were spotted only on limited locations where the mucosal surface was relatively flat. Nevertheless, capturing only a few wells where beads showed single swirl motion was sufficient to show that swarming occurred on a mucosal surface.

Evidence of genetic and epigenetic regulation[70, 94-96], as well as cell morphology changes (e.g., cell elongation and hyper-flagellation), indicates that swarming is a different phenotype from swimming. Lacking comparison under the same experimental conditions, one might suspect that bacterial swarming might be a dense group of cells swimming on a surface. Here, through geometry confinement, we show that *Enterobacter sp*. SM3 swarming manifests different biophysical characteristics from swimming. In fact, not only SM3, but other gram-negative swarming bacteria have shown similar properties based on our limited additional experiments (see Appendix A.1). This study's key experimental method differentiates swarming motility from swimming motility at mesoscopic or even macroscopic scales, providing a visual assay to detect swarming behavior on either an agar or tissue surface. This study's findings provide the rationale for developing applications such as isolating bacterial swarmers from a polymicrobial environment and developing

diagnostics for the presence of *in vivo* swarming (e.g., detecting urinary or fecal swarming bacteria in catheter infections or intestinal inflammation, respectively)[50, 97]. Additionally, the sensitivity to confinement size indicates that a quantitative ranking system for different swarmers could be established based on the characteristic well size that stabilizes the confined motion pattern into a single swirl. Such a ranking system may be significant for future investigations on the implications of swarming bacteria in host physiology and pathophysiology.

CHAPTER 4

BACTERIAL SWARMERS EXHIBIT PROTECTIVE EFFECT FOR INTESTINAL STRESS

4.1 Introduction

In the previous chapter, I discussed an interesting biophysical property of the novel swarming strain SM3. Here, the focus is shifted onto the probiotic property of SM3. As mentioned in Chapter 2, bacterial motility is essential in mucosal colonization and has long been associated with virulence and pathogenesis[12, 98]. Intestinal inflammation, such as inflammatory bowel disease (IBD), is attributed to dysbiosis and the mucosal immune system[99]. The disease is characterized by enrichment of motile flagellated bacteria resident in the microbiome and its encroachment into the inner mucus layer and the intestinal epithelial cells[18, 100, 101]. However, despite cues of the molecular mechanisms of flagella effects during intestinal health and disease[102],[103-105],[106], the functional importance and consequence of bacterial motility in a microbial consortium is unknown.

Swimming and swarming are the two primary and common forms of bacterial motility[5]. Swarming, driven by flagella, is a fundamental process in certain groups of bacteria characterized by collective and rapid movement across a surface[5, 29]. This process, in contrast with swimming, offers bacteria a competitive advantage in occupying specific niches (e.g., seeding colonization)[107]; however, the cost-benefits to bacteria[49, 108] and consequences to its host or the environment remain primarily unknown[109].

We hypothesized that bacterial swarming is a necessary adaptation to a noxious environment in a host such as bacteria within inflamed or stressed intestines. Since prototypical swarming bacteria (e.g., *Proteus mirabilis*, *Pseudomonas aeruginosa*) are associated with virulence[51, 109], we surmised that bacterial swarming might be well represented in colonoscopy aspirates from humans with bacterial virulence-associated pathologies (e.g., intestinal inflammation)[110]. This study aims to determine the occurrence and consequence of bacterial swarming in humans and in the animal kingdom, in the context of a stressed and non-stressed intestinal environment. In addition, we aim to uncover potential mechanisms by which swarming bacteria interact with the host.

4.2 Results

4.2.1 Presence of Bacterial Swarmers is a feature of a stressed intestine.

To test whether bacterial swarmers are associated with human and rodent gut health, we developed a modified swarming assay using feces based on an established soft-agar plate assay utilized for single species[111]. We obtained colonoscopy aspirates from individuals with a progressive illness (inflammatory bowel disease - Crohn's and ulcerative colitis and other common forms of intestinal stress like intestinal polyps[1, 112] as well as age and gender-matched controls (those without a clinically active illness)). Within our sampling pool, bacterial collective spreading on soft agar was over-represented in cases with overt or clinically active intestinal stress (Fig. 4.1A-B). As a preliminary assessment, we judged bacterial swarmers' presence in feces by the bacterial spread with a surfactant layer on soft-agar. Swarmers were isolated, identified by MALDI-TOF, and validated for their swarming motility (Table 4.1).

A

		Disease*	
		+	-
Age	Mean (± SD)	51 ± 14	50 ± 11
	Median (Range)	52 (21-81)	51 (24-70)
Gender	Females	27	8
	Males	17	9

* Defined as individuals with clinically established *active* inflammatory bowel disease (Crohn's disease n = 14, or Ulcerative colitis n = 5), intestinal dysplasia (n =1), intestinal polyps (n = 23), intestinal reactive hyperplasia and inflammatory changes not otherwise specified (n = 1). All other diagnoses were considered "negative" for disease.

B

		Disease*	
		+	-
Swarming test †	Swarming	25	3
	Non-swarming	20	22

* One patient consented for the study specimen but did not undergo colonoscopy; One patient had a poor colonoscopy preparation and aspirate sample was not obtained; 9 fecal samples obtained from OpenBiome (Boston, MA), one of which was contaminated inadvertently with a laboratory swarming strain and was excluded from analysis.
† "Swarming" defined as swarming score ≥ 1; "Non-swarming" defined as swarming score = 0.

C

Statistic*	Value	95% CI†
Sensitivity	55.56%	40.00% to 70.36%
Specificity	88.00%	68.78% to 97.45%
Positive Likelihood Ratio	4.63	1.55 to 13.81
Negative Likelihood Ratio	0.51	0.35 to 0.72
Disease Prevalence	64.29%	51.93% to 75.39%
Positive Predictive Value	89.29%	73.63% to 96.13%
Negative Predictive Value	52.38%	54.88% to 77.91%

* Computed with: https://www.medcalc.org/calc/diagnostic_test.php
† CI, confidence interval

D

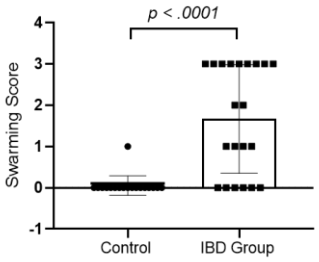

E

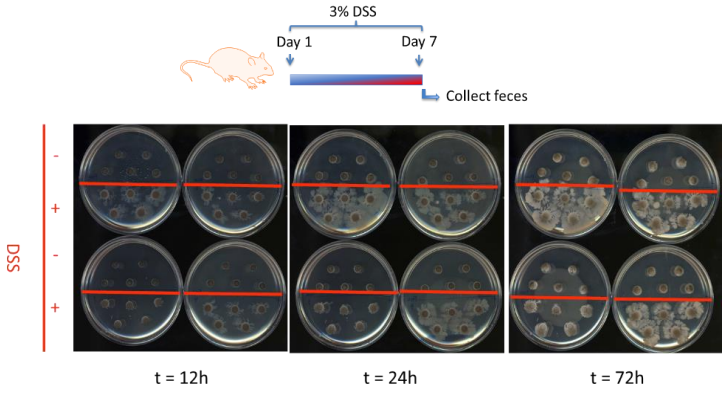

F

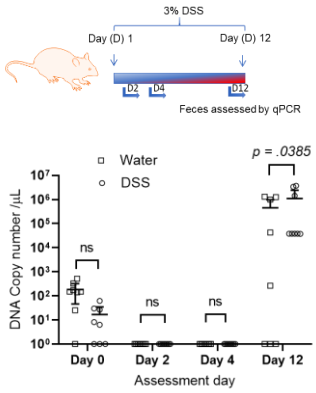

Figure 4.1 | Effect of intestinal inflammation on bacterial swarming. (A-D) Human colonoscopy aspirates (n = 45 intestinal disease; n = 25 non-disease) were spotted on 0.5% agar plates and the swarming assay performed. (A) Colonoscopic washes were obtained from individuals with active intestinal disease and matched controls. Swarming assays performed using aspirates were binned by disease as defined both clinically and by intestinal histopathology, where available. (B) Clinical demographics are described for the disease and non-disease population. (C) Swarming assays' clinical test characteristics. (D) Swarming assays (72h) of fecal samples collected from pigs with and without IBD. Swarming scores - 0: no swarming, 1: swarm within 72h, 2: swarm within 48h, 3: swarm within 24h or less (Control: n = 6; IBD: n = 7, each in triplicate, sampled from distinct regions of the semi-solid feces). (E) C57BL/6 mice (8-week-old) were exposed to water or DSS water for 7 days (n = 4 per group). Fecal samples of control group (above red line) and DSS group (below red line) were collected for swarming assay. Swarming plates were scanned at 12, 24 and 48 hours. (F) In a separate experiment, C57BL/6 mice (8-week-old) were exposed with water or DSS water for 12 days (n = 8 per group). Fecal samples were collected for DNA extraction and SM1/SM3-specific PCR analysis was performed, and DNA copy number ascertained. Data represented as mean and 95% CI, significance tested using Fisher's Exact test.

In this pilot evaluation, the specificity and positive predictive value of the test for disease as defined was approximately 88 and 89%, respectively. In comparison, the test's sensitivity and the negative predictive value was only approximately 56 and 52%, respectively (Fig. 4.1C). Similarly, feces collected from pigs with active inflammatory bowel disease also showed an increased prevalence of collective spreading and swarming compared to control pigs (Fig. 4.1D).

Table 4.1 | Bacterial Strains isolated in the swarming assay

Bacterial strains identified from luminal contents and isolated on swarming agar*

Strain Isolated	Swarming	Source
Escherichia coli #	+	Human IBD
Escherichia coli #	+	Human IBD
Escherichia coli	+	Human anal fistula
Klebsiella pneumoniae	+	Human IBD
Klebsiella pneumoniae	-	Healthy Human
Citrobacter koseri	+	Human IBD
Morganella morganii	-	Human IBD
Serratia marcescens	+	Human adenomatous polyp
Proteus mirabilis	+ ‖	Mouse colitis
Proteus mirabilis	+ ¶	Mouse colitis
Enterobacter sp.#	+	Mouse (DSS colitis)
Enterobacter sp.#	+	Mouse (TNBS colitis)

* Human or mouse feces was subject to the swarming assay and any swarm colony detected within 24 h was swabbed for strain identification. In addition, delayed swarmers were classified as negative but their swarm edge also yielded single species
‖, ¶ Mouse model: Msh2/-loxPTgfbr2 loxp Villin-cre
Also confirmed using Illumina Sequencing (PacBio)

4.2.2 Novel *Enterobacter* swarming strains were isolated from mouse feces.

To identify the relevance of swarmers on host health, we focused on isolating endogenous swarming bacteria residing in rodents and humans. An initial approach was to determine if a single dominant swarming species could always be isolated from a polymicrobial culture (such as mammalian feces). In a competitive swarming assay, a mix of different pure bacterial cultures gave rise to a single bacterial species populating the leading edge of the swarm colony on agar (Fig. B.1). Similarly, swarming assays using the pooled mouse or

individual human feces yielded single species of a dominant swarmer as identified by MALDI-TOF (Table 4.1; Fig. B.1B). To test whether swarming bacteria are also present in preclinical models, we screened feces of mice exposed to dextran sulfate sodium (DSS) that caused acute colonic inflammation[103, 113]. Swarmers (in feces) were uniformly absent in water exposed mice, while present in DSS exposed mice (Fig. 4.1E). In a single experiment, we found "nearly identical isolates" [>99% identical, one contig of 5,107,194 bp (NCBI BioProject PRJNA558971)] from two different mouse fecal specimens - *Enterobacter sp*. SM1 from mice exposed to water and *Enterobacter sp*. SM3 from mice exposed to DSS and SM3 swarmed significantly faster compared to SM1 (Fig. B.2). Taken together, using an agar-based assay, we were able to isolate nearly identical strains with striking differences in their swarming potential.

4.2.3 SM3 abrogates intestinal inflammation in a mouse model of colitis.

A quantitative PCR sequencing-based approach to accurately identify SM1 or SM3 like bacteria in feces showed a significant increase in its abundance during the evolution of DSS-induced colitis (>10,000 DNA copy number/μL) than water only group (Fig. 4.1F). To determine the functional consequence of bacterial swarmers in the host, we administered the "near-identical" swarming competent SM1 or SM3 strains to mice with DSS-induced colitis. In comparison with SM1, SM3 is a hyperswarmer (Fig. B.3A), but both strains possess the same swim speed (Fig. B.3B-C), surfactant production (Fig. B.3D) or growth rate (Fig. B.3E). In contrast to that observed with SM1, SM3 significantly protected mice from intestinal inflammation (Fig. 4.2A-F). Comparison of clinical parameters showed that SM3 significantly protected from body weight loss (Fig. 4.2A),

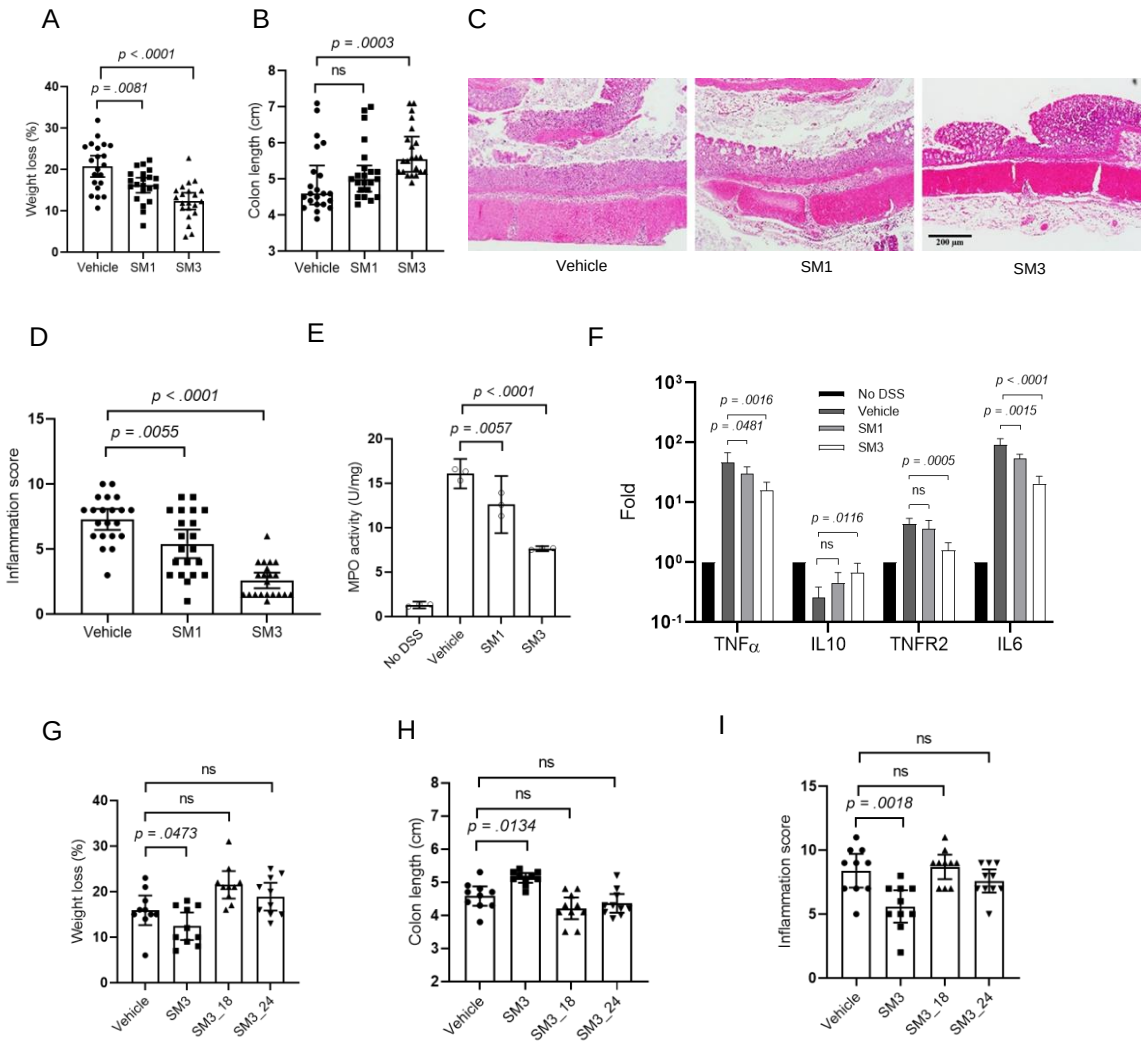

Figure 4.2 | Effects of *Enterobacter sp*. SM strains on DSS induced colitis in C57BL/6 mice. (A-F) 8-week-old mice were exposed to DSS water and treated with vehicle (LB), SM1 or SM3 by oral gavage for 10 days. A-B indicates weight loss (A) and colon length (B) (n = 21 per treatment group). (C) Representative images (100x magnification) of H&E-stained colonic section treated with vehicle (left), SM1 (middle) and SM3 (right). (D) Inflammation score (n = 21 per treatment group). **(**E-F) In a separate experiment, myeloperoxidase (MPO) enzyme activity was determined (n = 3, each in duplicate) (E). Colon total RNA (n = 4) was isolated and reverse transcribed to cDNA. RT-qPCR data show fold induction of mRNA (TNFα, IL10, TNFR2, IL6). PCR was repeated in quadruplicate. The expression was normalized to internal control, TBP. The entire experiment was repeated n = 2 for reproducibility (F). (G-I), In a separate experiment, C57BL/6 mice (8-week-old) were exposed to DSS water and administered vehicle (LB), SM3, or its mutants (SM3_18 or SM3_24) for 10 days. G-I indicates weight loss (G), colon length (H) and inflammation score (I) (n = 10 per treatment group). Unless otherwise noted, data are represented as mean and 95% CI, and significance tested using one-way ANOVA followed by Tukey's post hoc test. (B), data represented as median and interquartile range, and significance tested using Kruskal-Wallis followed by Dunn's multiple comparisons test. ns, not significant. H&E, Hematoxylin and Eosin; TBP, TATA-Box Binding Protein; CI, Confidence Interval.

increased colon length (Fig. 4.2B), reduced the colonic inflammation score (Fig. 4.2D), and had reduced expression of pro-inflammatory mediators compared to vehicle-treated colitic mice (Fig. 4.2E-F). To test the mucosal healing capacity of swarming bacteria, we administered strains SM1 and SM3 to mice during the recovery phase of DSS exposure[114]. When compared to the vehicle, SM3 significantly improved weight gain and colon length with reduced total inflammation and fibrosis at the microscopic level (Fig. B.4). To identify if the effect is flagella mediated, we used a TLR5KO IL-10R neutralization-induced colitis model of mice. SM3 also significantly protected from body weight loss (Fig. B.5A), reduced spleen and colon weight (Fig. B.5B-C), increased the cecum weight (Fig. B.5D), reduced serum KC level and lipocalin level (Fig. B.5E-F), reduced levels of fecal lipocalin (Fig. B.5G), reduced myeloperoxidase activity (Fig. B.5H), and had reduced the colonic inflammation score (Fig. B.5I), when compared to the SM1. SM3 and its isogenic transposon mutants (SM3_18 and SM3_24) only differed in swarming potential (Fig. B.3F), but not swimming speed (Fig. B.3G-H), surfactant production (Fig. B.3I), or growth rate (Fig. B.3J). In mice exposed to DSS, SM3, but not the swarming deficient mutants (SM3_18 and SM3_24), showed significant protection against weight loss (Fig. 4.2G), colon length (Fig. 4.2H), and inflammation (Fig. 4.2I). Together, however, these data indicated that SM3 with swarming properties, as opposed to swarming deficient strains, is associated with anti-inflammatory activity. In accordance with these results, a diverse set of commensal swarmers (*Bacillus subtilis* 3610 and *Serratia marcescens* Db10) exhibited protection against DSS induced inflammation in mice (Fig. B.6 and Appendix B.2.1).

4.2.4 SM3 mediated abrogation of intestinal stress is microbiome dependent.

To determine if the anti-inflammatory role of SM3 is dependent on the conventional intestinal microbiome composition, germ-free mice (GF/SPF) were exposed to DSS and treated with SM3. This strain was unable to abrogate intestinal inflammation in GF/SPF mice (Fig. 4.3A). We analyzed fecal samples of colitic mice (conventional and GF/SPF) with SM3 administered using 16S rRNA gene profiling. In contrast to GF/SPF mice, conventional mice feces showed specific enrichment of anaerobes belonging to the family S24-7 and Lactobacillaceae within SM3 treated mice when compared to vehicle mice (Fig. 4.3B). Specifically, in conventional mice, we found a significant increase in the abundance of S24-7 with SM3 gavage compared to vehicle in DSS exposed mice (Fig. 4.3C). However, quantitative PCR analysis of the levels of S24-7 in the feces of DSS-induced colitis mice gavaged with SM1 or SM3_18 or SM3_24, that did not exhibit protection from intestinal inflammation, was significantly reduced (Fig. 4.4A). In mice not exposed to DSS, the levels of S24-7 bacteria remain stable in SM3 treated group when compared with the untreated group (Fig. 4.3C). Within DSS exposed conventional mice, we observed that enriched S24-7 negatively co-occurred with pathogenic taxa such as the Peptostreptococcaceae and Enterobacteriaceae (Fig. 4.3D). Together, these data suggest that protection from intestinal inflammation by SM3 is associated with the presence of beneficial S24-7 group of bacteria[115].

4.2.5 SM3 promotes growth of *Muribaculum intestinale* in vitro.

A recent study has reported the first cultured bacterium *Muribaculum intestinale* (DSM 28989) that belongs to Bacteriodales S24-7 family[116] and this strain was verified to be one of the representative strains in our fecal sample S24-7 taxa. We used this strain to delineate any potential interspecies interaction with SM3 using an *in vitro* co-culture assay

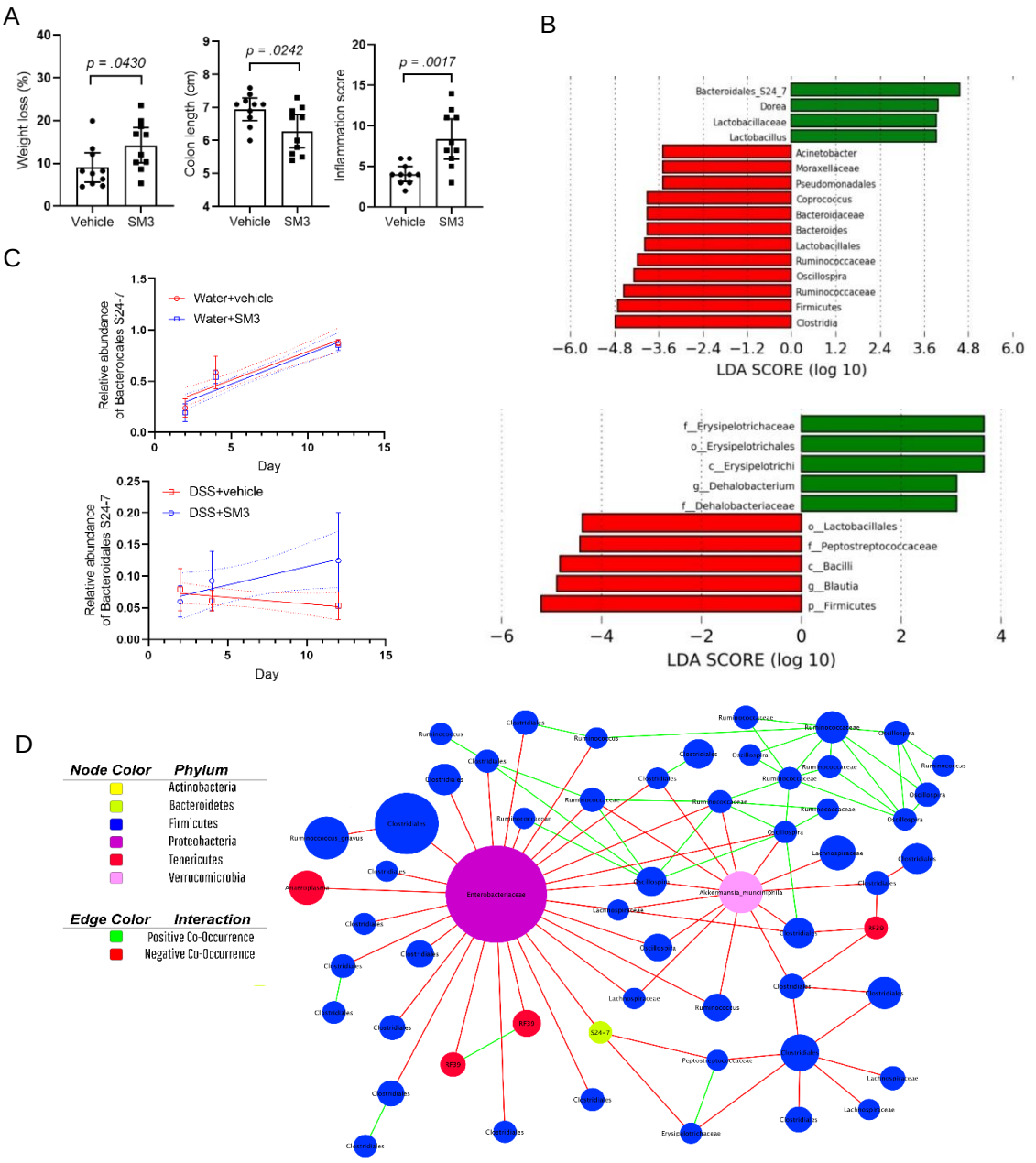

Figure 4.3 | Effects of SM3 on the intestinal microbiota of GF/SPF and conventional mice. C57BL/6 GF/SPF mice (5-week-old) were exposed to DSS water and treated with vehicle (LB) or SM3 for 6 days. (A) indicates weight loss (left), colon length (middle), and inflammation score (right) (n = 10). (B) Linear discriminant analysis Effect Size (LEfSe) plot of taxonomic biomarkers identified using feces of SM3 treated conventional (n = 10) (upper) and GF/SPF (n = 10) (lower) colitic mice on day 12 and day 6, respectively, as compared to vehicle (n = 10). Green and red bars indicate bacterial enrichment within SM3 treated and vehicle group respectively. (C) Relative abundance of S24-7 in the feces from DSS (lower) and control (upper) mice treated with SM3 or vehicle (n = 8). Linear regression line was fit to show the trend of the change (dotted lines show the 95% confidence bands). The slope of the SM3 treated group is similar to vehicle in water control group (P = 0.7827), but significantly different in DSS group (P = 0.0182). (D) Co-occurrence network plot showing strong positive and negative correlations between OTU abundances. Data are represented as mean and 95% CI, and significance tested using a two-tailed Student's t-test. OTU, Operational Taxonomic Unit; GF/SPF, Germ-Free mice transferred to specific pathogen free conditions.

system. We performed a broth-based co-culture assay using this strain and SM3 or SM1 or SM3_18. Interestingly, the proportion of *M. intestinale* during co-culture was higher compared to its monoculture at any tested time point. SM3 as well as the partially swarming deficient strains, SM1 and SM3_18, had a 2-4 fold increase in DNA copy number/µL, when analyzed by qPCR using S24-7 specific primers (Fig. 4.4B). We also designed and developed a plate-based co-culture assay to compare the effects of swarming bacteria SM3 and swarming-deficient variants, SM1 or SM3_18, on the growth of *M. intestinale*. In this assay, swarming plates harbored a central bore well containing *M. intestinale* that guarantees a direct or indirect interaction with the spreading bacteria on agar of the same plate. The plates were sealed so that the act of swarming generated an anaerobic environment suitable for the growth of *M. intestinale*. At 64 hours, in congruence with the broth co-culture assay results, we observed an increase in *M. intestinale* counts with SM3, SM3_18, and SM1 (Fig. 4.4C). To better understand if the observed increase in *M. intestinale* levels is mediated by a direct or an indirect interaction during the co-culture studies, and not solely due to the reduced oxygen concentration in the agar plate, we developed a separate plate-based co-culture assay. In this assay, the swarming region was physically separated from the central bore well containing *M. intestinale* to prevent any direct or indirect interaction with the swarming bacterium. In this system, as the bacteria swarmed on the agar surface over 64h, oxygen levels were reduced. *M. intestinale* showed no growth under the conditions tested (Fig. 4.4C, Divided/Sealed). Overall, our results suggest, that both planktonic and swarming cells of SM3, SM1, or SM3_18, when co-cultured *in vitro,* can promote the growth of S24-7 family (*M. intestinale*), independent of reduced oxygen concentrations in the environment. Coincidently, the development of

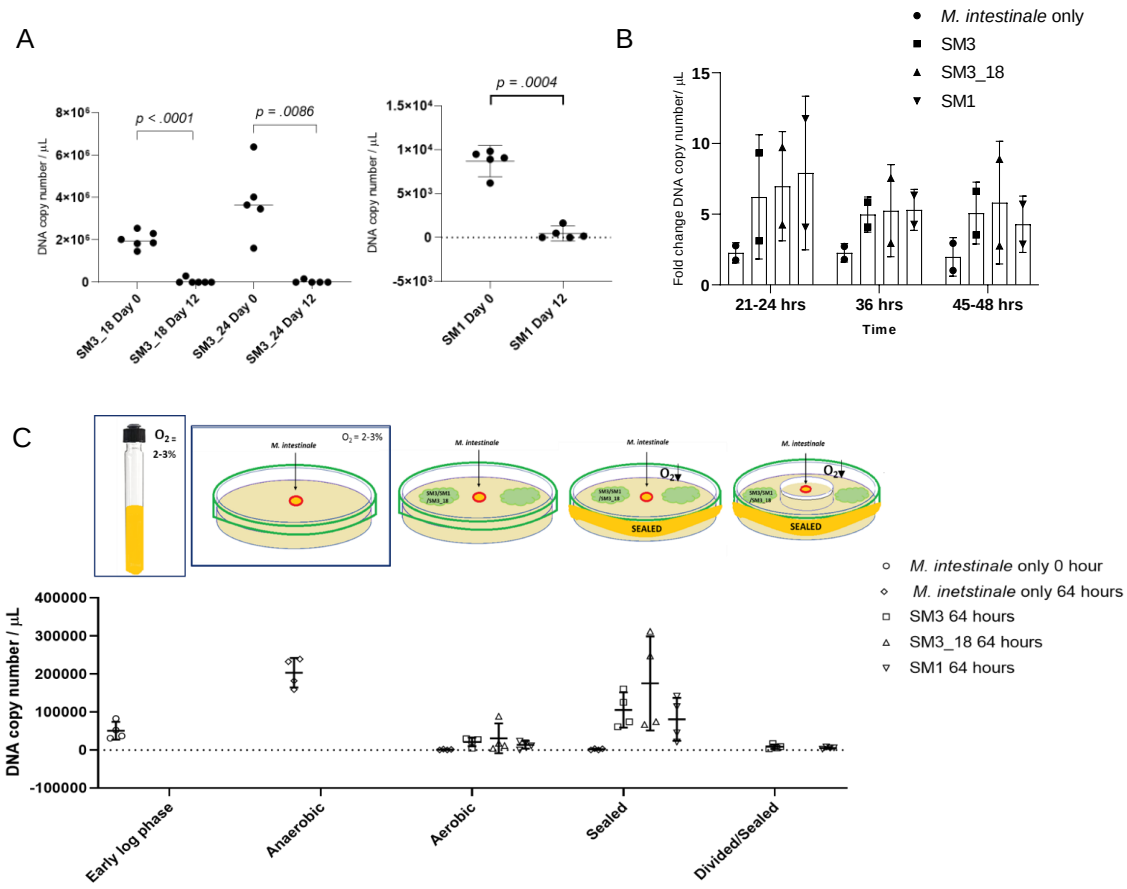

Figure 4.4 | Effect on S24-7 levels in the presence of SM3 and its swarming variants. (A) Eight (8)-week old C57BL/6 mice (n ≥ 5 per treatment group) were exposed to DSS water and treated with SM3_18, SM3_24, and SM1 by oral gavage for 12 days. Total DNA was extracted from feces collected on day 0 and day 12, processed and assessed using qPCR. Five (5) ng of total DNA in conjunction with S24-7 specific primers were used to quantify bacterial copy numbers. In each assay, DNA copy number/µL was calculated based on an internal standard curve. (B-C) *In vitro* co-culture assay using *M. intestinale* cells grown in Chopped meat medium under anaerobic condition until early log phase (OD_{600} ≈ 0.5) were used. (B) Fold change DNA copy number/µL relative to *M. intestinale* monoculture. In broth-based assay, 2µL of early log phase cells of SM3, SM3_18, or SM1 was added to *M. intestinale* cells and mixed cells or monoculture of *M. intestinale* was collected at regular intervals (21-24, 36, 45-48 hrs). (C) In swarming-plate based assay, early log phase *M. intestinale* was transferred in the bore-well and SM3, SM3_18, or SM1 was allowed to swarm either under aerobic or sealed condition at 37^0C and RH ≈ 50%. Plates were sealed using parafilm to create and maintain anaerobiosis due to the act of swarming. *M. intestinale* grown under anaerobic condition was used as a positive control. In Divided/Sealed condition, swarming region was physically separated from the bore -well containing *M. intestinale* and sealed using parafilm. Closed boxes represent incubation in an anaerobic chamber. DNA extracted from equal volume of culture and resuspended in equal volume of TE buffer was used for qPCR in conjunction with *M. intestinale* specific primers. (A), Data represented as mean and 95% CI, and significance tested using paired t-test. (B-C), Data represented as mean (± SD) (n = 2 independent experiments and 2 technical replicates for each). (*Credit to Arpan De*)

significantly reduced oxygen concentrations in the environment is also observed *in vivo* with SM3 only but not with SM1 or the other SM3 mutant bacteria (Fig. B.7 and Appendix B.2.2). Our results suggest that SM3 proximity to *M. intestinale* is necessary for the induction of the growth of the latter species.

4.2.6 Swarming is likely to happen *in vivo.*

The intestinal mucosa is relatively uneven during inflammation due to the loss of mucin (Fig. B.8)[117]. We conjectured, therefore, that swarmers might have an added advantage in niche dominance on inflamed tissue. Indeed, a race assay designed on mouse mucosal surface demonstrated the biological relevance of swarming. On mouse mucosa, it is not possible to visualize bacterial cells directly, so we developed the mucosa racing experiment to determine the dominant motility type. We developed a hyperswarmer strain of SM1, HS2B, that swims slower but swarms at a similar rate and extent to that of SM3, and an isogenic mutant Δ*flhE* SM1 that is swarm deficient but swim competent when compared to SM1 (Fig. B.9A-B). In this experiment, identically sized segments of "normal or control" mouse colon was placed on a hybrid agar plate (1%/0.3%) and equal concentration (CFU/mL) of bacteria spotted. As a negative control, sterile LB and a non-motile strain of Δ*mot*A SM1 when spotted did not show any motility across the mucosal surface even after 20 h. In comparing the "motility rates" across the normal colon mucosa, the hyperswarming HS2B demonstrated slow motility when compared to Δ*flhE* SM1 (Fig. B.9C). However, when the same experiment was performed using inflamed mouse colon after exposure to DSS *in vivo*, the motility of HS2B was significantly faster than swarming deficient Δ*flhE* SM1 (Fig. B.9D). We also used *S. marcescens* strains, swarming Db10 and non-swarming JESM267 (*swrA*) mutant to confirm our hypothesis. While on normal colon mucosa Db10

and JESM267 did not significantly differ in the motility rates, however, Db10 was significantly faster than JESM267 on colitic mucosa (Fig. B.9E-H). Similarly, SM3 had faster motility on colitic mucosal surface when compared to swarming deficient SM3_18 (Fig. B.9I). This indicates that swarming bacteria finds an advantage in motility on a colitic mucosa compared to normal mucosa. Parenthetically, we have recently developed and used a distinct Polydimethylsiloxane (PDMS) based confinement tool to show that a unique motility pattern associated with bacterial swarming is also seen on tissue from colitic mice (Fig. 3.6). Collectively, our data demonstrate the potential of bacterial swarming in vivo during colitis, suggesting that SM3 but not the non-swarming mutants have motility advantage during colitis realizing the proximity of SM3 and *M. intestinale*, and the later one is enriched and associated with the healing of intestinal inflammation.

4.3 Material and Methods

Isolation of bacterial swarmers from feces and colonoscopic aspirates. Patients diagnosed with either inflammatory bowel disease (Crohn's disease or Ulcerative colitis) or undergoing routine screening colonoscopy for colorectal polyps/cancer or required a colonoscopy as part of their medical management of any gastrointestinal disorder as clinically indicated, were recruited for the study. Sixty-three patients who consented to participate in a colonoscopy aspirate or fecal collection study was approved by the Institutional Review Board (IRB) (#2015-4465; #2009-446; #2007-554). Bacterial swarmers were isolated on Luria Bertani (LB) swarming agar medium containing 5 g/L agar with some modifications to an established method[111]. To isolate a singular dominant swarmer from a polymicrobial mix of bacteria (such as feces), we initially focused on developing an assay to isolate swarmers using known polymicrobial mixed

cultures of bacteria. Single bacterial species (up to seven strains belonging to different taxa) grown in LB [OD_{600} of 1.0-1.3] were mixed in a 1:1 ratio and, 5 µL of this mix was spotted on 0.5% agar plates. Following air drying at room temperature, the plates were incubated at 37°C, 40% RH (relative humidity) for 10 hours. Bacterial swarm front was swabbed using a sterile tooth-pick from the edge of swarming colony at different locations (see arrows in Fig. B.1) and after re-streaking on separate agar plates and scaled by growth in LB, samples were identified using Matrix Assisted Laser Desorption and Ionization-Time of Flight (MALDI-TOF). Swarmers present in the fecal or colonoscopic samples were isolated and determined using an identical approach. Fecal pellets and/or colonoscopy aspirates from the clinic and/or feces of mice and pigs were collected in sterile tubes, and freshly homogenized in PBS for swarming assays. Most bacterial swarmers were detected within the first 48-72h from incubation. Dominant swarmers from the edge of the colony were identified using MALDI-TOF. Once identified, cells from the same aliquot were plated on to 1.5% LB agar and serially passaged from a single colony to obtain a pure culture of the strain.

Characterization of the bacterial strains. Swarming ability of a single bacterial species using a pure culture of *Enterobacter sp*. SM1 and its isogenic mutant, *Enterobacter sp*. SM3 and its transposon mutants, *Serratia marcescens* Db10 and JESM267, clinical isolate *Bacillus subtilis* 3610 and its isogenic mutant DS215 was always determined on LB swarming agar at 37°C and 40% RH prior to any experiments using these strains. *B. subtilis* 3610 and its isogenic mutant were compared on LB swarming agar containing 0.7% agar[118]. In order to capture real time swarming motility, a temperature and humidity-controlled incubator equipped with time lapse photography was built and swarming area

was calculated using a python-based script (See Appendix C). Growth kinetics was observed in LB broth, while swimming potential of the strains were assessed in freshly grown cultures (OD_{600} ~ 0.6) or 0.3% LB agar. Surfactin synthesis was determined using blood agar hemolysis[119], drop-collapse[120] and drop-counting assay[121]. Swarming on mucosal surface was demonstrated using a colon tissue from mice that was treated with 3% DSS via a mucosal race experiment. Details of the techniques are present in Appendix B.3.

Mouse model studies. Four to six-week old female C57BL/6 mice (Jackson Laboratories, Bar Harbor, ME; # 000664) were co-housed for acclimatization at the vivarium for 2 weeks prior to randomization by coin toss as previously described[122]. Five-week old germ-free (GF) wildtype (WT) C57BL/6 mice were transferred to specific pathogen free (SPF) conditions[123] during the experimentations (GF/SPF). Acute colitis was induced by administering 3% (w/v) DSS. To determine the effect of swarming and swarming deficient strains during colitis, WT mice were orally gavaged with 100 µL (~ 4×10^9 CFU/mL) test bacteria or LB as vehicle, daily for 9-12 days until the weight of vehicle group dropped >20%. Swarming-deficient strains were generated either using recombineering and PCR Ligation mutagenesis approach[124, 125] or mariner-based transposon mutagenesis[126]. GF/SPF mice were gavaged with SM3 or LB and treated for 7 days, when most mice had >10% weight drop. Daily gavage of bacterial strains absolutely required use of unwashed bacterial strains grown in fresh LB (OD_{600} ~ 1.0). To determine the healing effect of SM3 in colitis, C57BL/6 mice were administered 3% DSS in drinking water for 7 days (when most mice had a weight loss >10% of their pre-DSS exposure weight). Subsequently, mice received animal facility drinking water without DSS and were further randomized by coin-

toss to a treatment group delivered 4×10^9 CFU/mL of bacterial cells or LB by oral gavage for 5 days. At the end of the experiment, mice were euthanized using isoflurane anesthesia or CO_2 asphyxiation and intestines harvested for Hematoxylin-Eosin (H&E) staining and histopathology. Lipocalin (LCN2) assay was performed using Mouse Lcn2/NGAL Duoset ELISA kit (R&D System, DY1857).

The role of TLR5 was assessed in chronic colitis model of TLR5KO mice administered anti-IL-10R monoclonal antibody[127]. Mice were orally gavaged with SM1 or SM3 once every three days from Day 1 onwards. Histology scoring for inflammatory damage was performed according to published criteria for colonic inflammation as a consequence of cytokine imbalance[100].

Fecal microbiome profiling. 16S rRNA meta-analyses of the fecal samples from mice were conducted at Wright Labs, LLC. DNA was isolated from feces using a Qiagen DNeasy Powersoil DNA Isolation kit following the manufacturer's instructions (Qiagen, Frederick, MD). The 16S rRNA gene was amplified using Illumina iTag Polymerase Chain Reactions (PCR)[128], pooled, gel purified at ~400bp and multiplexed with other pure libraries to form a sequencing library normalized to the final concentration of library observed within each sample. The sequencing library was sequenced using an Illumina MiSeq V2 500 cycle kit cassette with 16S rRNA library sequencing primers set for 250bp paired-end reads at Laragen Inc (Culver City, CA). The paired-end sequences were merged with a minimum overlap of 200 bases, trimmed at a length of 251 bp, and quality filtered at an expected error of less than 0.5% using USEARCH[129], analyzed using the QIIME 1.9.1[130, 131] and assigned operational taxonomic units (OTU) using UPARSE at 97%

identity[132]. The taxonomy was assigned using the Greengenes 16S rRNA gene database (13.5 release)[133].

In vitro co-culture assay using *M. intestinale*. A broth-based or swarm plate-based co-culture assay was designed to identify possible interaction bettween SM3 and *Muribaculum intestinale* (DSM 28989). Early exponential phase cells (OD_{600} 0.5-0.6) grown in Chopped meat carbohydrate broth, PR II (BD, BBL) (CMCB-PRII) in an anaerobic chamber, at 37^0C (O_2 = 2-3%) were used to establish the assay. For broth-based assay, *M. intestinale* was grown with fresh cells of SM3/SM3_18/SM1 in a Hungate tube and cells collected at different time points (21/24, 36, 45/48 hrs) for DNA extraction. For swarm-plate based assay, *M. intestinale* grown in CMCB-PRII was transferred into a bore-well at the center of a swarming plate on which SM3/SM3_18/SM1 swarmed. Plates were incubated at different conditions for 64 hours (aerobic, sealed or anaerobic) at 37^0C. For sealed condition, plates were taped carefully using parafilm to maintain anaerobiosis throughout the experiment. For Divided/Sealed condition (please see caricature in Fig. 4.4), a small Petri dish was placed inside a big Petri dish, both containing swarming agar. The bore well containing *M. intestinale* was stationed in the small Petri dish, while the swarming or less swarming strains were spotted on agar present in the big Petri dish. This allowed physical separation of *M. intestinale* from the swarming bacteria, nevertheless maintaining an anaerobic condition in this sealed system. DNA was extracted and qPCR analysis was performed using equal volume of each diluted DNA sample and *M. intestinale* specific primers.

4.4 Discussion

Our study finds that intestinal inflammation itself promotes a protective niche that allow enrichment of bacterial swarmers. Despite the caveat that our approach might preclude the selection of swarmers that do not produce surfactant[5], these pilot data indicate that collective spreading and swarming is a specific feature, and potentially a biomarker of an intestinal pathology as defined by harboring active intestinal inflammation or polyps. Surprisingly, however, these bacterial swarmers when dosed in sufficient abundance abrogate intestinal inflammation in mice. We focused on a newly isolated bacterium, *Enterobacter sp*. SM3, which is resident to the intestinal microflora of mice. *In vivo*, SM3, but not SM1, or SM3 swarming deficient mutants (poor swarmers), influenced the specific enrichment of S24-7 group of bacteria. Notably, the family of S24-7 (*Muribaculaceae*) are known to repair barrier function in inflamed mice intestines[2, 115]. However, the *in vitro* co-culture experiment proved that a close interaction between SM3 and S24-7 group of bacteria is essential for its enrichment. Thus, we hypothesized that it is the relative hyperswarming activity of SM3 (but not the weak swarming SM1 or SM3 mutants) that may facilitate a close interaction with S24-7 group of bacteria, *in vivo*. Further support of this hypothesis comes from the ability of bacteria to swarm on a mucosal surface afflicted only by colitis (ex vivo mucosal race assay). The present mechanism implicates swarming SM3 to directly enhance S24-7 (*Muribaculaceae*) which then suppresses host inflammation. Nevertheless, we do not exclude other direct or indirect effects of the swarming SM3 on mucosal inflammation and healing. However, if present, it would assist in suppressing host inflammation in conjunction with enrichment of S24-7 group of bacteria in the gut.

Swarming bacteria secrete surfactants, such as surfactin, that facilitate motility on a solid surface[5]. Surfactin is known to attenuate TNBS induced colitis, possibly by differentially regulating anti-inflammatory and pro-inflammatory cytokines[134]. However, none of the isogenic pairs showed significant difference in surfactant production, suggesting that the observed protection was not due to secreted surfactin (Fig. B.10 and Appendix B.2.3).

In a germ-free/SPF condition, SM3 lost protection allowing us to speculate the role of a full spectrum intestinal microbiome in the observed effect. Oral gavage of SM3 in conventional colitic mice enriched beneficial anaerobes. As intestinal inflammation creates a shift from anoxic to oxic[135] (Fig. B.7), it was unexpected to find enrichment of obligate anaerobes such as Bacteriodales S24-7 in SM3 treated mice. We observed SM3 fed colitic mice had significantly lower oxygen concentration compared with the colitic mice treated with swarming deficient variants. We conjectured the possible role of swarming movement of SM3, if occurring *in vivo*, in reducing oxygen concentration as also observed *in vitro*. It was further corroborated by the increase in anaerobic taxa in the feces of GF/SPF mice treated with SM3. Nevertheless, a steady increase of S24-7 specific OTU's in SM3 treated DSS-colitic mice pointed towards a potential mechanism underlying the observed protection. Hence, we designed a broth and plate-based co-culture assay to identify possible specific interaction between SM3 and the first cultured bacterium belonging to the S24-7 family, *M. intestinale*. Both SM3 and the less swarming variants promoted growth of *M. intestinale* in co-culture assay. However, linking this observation with decrease in the levels of S24-7 in the fecal DNA obtained from SM1, SM3_18, and SM3_24 led us to speculate the essential role of swarming by SM3 in exhibiting protection. We conjectured that in addition to an anaerobic environment generated by the act of swarming on the agar

plate, all the tested strains either required a direct cell-cell contact or produced a secretome, which promoted growth of *M. intestinale*. This was further validated by a plate-based assay that allowed physical separation of swarming SM3 from *M. intestinale*, but at the same time creating an anaerobic condition in the system suitable for the growth of *M. intestinale*.

Based on the evidence of swarming on mucosal surface, we conclude that swarming of SM3 *in vivo* may facilitate a close spatial interaction with S24-7 group of bacteria. SM3 may aid in re-establishing hypoxia, and consequently create an optimal condition for the enrichment of S24-7 and other anaerobes in a specific microenvironment. In summary, our work demonstrates the unique and unprecedented role that bacterial swarmers play in intestinal homeostasis. We forsee a new personalized "probiotic" approach stemming from the ability to isolate and bank swarming microbes during colitic episodes.

CHAPTER 5

CONCLUSIONS

Through the soft agar swarming assay of polymicrobial mixtures in fecal samples, we were able to isolate single bacterial strains from the swarming colony edge. From DSS induced colitic mice feces, we isolated a novel swarming bacterial strain, *Enterobacter sp*. SM3. At the same time, a swarming deficient strain, *Enterobacter sp*. SM1 was isolated from normal mice feces. Although SM3 and SM1 are genetically identical, and have the same swimming speed, growth rate, and surfactant production rate, SM3 is a hyperswarmer compared with SM1. In a DSS-induced colitis mouse model, SM3 shows protection against inflammation whereas SM1 and other swarming deficient isogenic mutant strains do not. Thus, the anti-inflammatory effect may correlate with the swarming phenotype of SM3.

Further experiments on germ-free mice and fecal sample 16SrRNA analysis reveals that the protection of SM3 is microbiota dependent. A family of bacteria S24-7 increased significantly in abundance in the feces of conventional mice treated with SM3. S24-7 are anaerobic bacteria associated with the healing of inflammation. In addition, in vitro co-culture assay shows that oxygen depletion only is not sufficient, but the proximity between SM strains and S24-7 is necessary for the enrichment of the later. Finally, the race assay on mouse mucosal surface shows that swarming bacteria move significantly faster than their swarming-deficient variant strains, implying that swarming may happen *in vivo*.

Together, we conclude that in colitic mice, the swarming phenotype of SM3 not only reduces lumen oxygen level, creating a favorable anoxic environment for the growth of anaerobic bacteria, but also adds advantage to the spread of SM3 on the mucosal surface.

The expansion and colonization of SM3 increases the chance of SM3 to interact with other bacteria, among which are the S24-7 bacterial family. S24-7 is associated with the abrogation of inflammation and it is enriched under close interaction with SM3. Thus, via symbiosis with S24-7 bacteria, the novel swarming strain SM3 manifests its unique probiotic property. With future work, SM3 may be cultivated into a new type of personalized probiotics that heal IBD.

Besides the probiotic property, swarming SM3 also exhibits unique biophysical properties. When swarming SM3 and planktonic SM3 are confined under PDMS microwells, as the well size increases, the single swirl motion pattern of confined swarming SM3 breaks into a pattern of multi vortices at a much larger well size. After excluding the factors such as cell length, swim speed, cell density and surfactant, we performed the dilution experiment on the colony edge of swarming and concentrated planktonic SM3. We observed dynamic clusters in diluted swarming SM3 but not planktonic SM3. The strong cell-cell alignment may count for the large single swirl motion pattern of confined SM3 swarmers because when SM3 swarmers are washed in LB and re-concentrated to original cell density, the large single swirl breaks into multi vortices and meanwhile the dynamic clusters also disappeared.

We adopted the Zonal model to simulate the confined system numerically and further validate our conjectures. By keeping other parameters the same and only assigning a stronger alignment among the swarmers in the simulation, we were able to recover the experimental results such as the VOP phase diagram, the dynamic clusters in the diluted swarmers. Thus, we conclude that the strong cell-cell alignment among SM3 swarmers

plays an important role in holding the big single swirl motion patterns when circularly confined.

Novel bacterium SM3 shows unique biophysical and probiotic properties associated with its swarming phenotype. However, these properties are not limited to SM3. Swarming bacteria *Bacillus subtilis* 3610 and *Serratia marcescens* Db10 show protection against inflammation too while swarming *Citrobacter koseri* H6 and *Serratia marcescens* H3 also show motion pattern differences compared with their planktonic counterparts. These common properties provide a strong motivation to study bacterial swarming motility more extensively since there may exist more exciting properties of swarming bacteria that have clinical implications.

The finding of new properties of novel bacteria SM3 plants the seeds for deeper and broader studies, such as the exact mechanism of the interaction between SM3 and S24-7, the demonstration of *in vivo* swarming, the molecules that involved in rafting formation, and the dynamic behavior during the phase transition of single swirl breaking into multi vortices. Thus, in a broader view, this thesis marks only the beginning of a long journey to explore more exciting scientific truth on bacterial swarming.

APPENDIX A

SUPPELEMENTARY INFORMATION FOR CHAPTER 3

A.1 Other swarming bacteria show similar biophysical property as SM3

We also tested other bacteria such as *Enterobacter sp.* SM1[74], *Serratia marcescens* (including one lab strain Db10 and another strain, H3, isolated from a human patient)[74], *Citrobacter koseri* (H6)[74], and *Bacillus subtilis* 3610[74]. All the tested strains, with the exception of *B. subtilis*, showed similar motion pattern divergence between confined planktonic cells and swarming cells like SM3 (Fig. A.1A). The bacteria tested, including SM1, H6, H3, and Db10, all behave like SM3. i.e., They all showed clustering when the swarming colony was diluted and uniformly dispersed when the concentrated planktonic cells were diluted.

One notable exception is *Bacillus subtilis.* Swarming and concentrated planktonic *Bacillus subtilis* 3610 show the same motion pattern across different confinement sizes. For well diameter $d \leq 90$ μm, both swarming and swimming *B. subtilis* form single swirls while for well diameter $d \geq 112$ μm, they both break into mesoscale vortices. *B. subtilis* is a Gram-positive bacterium, different from SM3, SM1, H6, H3, and Db10. We speculate that swarming *B. subtilis* does not have as strong a cell-cell interaction as SM3 and its gram-negative cohort we tested. The interaction is not so different between the swarming and planktonic *B. subtilis* 3610 cells since we found the diluted swarming cells to disperse uniformly, and with no clustering behavior, much like diluted planktonic cells. The swarming colony thickness for *B. subtilis* may also play a role in defining the differences between this bacterium and the other strains. It is known that swarming *B. subtilis* produces

abundant surfactant, resulting in a wide-spread, monolayer, non-compact colony[29, 136]. In contrast, swarming SM3 and the other tested bacteria are multilayer colonies that can be as thick as 20 - 40 μm. The thickness of SM3 swarm and that of its gram-negative cohort on agar may extend the strong cell-cell alignment through the entire depth of PDMS wells, which is lacking among planktonic cells of comparable concentration (Fig. A.1B).

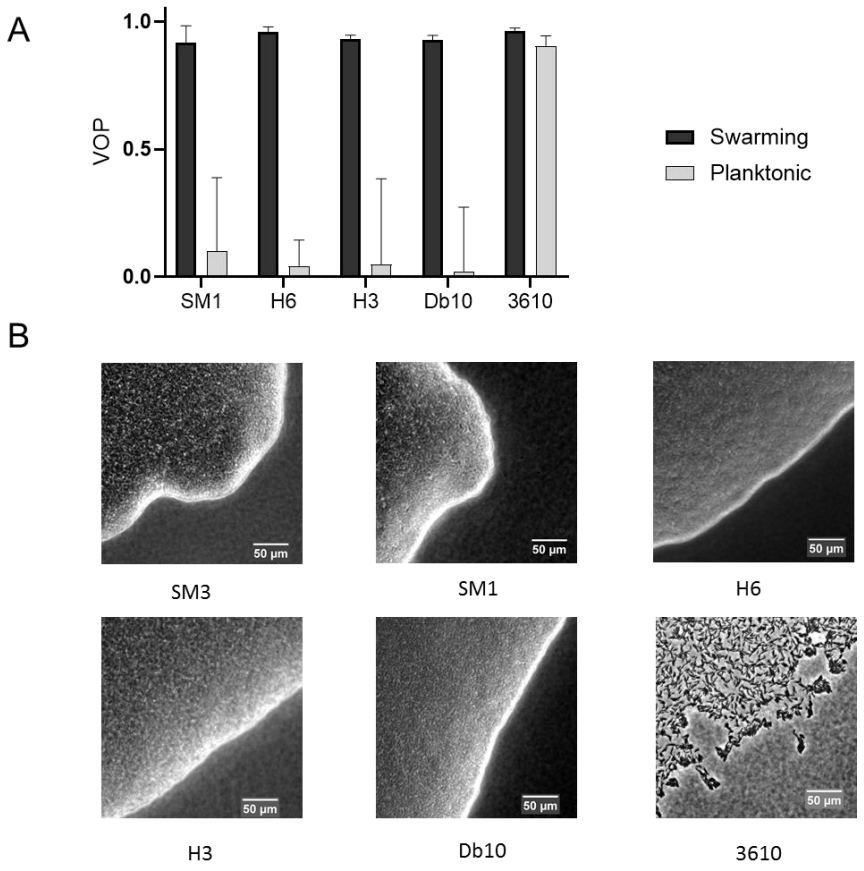

Figure A.1 | Comparison of Vortex Order Parameter (VOP) under confinement and swarm front among several bacteria species. (A) VOP of concentrated planktonic (SM1) and swarming (SM3) Enterobacter *sp.*, *Citrobacter koseri* (H6), *Serratia marcescens* (H3), *Serratia marcescens* (Db10), and *Bacillus subtilis 3610* confined in the PDMS microwells of 58 μm in diameter and 22 μm in depth. The bars indicate averages with standard deviation (+SD) over five microwells. (B) Swarm in front of the tested bacteria. *B. subtilis* 3610 forms a monolayer, loose swarming colony while all the other bacteria strains form multilayer, compact swarming colonies.

A.2 Mathematical modelling and computer simulation

The simulation results presented in this thesis are largely the work of Dr. Hamid Karani, a close collaborator on the project. Below, the method applied for the simulations is detailed by him. It is included in this appendix just so that the details are readily available to the readers of my PhD thesis. Readers are also urged to look in the future for updates of the simulation work in forthcoming publications co-authored by H. Karani.

A.2.1 A simplified treatment of swarming bacteria

Most particle-based models for self-propelled microswimmers incorporate detailed hydrodynamics of elongated rods in a low Reynolds number environment [79, 137-139]. However, the dynamics of bacterial swarming comprise a complex interplay between several physical and chemical interactions that go beyond hydrodynamic and steric effects. Cell interactions with the extracellular polymeric network, mechanical locking, and intertwining of flagella and formation of intercellular bundles between adjacent swimming cells[5, 140] are a few examples whose underlying mechanisms are not fully understood. In the absence of a comprehensive model that captures many interactions among swarming bacteria, we seek a simplified description of active particles interacting via competing interactions that capture the essential dynamics of both swarming and planktonic bacteria. Our focused aim in connection with the experimental study in this report is to discern the distinct, collective behaviors of swarming bacteria from their planktonic counterpart, in comparable concentration, and under the extent of same spatial confinement.

There are numerous approaches for incorporating the relevant physical interactions between active particles[85, 86, 141, 142] (readers are referred to Bär *et al.* for a recent

review[143], for example, on models for dry and wet interacting self-propelled rods). Here, we choose the binary interaction model introduced by Großmann et al.[85, 86] based on the fact that hydrodynamic couplings among the swimmers can induce both alignment and anti-alignment effects[144]. The simplified model we employ also allows us to implicitly embed the unknown interactions of cells with extracellular polymeric network and possibly, mechanical locking of flagella between adjacent cells in alignment, anti-alignment, and repulsion torque terms.

A.2.2 Numerical model and simulation

The dynamics of N interacting active particles have been modeled in a 2-dimensional space using the overdamped Langevin-based equations, assuming that inertia is negligible in a low Reynolds number environment. The position $\boldsymbol{r}$ and orientation θ of particle i are calculated using the following stochastic differential equations:

$$\partial_t \boldsymbol{r_i} = v_0 \widehat{p_\iota} - \sum_{j \neq i} G_\theta\left(d_{ex}, r_{ji}\right) + \sqrt{2D_T}\xi_i$$
$$= v_0 \widehat{p_\iota} - \sum_{j \neq i} k_{ex} r_{ji} \mathcal{H}(d_{ex} - r_{ji}) + \sqrt{2D_T}\xi_i \quad (1)$$

$$\partial_t \theta_i = \sum_{j \neq i} F_\theta(\boldsymbol{r_{ji}}, \widehat{p_\iota}, \widehat{p_j}) + \sqrt{2D_r}\zeta_i \quad (2)$$

In Eq. (1), the particles' self-propulsion speed is set to be a constant v_0 along the direction $\widehat{p_\iota} = [\cos(\theta_i), \sin(\theta_i)]$. This simple assumption is based on our experimental observations, suggesting that the bacterial velocity in the suspension is largely independent of the local cell density. The second term incorporates the central exclusion force term with a spring constant k_{ex}, which acts over the relative distance r_{ji} with all the neighboring particles j. This exclusion force term applies only when r_{ji} gets smaller than the exclusion

range d_{ex} (represented as a Heaviside function $\mathcal{H}$). The last term in Eq. (1) is the Brownian fluctuation term with the corresponding translational diffusivity D_T and ξ_i is the white noise with zero mean and correlation $\delta(t)$.

Two terms influence the temporal change in the orientation of each particle. The first term on the right-hand side of Eq. (2) includes all the binary interaction terms. The last term on the right-hand side of Eq. (2) is the contribution from the angular Brownian fluctuation with the rotational diffusion D_r and a zero mean and delta-correlated stochastic white noise ς. In the present study, we employ the pair-wise interaction model introduced by Grossman and co-workers[85, 86], which successfully reproduces various macroscopic patterns that occur in dense bacterial suspensions. The pair-wise interaction term is based on a zonal model (illustrated in Fig. A.2 below), capturing the alignment, anti-alignment, and repulsion effects. It is formulated in the following form[85, 86]:

$$F_\theta\left(\boldsymbol{r_{ji}}, \widehat{p_i}, \widehat{p_j}\right) = k_r\, \mathcal{H}\left(r_r - r_{ji}\right)\sin\left(\theta_i - \theta_{ji}\right) + \mu \sin\left(\theta_j - \theta_i\right) \qquad (3)$$

k_r is the magnitude of the constant repulsion interaction that applies over a distance of r_r around the particle (Fig. A.2). The second term in Eq. (3) represents the alignment and anti-alignment effects, which operate over a range of r_a and r_{aa}, respectively. The magnitude of the aligning interaction μ is distance-dependent and is defined as[85, 86]:

$$\mu = \begin{cases} \mu^+\left(1 - \left(r_{ji}/r_a\right)^2\right) & 0 \le r_{ji} \le r_a \\ -\mu^- \dfrac{4(r_{ji} - r_a)(r_{aa} - r_{ji})}{(r_{aa} - r_a)^2} & r_a \le r_{ji} \le r_{aa} \end{cases} \qquad (4)$$

where μ^+ and μ^- are the strength of alignment and anti-alignment interactions, respectively.

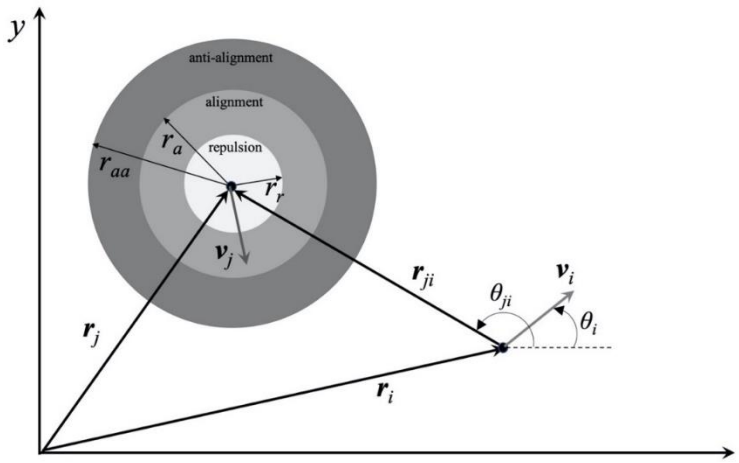

Figure A.2 | Schematic of the zonal pair-wise interaction model. Anti-alignment, alignment, and repulsion zones correspond to interaction radii r_{aa}, r_a, and r_r.

We numerically integrate Eqs. (1) and (2) using the first-order Euler scheme. Initially, the particles are randomly distributed with random orientations. The integration time step Δt is selected sufficiently small to ensure both numerical stability and also independence of long-term statistics from Δt. The simulation time is set long enough to let the system reach a dynamic steady-state. The interaction of particles with the bounded circular domain is modeled via a reflective boundary condition.

A.2.3 Assessment of simulation parameters

Swarming cells secrete large amounts of surface-active compounds that modify the surface tension locally[145, 146], as well as micro-viscosity of the fluid[140], which along with the formation of intercellular bundles between neighboring cells, can enhance the cohesive interaction and alignment in swarmer cells. Thus, simulation parameters must be chosen to capture different behaviors between the planktonic and swarmer cells.

Two different sets of interaction parameters have been used to differentiate the swarming and planktonic cases, and these parameters are summarized in Table A.1. The values are unitless. We set the exclusion parameters k_{ex} and d_{ex} to fixed values of 0.02 and 0.035, respectively. It is also assumed that particles only experience a rotational diffusion D_r of 0.75. The simulations for both swarming and planktonic forms have been studied at two particle densities $\rho = N/A_{dom}$, where N is the number of particles, and A_{dom} is the simulation domain area. In the high-density case, $\rho = 4300$, and in the dilute case, we set $\rho = 235$. In the dilute case, to further minimize the boundary effects, we replace the bounded domain with a periodic boundary.

		Swarming	**Planktonic**
repulsion	k_r	2	3
	r_r	0.05	0.08
alignment	μ^+	0.5	0.2
	r_a	0.2	0.2
Anti-alignment	μ^-	0.5	4.0
	r_{aa}	0.25	0.25

Table A.1 | Simulation parameters used for Swarming and Planktonic cases

The simulation results at high particle density $\rho = 4300$ for some representative confinement sizes are shown in Fig. A.3. As Fig. A.3 illustrates, the macroscopic behavior of both swarming and planktonic cells is affected by the confinement size. The corresponding change in Vortex Order Parameter (VOP) marks the transition from a single vortex to multiple swirls. Compared to the swarming case, the higher values of anti-

alignment and repulsive interactions in the planktonic case trigger an earlier onset of the transition.

The set of simulation parameters in Table A.1 implies that (1) alignment interactions in planktonic cells are suppressed via lower alignment and higher anti-alignment magnitudes, and (2) the repulsive interaction in planktonic cells is more pronounced, in terms of higher values of the magnitude and range of repulsive torque. Despite the empirical nature of these parameter values, we found them to capture the competing interactions between planktonic and swarmer cells. The simulation results provide valuable physical insights as the patterns predicted closely resemble the experimental observation. More advanced real-time visualization of bundling dynamics in swarmer cells[140], along with biochemical characterization of the bacterial fluids, and the micro-rheology measurements within local, extracellular polymeric network[147] will shed light on the underlying nature of complex physical and chemical interactions. These properties rely on experimental effort beyond the scope of this report. If determined, they will facilitate the development of more comprehensive particle-based models.

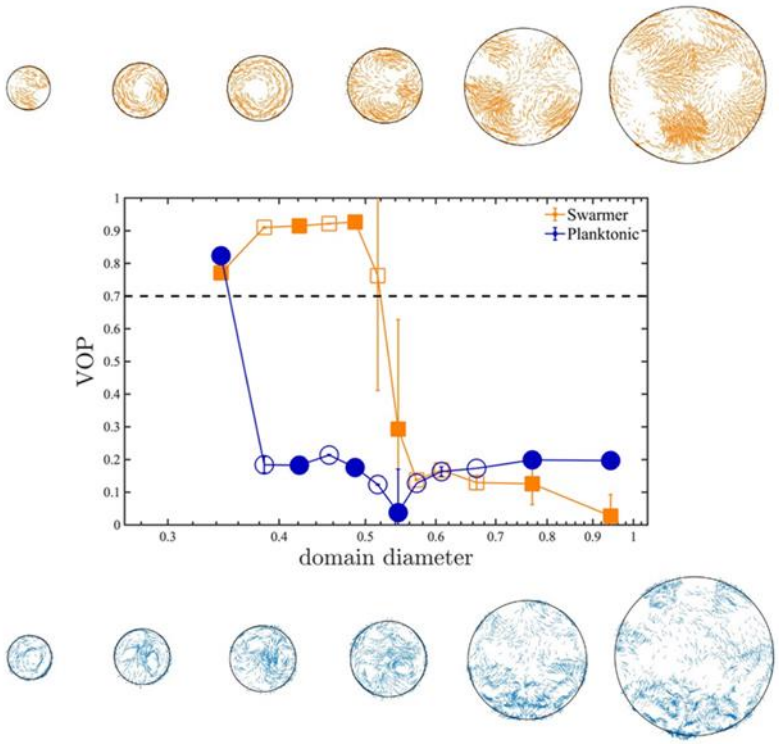

Figure A.3 | Representative patterns at different sizes of the bounded domain. Top row: Swarming; Bottom row: Planktonic. The corresponding domain sizes and VOP values are marked as filled symbols. The particle density is kept constant as the area of the simulated region increases. Simulation parameters are based on the values summarized in Table S1. $\rho = 4300$ in all cases.

APPENDIX B

SUPPELEMENTARY INFORMATION FOR CHAPTER 4

B.1 Supplementary Figures

Figure B.1

A

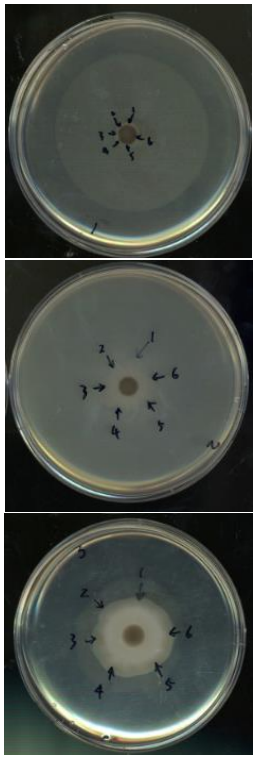

B

Sample Number	MALDI Identification	MALDI Identification Score (Mean) *
A-1	*Klebsiella pneumoniae* *Escherichia coli*	2.26 2.06
A-2	*Klebsiella pneumoniae* *Escherichia coli*	2.24 2.33
A-3	*Klebsiella pneumoniae* *Escherichia coli* *Acinetobacter sp.*	2.20 2.33 1.82
A-4	*Klebsiella pneumoniae* *Acinetobacter sp.*	2.12 1.76
A-5	*Klebsiella pneumoniae*	2.12
A-6	*Klebsiella pneumoniae* *Escherichia coli*	2.24 2.14
B-1	*Bacillus sp.*	1.81
B-2	*Bacillus sp.*	1.83
B-3	*Bacillus sp.*	1.79
B-4	*Bacillus sp.*	1.80
B-5	*Bacillus sp.*	1.80
B-6	*Bacillus sp.*	1.84
C-1	*Enterobacter asburiae*†	2.24
C-2	*Enterobacter asburiae*	2.28
C-3	*Enterobacter asburiae*	2.31
C-4	*Enterobacter asburiae*	2.25
C-5	*Enterobacter asburiae*	2.27
C-6	*Enterobacter asburiae*	2.21

* MALDI identification scores ≥ 2.0 indicate reliable species level identification. Identification scores between 1.7-1.99 indicate a reliable identification to the genus level only.
† *Enterobacter asburiae* is a member of *Enterobacter cloacae* complex. The species level identification *of E. cloacae* complex members by MALDI was confirmed using 16S sequencing.

Figure B.1 | Identification of dominant swarming bacteria within a polymicrobial culture. (A) 1:1 ratio mix of bacteria were used for swarming assay on 0.5% LB agar for 10 hours. *Top*: five non-swarming bacteria were mixed and applied on 0.5% agar. Six random picks as shown in arrows were placed on the edge of colony (1. *Klebsiella pneumoniae* 2. *Escherichia coli* 3. *Acinetobacter sp*. 4. *Bordetella hinzii* 5. *Staphylococcus xylosus*) and 1.5% LB agar streaks performed - single viable colonies were subjected to MALDI-TOF identification. *Middle*: five non-swarming bacteria as above plus two known swarming bacteria SM3 (*Enterobacter asburiae*) and *Bacillus* sp. were mixed, and experiment repeated as per *Top* panel. Six random picks as shown in arrows were placed on the edge of the complex. *Bottom*: five non-swarming bacteria as above plus one known swarming bacteria SM3 (*Enterobacter asburiae*). Six random picks as shown in arrows were placed on the edge of complex**.** (B) Table showing results of MALDI-TOF identification of bacterial colonies isolated from swarming edge. A1-A6 are picks from (A) *Top*. B1-B6 from (A) *Middle*, and C1-C6 from (A) *Bottom*. "A" represents mix of bacterial species *Klebsiella pneumoniae*, *Escherichia coli*, *Acinetobacter sp*., and *Bordetella hiuzii*, *Staphylococcus xylosus*; "B" represents mix of "A", *Bacillus pumilus*, and SM3; "C" represents mix of "A" and SM3.

Figure B.2

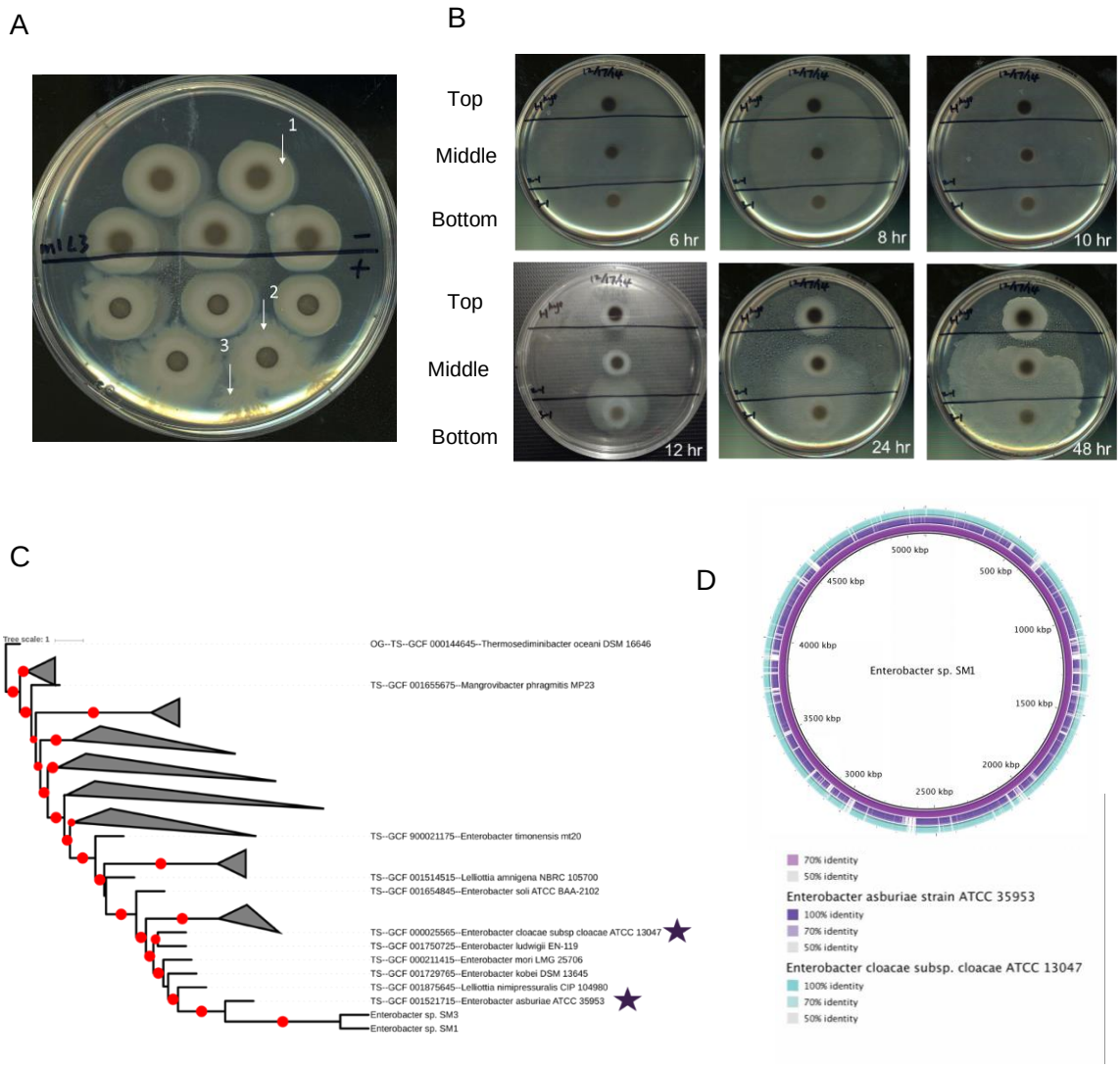

Figure B.2 | Isolation and characterization of *Enterobacter sp.* (A) Five replicate fecal spots from pooled fecal pellets of mice administered water (above black line) or 3% DSS water (below black line) (n = 3, day 7). The white arrows indicate 1, swarm edge isolation from control feces (SM1); 2, swarm edge isolation from feces of mice exposed to DSS (SM2); 3, swarm colony isolation from spontaneous "burst" activity from feces at 24h from plating (SM3). The mouse experiments were repeated at least twice. (B) The bacterial clones isolated from (A) were re-plated as pure strains on 0.5% LB agar and the swarming assay performed over time. Two solid black marker lines divide each plate into 3 regions, holding spots of the 3 strains – Top: Strain 1 (SM1), Middle: Strain 2 (SM2), Bottom: Strain 3 (SM3). These strains have been repeatedly (≥25 times) plated in swarming assays from all aliquots stored from the original isolation (August 2014) and the results confirm that SM3 is a stable hyperswarmer. (C) Phylogenetic tree showing multi-locus sequencing typing-based genetic relatedness between *Enterobacter sp.* SM1, SM3 and reference genomes. Tree was generated with autoMLST (CITE) and drawn using iTOL (CITE). Red dots indicate bootstrap support > 0.8. Stars represent related strains used for comparison with the genome sequences of SM1 and SM3 in panel (D). (D) Genome comparison of related *Enterobacter* strains. *Enterobacter sp.* SM1 was compared to *Enterobacter sp.* SM3 (purple) and the related strains *Enterobacter asburiae* ATCC 35953 (violet) and *Enterobacter cloacae* ATCC 13047 (cyan) and plotted in BLAST Ring Generator (BRIG) http://brig.sourceforge.net/ PMID: 21824423.

Figure B.3

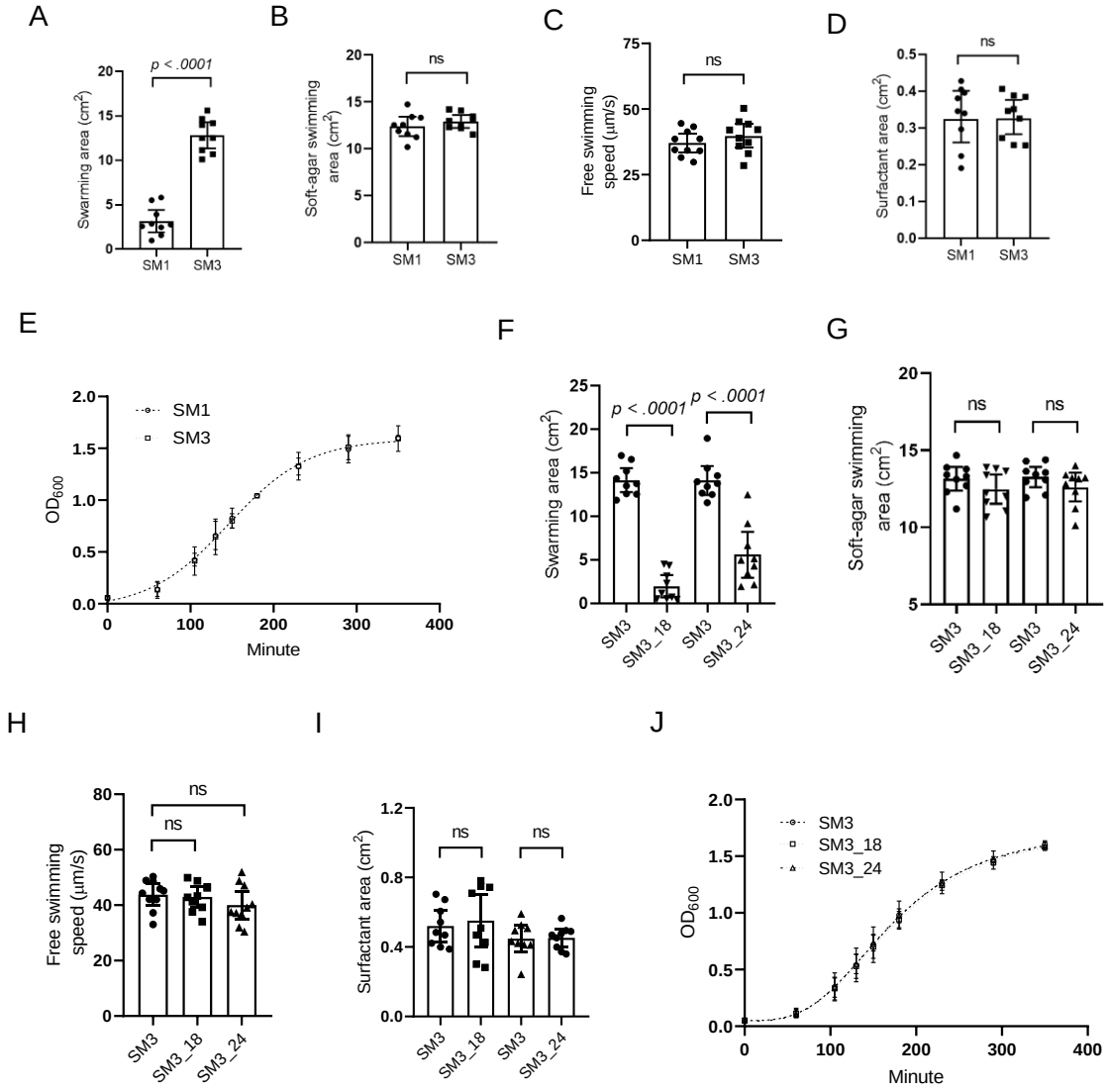

Figure B.3 | Characterization of motility, growth, and surfactant production by *Enterobacter sp*. SM1, SM3 and its mutant strains. (A-E) SM3 and SM1, swarming motility (A), soft-agar swimming motility (B), free swimming motility (C), surfactant production (D) and growth rate (E) (n = 3, each in triplicate except for E, n = 3, each in singlet). (F-J) SM3 and mutants (SM3_18 and SM3_24), swarming motility (F), soft-agar swimming motility (G), free swimming motility (H), surfactant production (I), and growth rate (J) (n = 3, each in triplicate except for J, n = 3, each in singlet). Unless otherwise noted, data are presented as mean and 95% CI, and significance tested using a two-tailed Student's t-test. H, significance tested using one-way ANOVA followed by Tukey's post hoc test.

Figure B.4

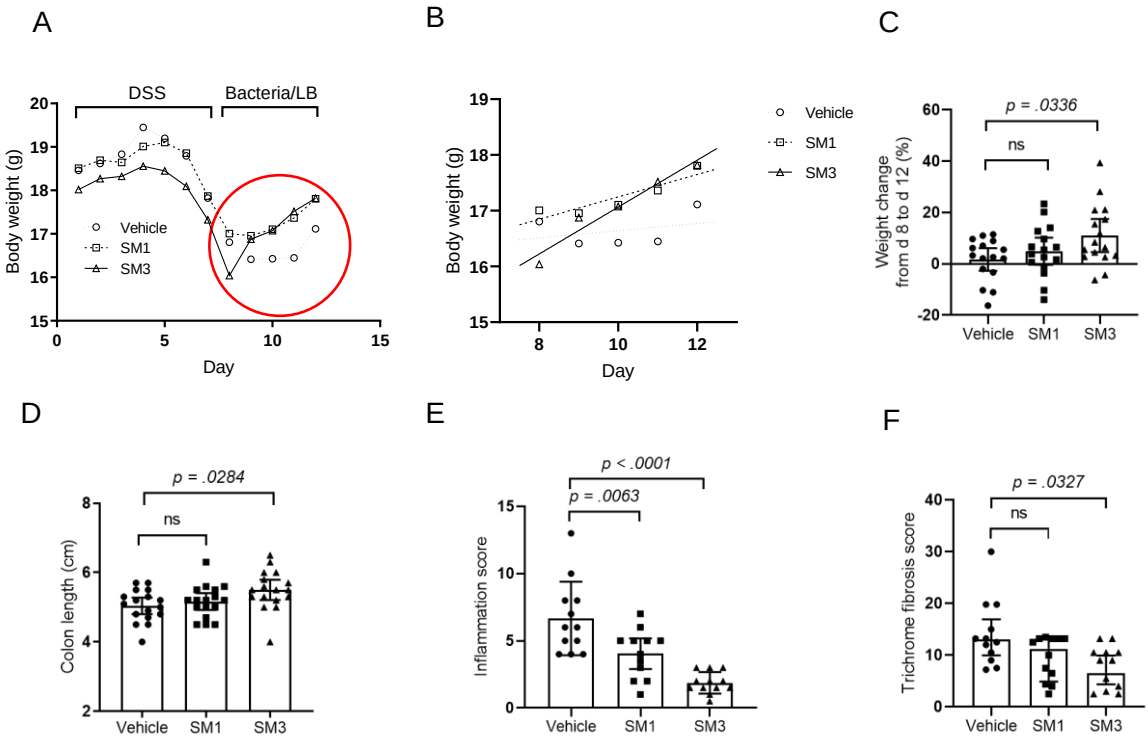

Figure B.4 | Effect of *Enterobacter sp*. SM strains on DSS induced colitis in C57BL/6 mice during recovery phase. 8-week-old mice were exposed to DSS water for 7 days. On day 8, DSS water was replaced with drinking water and mice were administered vehicle (LB), SM3 or SM1 for 5 days. [1] indicates the weight change. (A) Day by day weight change. (B) Day by day weight change from day 8 to day 12 (healing phase, red circle in (A) was separately plotted, and the best fitting line was added to each group using linear regression. The slopes for the regression lines are 0.421 (SM3), 0.201 (SM1) and 0.065 (Vehicle). The slope of SM3 group is significantly deviated from zero (P = 0.013), while the SM1 and vehicle group are not (P = 0.240, 0.754 respectively). (C) Percent weight change from day 8 to day 12. (D-F) indicates colon length (D), inflammation score (E), and trichrome fibrosis score (F) (n = 16 per treatment group except for E and F, four colon specimens per group were used for other experiments). Unless otherwise noted, data represented as mean and 95% CI, and significance tested using one-way ANOVA followed by Tukey's post hoc test. F, data represented as median and interquartile range, and significance tested using Kruskal-Wallis followed by Dunn's multiple comparisons test.

Figure B.5

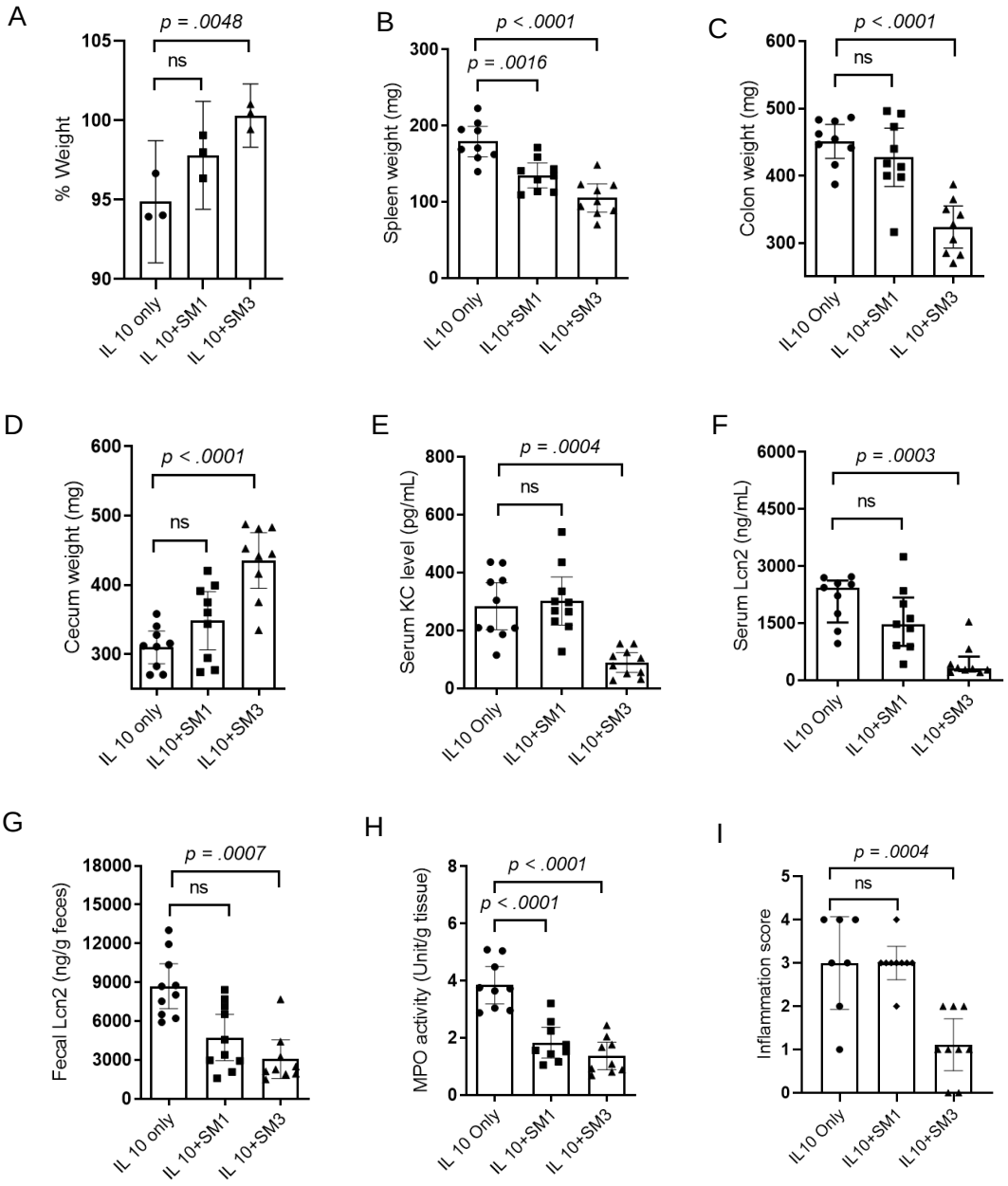

Figure B.5 | Effects of *Enterobacter sp*. SM strains on IL-10R neutralization-induced colitis in T5KO mice. 8-week-old Tlr5KO mice were administered rat anti-IL-10R monoclonal antibody (1.0 mg/mouse, i.p.) (BioXcell) at day 0 and 7. SM1 or SM3 was gavaged every 3 day from day 1 until day 18. (A) Weight percentage compared with day 0 (n = 3 per treatment group). (B) Spleen weight (n = 9 per treatment group). (C) Colon weight (n = 9 per treatment group). (D) Cecum Weight (n = 9 per treatment group). (E) Serum KC level (n = 10 per treatment group). (F) Serum lipocalin (n = 9 per treatment group). (G) Fecal lipocalin (n = 10 for each group, 1 fecal sample in SM3 group was used for other study). (H) Myeloperoxidase (MPO) (n = 9 per treatment group). (I) Inflammation score (n = 9 for each group, 2 tissue samples in IL 10 only group were used for other study). Unless otherwise noted, data are represented as mean and 95% CI, and significance tested using one-way ANOVA followed by Tukey's post hoc test. F-G, data represented as median and interquartile range, and significance tested using Kruskal-Wallis followed by Dunn's multiple comparisons test.

Figure B.6

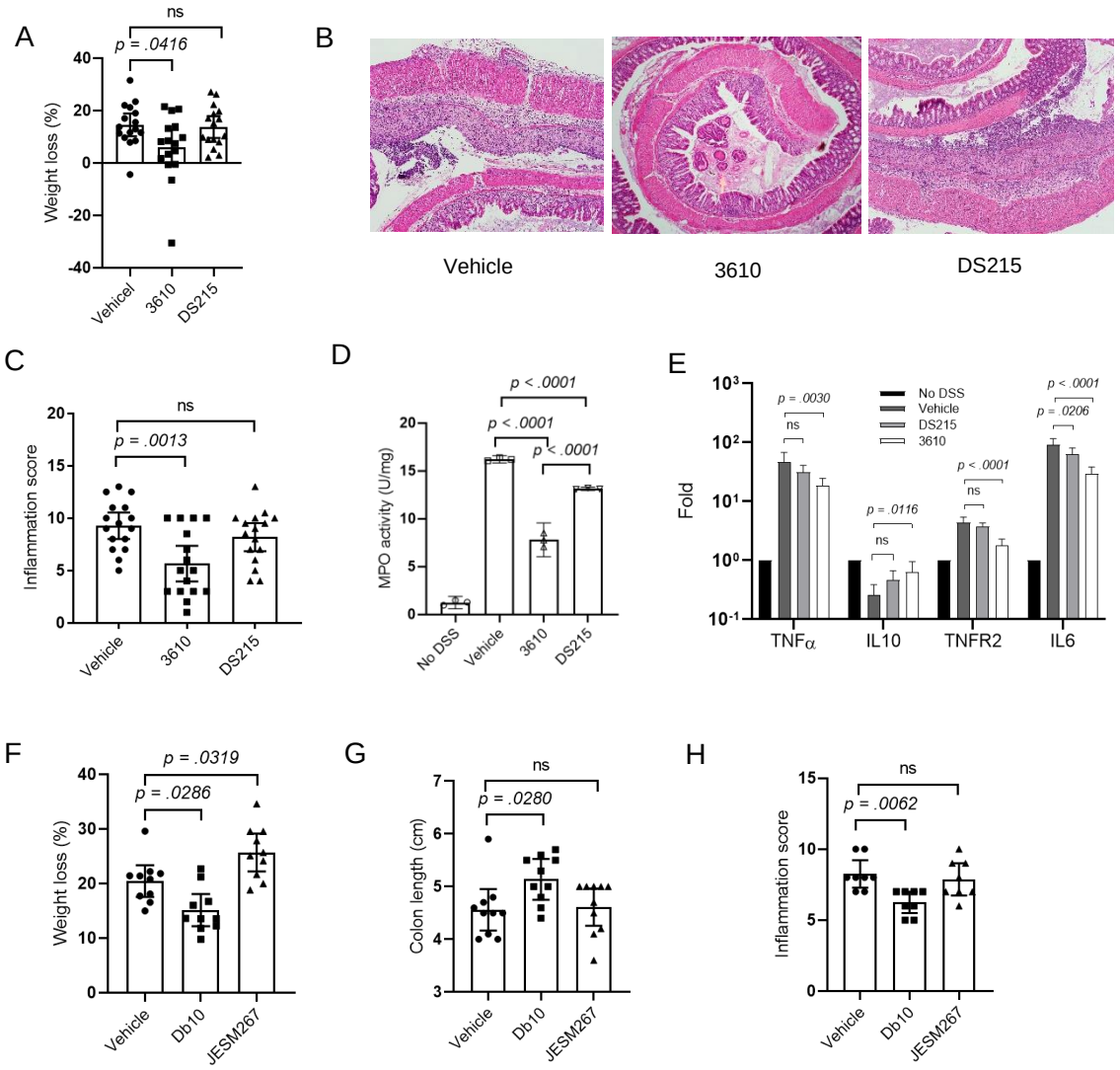

Figure B.6 | Effects of *B. subtilis* and *S. marcescens* on DSS induced colitis in C57BL/6 mice. [1] 8-week-old mice were exposed to DSS water and treated with vehicle (LB), *B. subtilis* 3610 or *B. subtilis* DS215 by oral gavage for 10 days. (A) Weight loss (n = 16 per treatment group). (B) Representative images (100x magnification) of H&E-stained colonic section treated with vehicle (left), 3610 (middle) and DS215 (right). (C) Inflammation score (n = 16 per treatment group). (D-E) In a separate experiment, myeloperoxidase (MPO) enzyme activity was determined (n = 3, each in duplicate) (D). Colon total RNA (n = 4) were isolated and reverse transcribed to cDNA. RT-qPCR data show fold induction of mRNA (TNFα, IL10, TNFR2, IL6). PCR was repeated in quadruplicate. The expression was normalized to internal control, TBP. The entire experiment was repeated n = 2 for reproducibility (E). (F-H) In a separate experiment, C57BL/6 mice (8-week-old) were exposed to DSS water and administered vehicle (LB), *S. marcescens* Db10 or *S. marcescens* JESM267 for 10 days. (F-H) indicates weight loss (F), colon length (G) and inflammation score (H) (n = 10 per treatment group except for H, for which n = 8; two colon specimens per group were used for other experiments). Unless otherwise noted, data represented as mean and 95% CI, and significance tested using one-way ANOVA followed by Tukey's post hoc test. G, data represented as median and interquartile range, and significance tested using Kruskal-Wallis followed by Dunn's multiple comparisons test.

Figure B.7

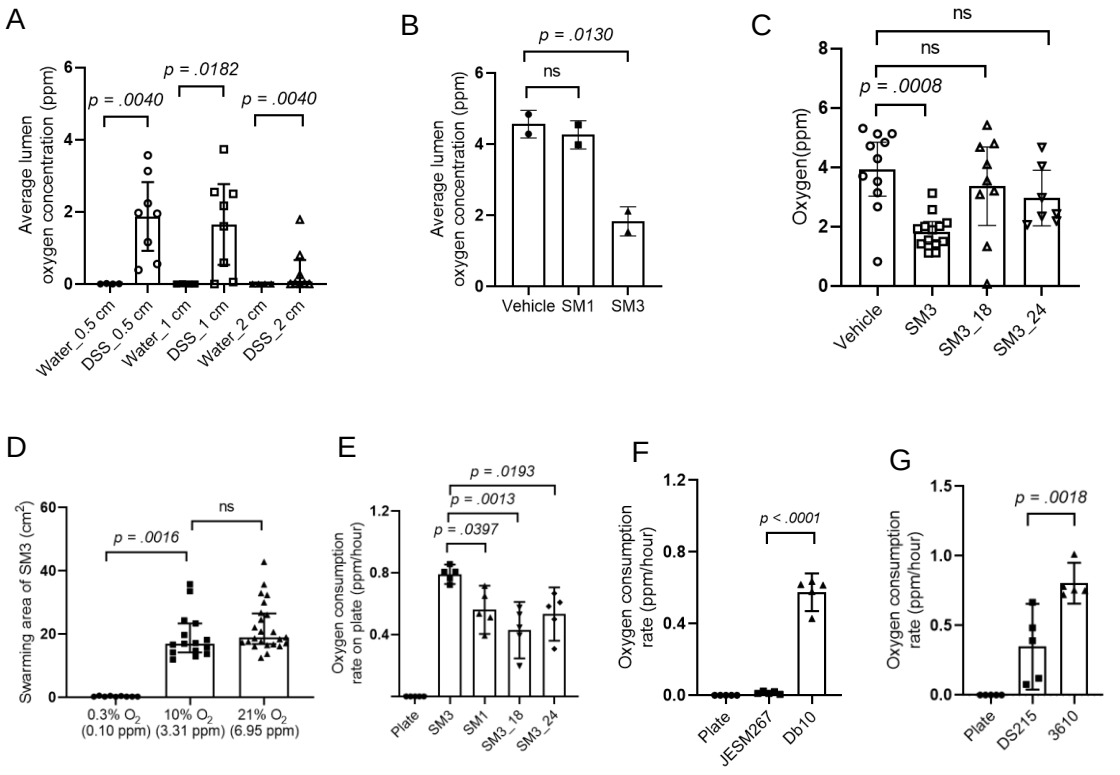

Figure B.7 | Oxygen measurements *in vivo* and *in vitro* using a microsensor probe. (A) C57BL/6 mice were exposed to water or DSS water for 10 days. Average lumen oxygen concentration (0.5, 1, and 2 cm from the anus) was measured (normal, n = 4; DSS, n = 8). (B) C57BL/6 mice were exposed to DSS water and treated with SM3 and SM1 for 10 days. Average lumen oxygen concentration was measured in a single experiment (n = 2). (C) In a separate experiment, C57BL/6 mice were exposed to DSS water and treated with SM3 or its mutants (SM3_18 or SM3_24) for 10 days. Average lumen oxygen concentration was measured (n = 3, at least 2 mice each separate experiment). (D) The swarming area of SM3 on LB agar plate in 8 hours under different concentration of oxygen (0.3%: n = 3, each in triplicate; 10%: n = 5, each in triplicate; 21%: n = 6, each in quadruplicate). [1] Oxygen consumption rate was measured for different strains: SM1, SM3, and its mutant strains (E); Db10 and JESM267 (F); 3610 and DS215 (G) on LB agar plate (n = 5, each in singlet). "Plate" indicates oxygen consumption rate in LB agar with no bacteria. Unless otherwise noted, data are presented as mean and 95% CI, and significance tested using one-way ANOVA followed by Tukey's post hoc test. A, data are presented as median and interquartile range, and significance tested using Mann Whitney test. D, data are presented as median and interquartile range, and significance tested using Kruskal-Wallis followed by Dunn's multiple comparisons test.

Figure B.8

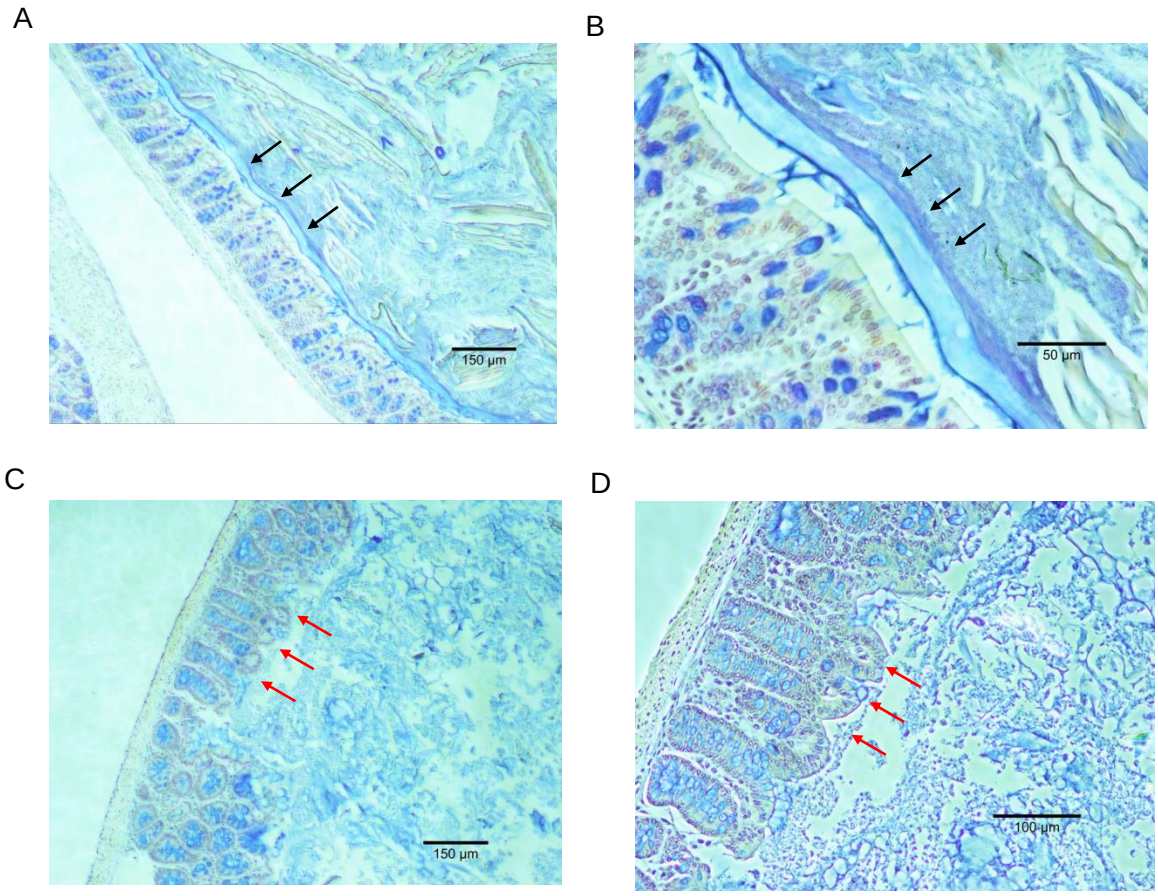

Figure B.8 | Representative images of mucin-stained mice intestinal tissue. Large intestine obtained from 8-week-old C57BL/6 mice exposed to water (A-B) or DSS water (C-D) for 10 days and stained for mucin using Alcian Blue. (A-B) Black arrows indicate the mucin layer on normal large intestine. (C-D) Red arrows indicate the loss of mucin layer on colitic tissue. A, C, 10x objectives; B, 40x objectives; D, 20x objectives.

Figure B.9

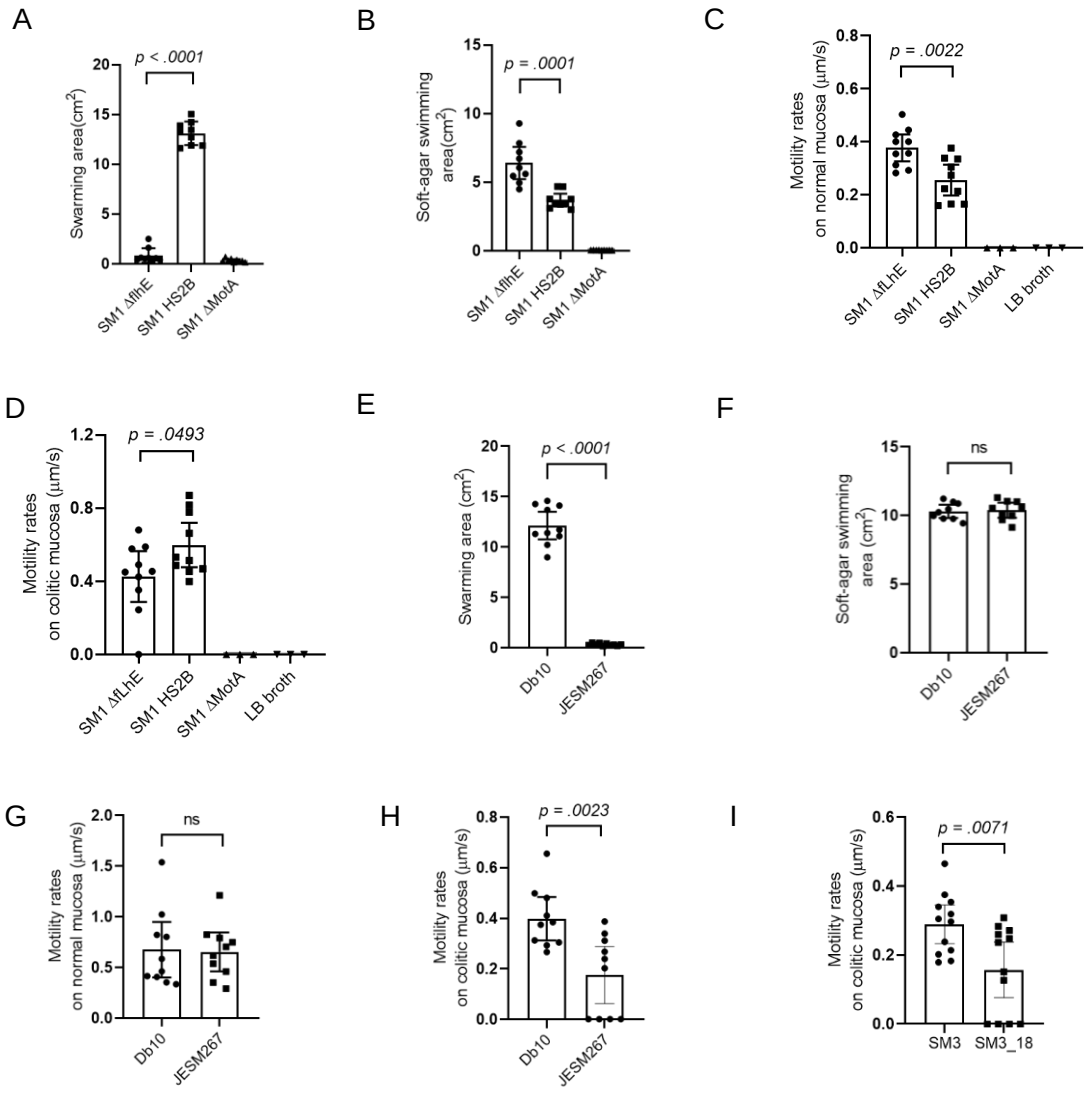

Figure B.9 | Bacterial motility rates on different media. (A-B) *ΔflhE* SM1, HS2B SM1 and Δ*motA* SM1 swarming motility (A), soft-agar swimming motility (B) (n = 3, each in triplicate). (C-D) *ΔflhE* SM1, HS2B SM1, Δ*motA* SM1 and LB (spotted as negative control), motility rates on normal (C) and colitic (D) mucosal surface of C57BL/6 mouse (n = 10, and n = 3 for Δ*motA* SM1, LB). (E-F) *S. marcescens* Db10 and *S. marcescens* JESM267, swarming motility (E), soft-agar swimming motility (F) (n = 3, each in triplicate). (G-H) *S. marcescens* Db10 and *S. marcescens* JESM267, motility rates on normal (G) and colitic (H) mucosal surface of C57BL/6 mouse (n = 4, at least in duplicate). (I) SM3 and SM3_18, motility rates on colitic mucosal surface of C57BL/6 mouse (n = 4, eachi in triplicate). Unless otherwise noted, data are represented as mean and 95% CI, and significance tested using a two-tailed Student's t-test.

Figure B.10

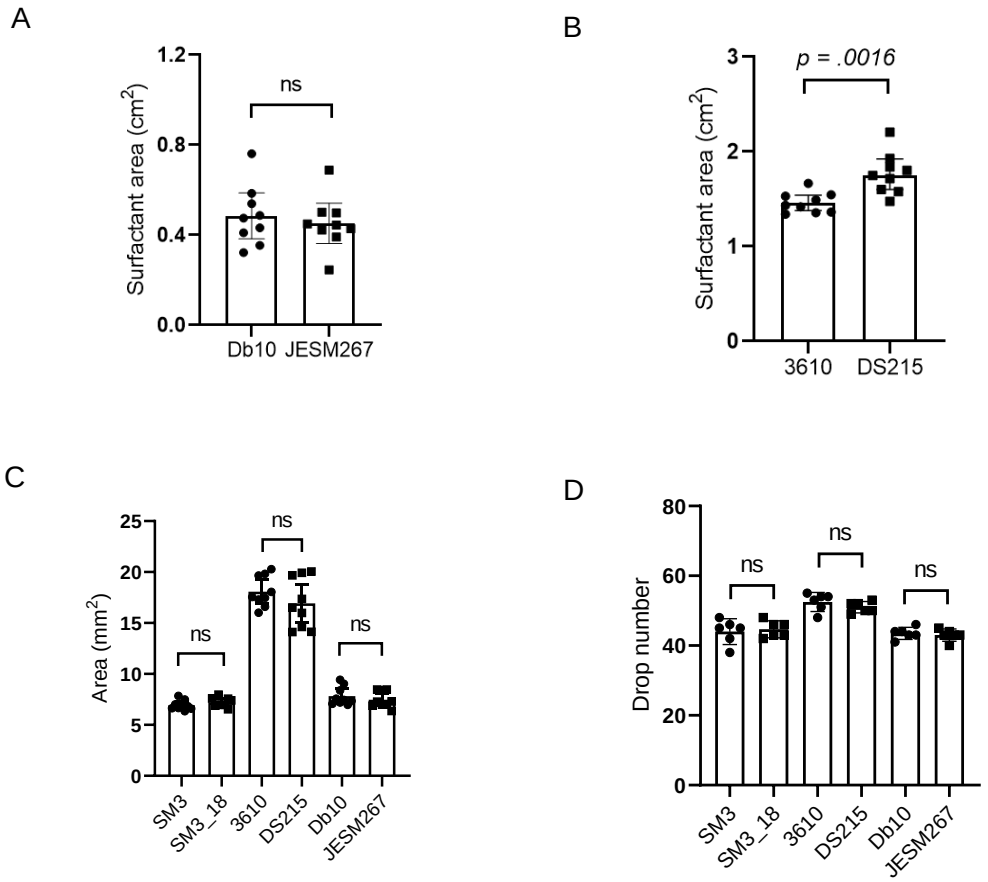

Figure B.10 | Surfactant production by swarming bacteria and their swarming deficient mutants. (A) Overnight bacterial cultures of wildtype *S. marcescens* Db10 and its non-swarmer mutant JESM267 spotted on 2.5% blood agar and incubated at 37°C (n = 3, each in triplicate) for 36-48 hours. (B) Identical method was used to estimate surfactant production by swarmer strain of *Bacillus subtilis* 3610 and its non-swarmer mutant DS215 at 37°C for 36-48 hours (n = 3, each in triplicate). (C) Cross-sectional area of bacteria supernatant droplets (5 µL) on 96-well polystyrene plate lid (n = 3, each in triplicate). (D) Drop numbers of bacteria supernatant droplets dropping from a glass Pasteur pipet to refill the volume of 1 mL (n =3, each in duplicate). Data are represented as mean and 95% CI, and significance tested using a two-tailed Student's t-test. ns, not significant; CI, Confidence Interval.

B.2 Supplementary Text on other bacteria's probiotic effect, luminal oxygen reduction, and surfactant production

B.2.1 Commensal bacterial swarmers also abrogate intestinal stress.

To generalize this concept across multiple strains, mice with DSS induced colitis were administered *Bacillus subtilis* 3610 (wildtype)[148] or its swarming deficient *swrA* isogenic mutant DS215[149] using the identical protocol as that used for SM3. In comparison with strain DS215, the wildtype significantly protected mice from intestinal inflammation (Fig. B.6A-E). Similarly, swarming *Serratia marcescens* Db10, in contrast to the swarming deficient JESM267 isogenic mutant[150], protected against inflammation in the identical mouse model (Fig. B.6F-H). Together, our results confirm that from a diverse set of genes and pathways altered in different bacterial strains, the swarming phenotype of bacteria correlates with protection against inflammation.

B.2.2 Bacterial swarmers reduce luminal oxygen concentration *in vivo*.

The enrichment of certain specific anaerobes when treated with SM3 suggested a reduction in oxygen content in the intestine; however, during inflammation, the median oxygen concentration in the lumen increases (Fig. B.7A). Similarly, fecal 16S rDNA profile of GF/SPF mice exposed to DSS and treated with SM3 also showed enrichment of anaerobic and microaerophilic taxa compared to the vehicle group. By contrast, the fecal microbiota of vehicle group was enriched in taxa that are aerobic and/or facultative anaerobic. Hence, we determined the oxygen concentrations within the intestinal lumen of mice at various lengths along the colon. In control conventional C57BL/6 mice, the colonic lumen is uniformly "hypoxic or anoxic". In colitic mice, however, we found a significant increase

in the oxygen levels (ppm) in the colonic lumen (measured at different lengths from 0.5 to 2 cm proximal to the anal verge) (Fig. B.7A). In DSS exposed mice treated with SM3, we observed a significant reduction in the luminal oxygen concentrations when compared to the mice that were treated with SM1 and the swarming deficient mutant strains (Fig. B.7B-C). SM3_18 and SM3_24 did not significantly affect oxygen concentrations compared with vehicle control (Fig. B.7C). In vitro experiments further proved that the swarming behavior of SM3 is dependent on oxygen concentration (Fig. B.7D), which in turn reduces the oxygen levels in a closed system at a significantly higher rate than the slow swarming variants (Fig. B.7E-G). Hence, we hypothesize that it is likely the act of swarming by SM3, *in vivo*, which might contribute to reducing the median oxygen concentrations in the intestinal lumen and concomitantly aid in establishing an anaerobic microenvironment. Indeed, the events leading to healing could also contribute to the reduced luminal oxygen levels.

B.2.3 Anti-inflammatory effect is likely not due to surfactant production.

Swarming bacteria secrete surfactants, such as surfactin, which reduce surface tension during motility on a solid surface[5]. Surfactin is reported to attenuate TNBS induced colitis, possibly by differentially regulating anti-inflammatory and pro-inflammatory cytokines[134]. This finding leads us to speculate that higher levels of protection exhibited by SM3 in comparison to its identical strain SM1 could likely be due to differences in surfactin levels secreted by these strains. We used an indirect blood hemolysis readout assay to test for the presence or absence of surfactin (or equivalent surfactants with surfactin-like activity). In this assay, blood agar hemolysis by SM1 and SM3 demonstrated similar zones of hemolysis. This observation suggested that the expression of surfactins

might be similar in SM1 and SM3, at least under the conditions tested. We observed similar results for *Bacillus subtilis* 3610 and its isogenic *swr*A mutant, and *S. marcescens* Db10 and its swarming deficient mutant JESM267 at 37°C (Fig. B.10A-B). In addition to the blood agar assay, drop-collapse assay[120] and drop-counting assay based on modified Stalagmometric Method[121] did not show any significant difference between the isogenic pairs of SM3, *B. subtilis* 3610 and *S. marcescens* Db10 (Fig. B.10C-D).

B.3 Supplementary Method

Clinical Study. From August 2014 through January 2018, sixty-three (63) patients were consented to participate in a colonoscopy aspirate study that was approved by the Institutional Review Board (IRB) (#2015-4465; #2009-446; #2007-554). The patients eligible for colonoscopy were enrolled sequentially after they provided study consent (#2015-4465; NCT 04089501). This study was audited by the IRB on April 24, 2019. All patients were screened and consented by a single gastroenterologist and Inflammatory Bowel Disease specialist (DL). Patients were enrolled if they had a diagnosis of inflammatory bowel disease (Crohn's disease or Ulcerative colitis) or were undergoing routine screening colonoscopy for colorectal polyps/cancer or required a colonoscopy as part of their medical management of any gastrointestinal disorder as clinically indicated. The following information was collected in the clinic and codified (numerically) by the gastroenterologist (DL). Laboratory personnel receiving the aspirate sample were blinded to the patient, diagnosis and therapy outcome. The results of the swarming assay were then associated by un-blinding the clinical diagnosis (MB, DL). The clinical data collected included age, gender, and clinical diagnoses at the time of the colonoscopy. Clinical disease activity was estimated using Harvey-Bradshaw Index for Crohn's disease (inactive < 5)

and Partial Mayo Score for Ulcerative colitis (inactive ≤ 2). There were no dietary restrictions or special instructions for patients to follow prior to colonoscopy except for routine fasting prior to the procedure. The colonoscopy preparative regimen (split dose polyethylene glycol) was used for all patients. Patients (n = 62 of 63) successfully underwent complete colonoscopy and aspirates were taken from the region or mucosa of pathology (over active inflammation, polyp) or from descending colon while exiting from a grossly "normal" colonoscopy. One patient had a truncated colonoscopy due to incomplete cleansing and no specimen was obtained in this case. Specimens were collected in sterile fecal specimen cups without any preservative (Fisher, 650 mL), kept at 4°C for at most 15 minutes prior to transport to the laboratory. The specimens were then transported at ambient temperature (~ 15 minutes) to the laboratory for processing. Ten (10) de-identified random frozen fecal samples from pre-screened healthy volunteers were also obtained from OpenBiome (Boston, MA) (www.openBiome.org). Glycerol can facilitate swarming of bacterial cells on soft agar medium. Samples from OpenBiome are stored in glycerol. In order to avoid any external determinant that can influence swarming of bacterial species in these fecal samples, we washed the fecal samples in sterile PBS and then incubated in 2 mL LB broth overnight at 37^{o}C, 200 rpm. Swarming assay was performed using these revived fecal cultures. Qualitative scoring of the swarmers in the clinical specimens was made based on the detection of bacterial spread with surfactant rim over a 72-hour incubation period. Samples showing swarming were scored as ≤ 24 hours (Score 3), 24-48 hours (Score 2) and 48-72 hours (Score 1). Samples that didn't show swarming over 72 hours of incubation were considered as "non-swarmers" (Score 0).

Swimming assays. Free swimming of bacterial cells was observed in fresh cultures that were grown in LB from an overnight culture (1:100 dilution in fresh LB) until OD_{600} ~ 0.3. At this point, cells were further diluted in PBS (1:50) and spotted on a glass slide with a cover slip placed on top of it. Swimming cells were observed under a phase contrast microscope (OMAX M837ZL, 40X) and videos captured using software (OMAX ToupView 3.7). The videos were captured at a frame rate of 18 fps for ~1 second for each trajectory and then processed in ImageJ (ver. 1.52g) to analyze swimming speeds of the test bacterium. Ten (10) straight trajectories of motion were picked randomly, and the average speed was calculated as trajectory length/time.

For soft-agar swimming assay that may be relevant to *in vivo* conditions, 2 µL of overnight culture of the test bacterium was inoculated on LB swimming plate (10 g/L tryptone, 5 g/L, 10 g/L NaCl, 3 g/L agar) and incubated at 37^{o}C, 40% RH in our indigenously made incubator. To compare swimming potential of isogenic mutants, the isogenic pairs were inoculated on the same swim agar plate equal distance from the plate middle line, and the area covered by the swimmers were measured when whichever faster swimmer reached the middle line of the plate.

Measurement of microlevels of oxygen in mouse lumen. Oxygen concentration in the mouse lumen was assessed using a profiling oxygen microsensor (PresensIMP-PSt7-02) with a flat tip that has the ability to detect in the range of 0-1400 µM oxygen with an accuracy of ± 3%. The control or DSS treated mice were first anesthetized in isoflurane for at least 3 minutes, and then the microsensor probe was inserted from the anal verge. The oxygen concentration was monitored for one minute at different locations across the colon (0.5, 1 and 2 cm from the anus) using "Presens Measurement Studio 2 (version

3.0.1.1413)". In order to avoid damage of the probe and mucosa while inserting through the anus, we used an Ethylenetetrafluoroethylene (ETFE) tube (outer diameter: 1mm; inner diameter: 0.7 mm) to house the probe. The housing was retracted to expose the probe in the designated location and cleaned before moving to the next location within the colon.

Consumption of residual oxygen on swarming plates. Swarming plates were prepared as described previously and a fine hole (3 mm × 1mm) was made on the lid of the plate to fix a syringe-based oxygen microsensor probe (Presens, NTH-PSt7-02). After inoculation of the test bacterial culture, the probe was inserted into the swarming agar medium through the hole on the lid, finely adjusted using a manual micromanipulator (Presens) and then sealed using silicon oil. The side of the Petri dish was sealed using parafilm, and this whole unit was placed in the indigenously built environmental controlled incubator at 37^0C. The oxygen consumption within the agar plate over time was monitored every 5 minutes for 20 hours using "Presens Measurement Studio 2". The average oxygen consumption rate in a sealed container was calculated by dividing the change in oxygen concentration with time at which the oxygen levels reached a plateau phase. Consistently, we have observed that during swarming activity of SM3, the plateau phase stabilizes at an oxygen concentration of 0.003 ppm. This validated that the system used in this study was properly sealed from the outside environment.

Qualitative measurement of surfactant production using 1) blood agar hemolysis. Blood agar hemolysis assay was optimized based on previously established method[119]. Briefly, 10 µL of overnight culture was inoculated on 15 mL Columbia Base agar plate supplemented with 2.5% defibrinated sheep blood. All the plates were incubated for 48h at 37ºC, unless otherwise stated. The area of the zone of hemolysis was calculated using

"Oval selection" tool in ImageJ. **2) drop-collapse assay.** Overnight bacteria culture was spun down at 4,500 rpm for 4 minutes. 5 μL of bacteria supernatant were pipetted on a polystyrene 96-well plate lid (Falcon). The droplet was placed at the center of a well and the lid was scanned [120]. Cross-sectional area of the droplet was calculated using "Free selection" tool in ImageJ. **3) drop-counting assay.** Drop-counting assay was performed with some modifications to an established method [121]**.** Overnight bacteria culture was spun down at 4,500 rpm for 4 minutes. A glass Pasteur pipet was then used to transfer the supernatant to a plastic cuvette drop by drop. Number of droplets was counted for the spent medium supernatant to reach a total volume of 1 mL.

Swarming on mucosal surface. We used colon tissue from mice that had received 3% DSS water or water for 10 days to develop a mucosal race experiment. Normal or DSS treated mice were euthanized, and the large intestines were cut open and cleaned to remove residual feces. After rinsing thoroughly twice in 35% (v/v) ethanol and PBS, the intestines were sectioned into small segments of around 1.5-2.5 cm each. A hybrid plate with sterile swimming agar (3 g/L) and hard agar (15 g/L) was prepared, where one half of the plate had 1.0% agar and the other half was filled with 0.3% agar containing LB. To make such hybrid agar plate, 1.0% agar was poured first and once solidified half of the gel was removed using a sterilized spatula to fill the rest of the Petri dish with swimming agar. The tissue pieces were placed on 1.0% agar in a way so as to have one end of the tissue precisely overlapping with the border between 1.0% agar and the swimming agar. Overnight bacterial cultures were serially diluted 10^6 times to reach cell concentration of 10^6 CFU/mL, 2 μL of which was inoculated on a 2 mm × 2 mm sterilized filter membrane (MF-Millipore, 0.45 μm). Bacterial cells adsorbed on membrane was then used as a source of

inoculum on the mucosal surface. This avoided wetting of tissue surface that may facilitate free swimming and free flowing of bacterial cells on tissue surface. The motility of a swarming deficient and its wild type was always compared using a piece of tissue that belonged to the same region of the colon in mice. The plates were dried in the laminar hood for 20-30 minutes before incubating at 37^{0}C and 40% RH overnight. Drying of plates allowed removal of excess moisture from the topmost layer of the tissue. Time-lapse photos were captured to evaluate the time at which bacterial test strain reached the other end of the intestinal tissue indicated by the swimming of bacteria on 0.3% LB agar. Distance travelled by the bacterial strain was measured in ImageJ according to the pixel/length ratio. The motility rates were calculated as distance travelled/time duration in which the test strain reached the swim agar.

APPENDIX C

PROTOCOL FOR MAKING AN ENVIRONMENTAL CONTROLLED INCUBATOR WITH TIME-LAPSE PHOTOGRAPHY

C.1 Introduction

In order to perform reproducible bacterial swarming experiment, I built an environment-controlled incubator with time-lapse photography. Inside the incubator, a digital camera was mounted on the top to take time-lapse images of the swarming activity. After the recording, images were transferred to a laptop for quantification of the swarming rate. In this appendix, I present the material needed and the procedure for making this chamber. By strictly following the procedure, one can get a homemade bacteria incubator with stable swarming results and high-quality.

At first glance, one may think swarming assay is simple: just inoculate bacteria on an agar Petri dish, then taking a picture of the plate after a period of incubation. However, it can be challenging to perform swarming assays with reproducible results and record high quality images for further analysis. Here, I listed a few technical challenges one may encounter and provide the corresponding solutions:

- A typical swarming event may take about 10 to 20 hours for the bacteria to cover a 9-cm Petri dish. Besides the full coverage time, sometimes we need to know how long the lag phase lasts, by what time branches form at the colony edge, and at the microscopic level, when cell elongation happens. Thus, the researcher needs to check at the plate regularly. Suppose one starts the assay during daytime, he/she may need to scan the plates every 30 minutes over night. Otherwise, he/she may

miss the details. In our protocol, time-lapse photography helps to capture the key frames so that the researcher does not have to stay up late or regularly check in order not to miss key events.

- Bacterial swarming is highly sensitive to the environment. Fluctuations in temperature and humidity will cause large differences in swarming rate and colony pattern. In this case, a stable humidity and temperature-controlled environment is critical for the assay. In our system, we utilized a thermo-insulated tent, a humidity control unit, and a temperature control unit to minimize the environmental fluctuation during the assay. One can readily set different humidity and temperature for swarming strain screening.
- Since agar gel contains nearly 99% water, condensation readily forms on the plate lid, which obscures photo taking. We designed the incubator in such a way that when the plates are invertedly placed on the platform, the temperature of the lid is slightly higher than that of the agar, which prevents condensation.
- Taking a clean and clear photo of swarming plates is tricky. The swarming plate has three optical surfaces: the plate lid, the agar surface and the plate bottom. When the camera flashlight or auxiliary front light is used, some light is reflected by the lid and bottom of the plate to the camera, forming unexpected light spots in the photos. In our design, LED light strip was used for illumination where the light field is well calibrated for arbitrary number of plates (1-9).

C.2 Materials

- Hydroponic Grow Tent (24" x 24" x 48", Yaheetech, model no. YT-2801)
- Digital camera (Panasonic, model no. DMC-FZ50)

- LCD Timer Remote Control (JJC, model no. TMD)
- AAA battery (2 pcs, Duracell)
- Zinc-plated slotted angle (4 pcs, 1.5’’ x 14 Gauge x 36’’, Crown Bolt)
- Zinc-plated slotted angle (10 pcs, 1.5’’ x 14 Gauge x 18’’, Crown Bolt)
- Aluminum flat bar (0.75’’ x 36’’ x 0.125’’, Everbilt)
- Black polyester cloth (20’’ x 20’’, Dazian)
- Bolts and Nuts (40 pairs, M5, Crown Bolt)
- Black acrylic sheet (2 pcs, 18’’ x 18’’ x 0.125’’, National Security Mirror)
- LED light strip (3 meters, White, GuoTonG)
- Power strip (6-outlet, Belkin)
- Heated control module (Coy Lab, serial no. DC1807)
- Fan (AC Infinity, model no. LS1225A-X)
- Digital humidity controller outlet (Inkbird, model no. IHC200S)
- Reptile humidifier (2L, Evergreen)
- Metal tray

C.3 Procedure

1. Setup the Yaheetech hydroponic tent according to the instruction manual. The manual comes with the product package. Assemble the skeleton first and then cover it with the polyester material.
2. Use M5 bolts and nuts to assemble the camera frame, as illustrated in figure C.1. Connect the Zinc-plated slotted angles first and then the aluminum bars. A rough estimation of the position of the aluminum bars is enough since they are just used to

stabilize the structure. The slotted angles have holes by the side, but the aluminum bars do not. Drill holes by the ends of the aluminum bars with hand drill or table drill.

3. Use acrylic cutter to cut the sides of acrylic sheets to fit in the sample platform.

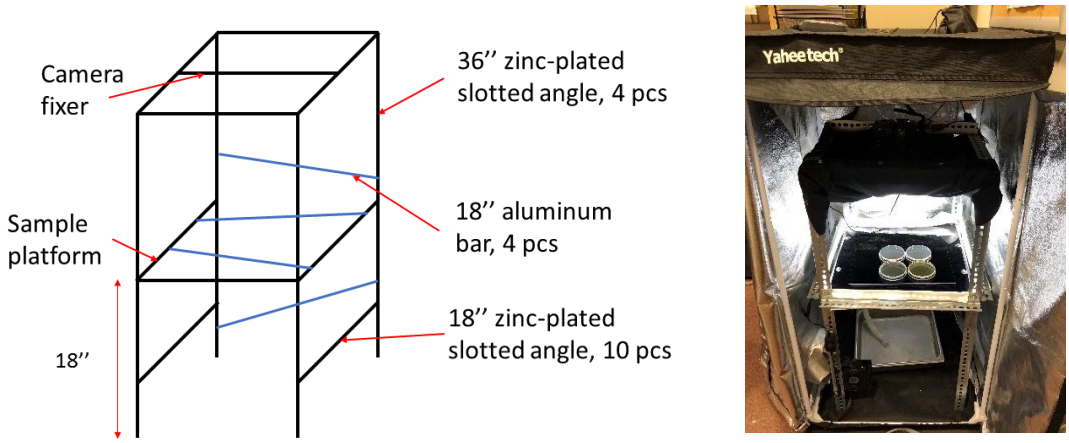

Figure C.1 | Schematics showing the structure of the camera frame. 4 pieces of 36'' zinc-plated slotted angle stand perpendicular to the ground and connected by 10 pieces of 18'' zinc-plated slotted angle using M5 bolts and nuts. The aluminum bars stabilize the whole structure with no specific position requirement. On the right is the real camera stand.

4. Drill appropriate holes on the side of the acrylic sheets to allow bolts to go through all the way down to the holes of slotted angles.

5. Fix the camera on the camera fixer with its lens facing downwards. Adjust the fixer back and forth to align the camera with the circle on the acrylic sheet.

6. Tape the LED strip around the sample platform 1 inch above the acrylic sheet on the slotted angle. The position of the light cannot be too high because we want to avoid unnecessary reflections of the light from the plates.

7. Cut two pieces of black cloth around 20'' x 20'' in size. Place one of them on the bottom of the tent as black photography background. For the other piece, cut a hole in

the center to let the camera lens go through and hang the cloth onto the camera platform to shield any reflection from the top.

8. Place the camera stand inside the tent.

9. Load batteries for the LCD timer remote control and connect it with the camera through the hole on the top of the tent. Tighten the hole using the elastic cord.

10. Put the heat control module inside the tent on the side of the bottom so that it will not show up in the swarming photos when using the light shield. Adjust the temperature setting to the desired temperature for swarming assay.

11. Set the humidifier outside the tent and connect the power cord to the humidity controller outlet. Extend the extractable plastic mist tube through the hole on the tent wall into the tent beneath the sample platform.

12. Fill the humidifier tank with water. Plug in the humidity controller to the power strip and adjust the humidity value with tolerance range according to the controller manual. For *Enterobacter sp*. SM3, set the humidity for 40% RH ± 5%RH tolerance (tol).

13. Place a tray under the mist tube to collect water droplets from the mist tube.

14. Fix the AC fan on one of the slotted angle legs facing the beaker using the bolts and nuts that come with the fan. The fan is used not only to blow the mist from the humidifier to avoid the fog showing up in the photos but also to improve ventilation and uniformity of the temperature and humidity in the chamber.

15. Tighten all the holes and seal the zip of the tent.

16. To perform swarming assays, turn on the LED light strip and place the swarm plates inverted on the acrylic sheet so that water will not condensate on the lid.
17. Check the camera preview to make sure all the plates are within the range of the screen. Adjust the position of the plates if necessary.
18. Set the frame rate and frame number of the LCD camera timer control according to the manual. In the case of SM3, we set the frame number to 50 and time interval between frames as 15 min. Press “start” button to start time-lapse photo shooting.
19. The swarming assay may take about 10 h. You can leave the camera on for overnight and collect the images the next morning. During the photo taking process, DO NOT shake the incubator.
20. Make sure there is enough water in the humidifier water tank. If you want to check the condition inside the chamber, you may gently open the window on the top of tent to see the camera screen without disturbing the photographing.
21. Stop the timer controller when the swarming is finished and download the images.
22. Images can be analyzed using software such as ImageJ or MATLAB.

REFERENCES

1. Crespo-Sanjuán, J., et al., *Early detection of high oxidative activity in patients with adenomatous intestinal polyps and colorectal adenocarcinoma: myeloperoxidase and oxidized low-density lipoprotein in serum as new markers of oxidative stress in colorectal cancer.* Lab Med., 2015. **46**(2): p. 123-35.
2. Osaka, T., et al., *Meta-Analysis of Fecal Microbiota and Metabolites in Experimental Colitic Mice during the Inflammatory and Healing Phases.* Nutrients, 2017. **9**(12).
3. Henrichsen, J., *Bacterial surface translocation: a survey and a classification.* Bacteriol Rev, 1972. **36**(4): p. 478-503.
4. Sun, E., S.J. Liu, and R.E.W. Hancock, *Surfing Motility: a Conserved yet Diverse Adaptation among Motile Bacteria.* Journal of Bacteriology, 2018. **200**(23).
5. Kearns, D.B., *A field guide to bacterial swarming motility.* Nature Reviews Microbiology, 2010. **8**(9): p. 634-644.
6. Saintillan, D., *Rheology of Active Fluids.* Annual Review of Fluid Mechanics, Vol 50, 2018. **50**: p. 563-592.
7. Purcell, E.M., *Life at low Reynolds number.* American Journal of Physics, 1977. **45**: p. 3.
8. Howard C. Berg, D.A.B., *Chemotaxis in Escherichia coli analysed by Three-dimendional Tracking.* Nature, 1972. **239**.
9. Luchsinger, R.H., B. Bergersen, and J.G. Mitchell, *Bacterial swimming strategies and turbulence.* Biophysical Journal, 1999. **77**(5): p. 2377-2386.
10. Stecher, B., et al., *Flagella and chemotaxis are required for efficient induction of Salmonella enterica serovar Typhimurium colitis in streptomycin-pretreated mice.* Infect Immun, 2004. **72**(7): p. 4138-50.
11. Stecher, B., et al., *Motility allows S. Typhimurium to benefit from the mucosal defence.* Cell Microbiol, 2008. **10**(5): p. 1166-80.
12. Wiles, T.J., et al., *Swimming motility of a gut bacterial symbiont promotes resistance to intestinal expulsion and enhances inflammation.* PLoS Biol, 2020. **18**(3): p. e3000661.
13. Chelvam, K.K., L.C. Chai, and K.L. Thong, *Variations in motility and biofilm formation of Salmonella enterica serovar Typhi.* Gut Pathogens, 2014. **6**.
14. Ayres, J.S., N.J. Trinidad, and R.E. Vance, *Lethal inflammasome activation by a multidrug-resistant pathobiont upon antibiotic disruption of the microbiota.* Nat Med, 2012. **18**(5): p. 799-806.
15. Rui, H., et al., *Reactogenicity of live-attenuated Vibrio cholerae vaccines is dependent on flagellins.* Proc Natl Acad Sci U S A, 2010. **107**(9): p. 4359-64.
16. Zeng, H., et al., *Flagellin is the major proinflammatory determinant of enteropathogenic Salmonella.* J Immunol, 2003. **171**(7): p. 3668-74.
17. Fulde, M., et al., *Neonatal selection by Toll-like receptor 5 influences long-term gut microbiota composition.* Nature, 2018. **560**(7719): p. 489-493.
18. Okumura, R., et al., *Lypd8 promotes the segregation of flagellated microbiota and colonic epithelia.* Nature, 2016. **532**(7597): p. 117-21.
19. O'Loan, O.J. and M.R. Evans, *Alternating steady state in one-dimensional flocking.* Journal of Physics a-Mathematical and General, 1999. **32**(8): p. L99-L105.
20. Partridge, J.D. and R.M. Harshey, *Swarming: Flexible Roaming Plans.* Journal of Bacteriology, 2013. **195**(5): p. 909-918.
21. Desai, J.D. and I.M. Banat, *Microbial production of surfactants and their commercial potential.* Microbiol Mol Biol Rev, 1997. **61**(1): p. 47-64.

22. Verstraeten, N., et al., *Living on a surface: swarming and biofilm formation.* Trends in Microbiology, 2008. **16**(10): p. 496-506.
23. Mattick, J.S., *Type IV pili and twitching motility.* Annual Review of Microbiology, 2002. **56**: p. 289-314.
24. Mignot, T., *The elusive engine in Myxococcus xanthus gliding motility.* Cell Mol Life Sci, 2007. **64**(21): p. 2733-45.
25. Yeung, A.T.Y., A. Parayno, and R.E.W. Hancock, *Mucin Promotes Rapid Surface Motility in Pseudomonas aeruginosa.* Mbio, 2012. **3**(3).
26. Bhattacharjee, T. and S.S. Datta, *Bacterial hopping and trapping in porous media.* Nature Communications, 2019. **10**.
27. Kuhn, M.J., et al., *Bacteria exploit a polymorphic instability of the flagellar filament to escape from traps.* Proceedings of the National Academy of Sciences of the United States of America, 2017. **114**(24): p. 6340-6345.
28. Dell'Arciprete, D., et al., *A growing bacterial colony in two dimensions as an active nematic.* Nature Communications, 2018. **9**.
29. Be'er, A. and G. Ariel, *A statistical physics view of swarming bacteria.* Movement Ecology, 2019. **7**.
30. Patteson, A.E., A. Gopinath, and P.E. Arratia, *The propagation of active-passive interfaces in bacterial swarms.* Nature Communications, 2018. **9**.
31. Be'er, A. and R.M. Harshey, *Collective Motion of Surfactant-Producing Bacteria Imparts Superdiffusivity to Their Upper Surface.* Biophysical Journal, 2011. **101**(5): p. 1017-1024.
32. Partridge, J.D., et al., *Tumble Suppression Is a Conserved Feature of Swarming Motility.* mBio, 2020. **11**(3).
33. Ariel, G., et al., *Swarming bacteria migrate by Levy Walk.* Nature Communications, 2015. **6**.
34. Jones, B.V., et al., *Ultrastructure of Proteus mirabilis swarmer cell rafts and role of swarming in catheter-associated urinary tract infection.* Infect Immun, 2004. **72**(7): p. 3941-50.
35. Sokolov, A., et al., *Concentration dependence of the collective dynamics of swimming bacteria.* Physical Review Letters, 2007. **98**(15).
36. Ilkanaiv, B., et al., *Effect of Cell Aspect Ratio on Swarming Bacteria.* Phys Rev Lett, 2017. **118**(15): p. 158002.
37. Andersen, J.B., et al., *Surface motility in Pseudomonas sp. DSS73 is required for efficient biological containment of the root-pathogenic microfungi Rhizoctonia solani and Pythium ultimum.* Microbiology (Reading), 2003. **149**(Pt 1): p. 37-46.
38. Arino, S., R. Marchal, and J.P. Vandecasteele, *Involvement of a rhamnolipid-producing strain of Pseudomonas aeruginosa in the degradation of polycyclic aromatic hydrocarbons by a bacterial community.* J Appl Microbiol, 1998. **84**(5): p. 769-76.
39. Zhang, Y. and R.M. Miller, *Enhanced octadecane dispersion and biodegradation by a Pseudomonas rhamnolipid surfactant (biosurfactant).* Appl Environ Microbiol, 1992. **58**(10): p. 3276-82.
40. Zhang, Y. and R.M. Miller, *Effect of a Pseudomonas rhamnolipid biosurfactant on cell hydrophobicity and biodegradation of octadecane.* Appl Environ Microbiol, 1994. **60**(6): p. 2101-6.
41. Gavin, R., et al., *Lateral flagella of Aeromonas species are essential for epithelial cell adherence and biofilm formation.* Mol Microbiol, 2002. **43**(2): p. 383-97.
42. Callegan, M.C., et al., *Role of swarming migration in the pathogenesis of bacillus endophthalmitis.* Invest Ophthalmol Vis Sci, 2006. **47**(10): p. 4461-7.

43. Allison, C., H.C. Lai, and C. Hughes, *Co-ordinate expression of virulence genes during swarm-cell differentiation and population migration of Proteus mirabilis.* Mol Microbiol, 1992. **6**(12): p. 1583-91.
44. Ammendola, A., et al., *Serratia liquefaciens swarm cells exhibit enhanced resistance to predation by Tetrahymena sp.* FEMS Microbiol Lett, 1998. **164**(1): p. 69-75.
45. Givskov, M., et al., *Induction of phospholipase- and flagellar synthesis in Serratia liquefaciens is controlled by expression of the flagellar master operon flhD.* Mol Microbiol, 1995. **15**(3): p. 445-54.
46. Kim, W., et al., *Swarm-cell differentiation in Salmonella enterica serovar typhimurium results in elevated resistance to multiple antibiotics.* J Bacteriol, 2003. **185**(10): p. 3111-7.
47. Lai, S., J. Tremblay, and E. Deziel, *Swarming motility: a multicellular behaviour conferring antimicrobial resistance.* Environ Microbiol, 2009. **11**(1): p. 126-36.
48. Overhage, J., et al., *Swarming of Pseudomonas aeruginosa is a complex adaptation leading to increased production of virulence factors and antibiotic resistance.* Journal of Bacteriology, 2008. **190**(8): p. 2671-2679.
49. Butler, M.T., Q. Wang, and R.M. Harshey, *Cell density and mobility protect swarming bacteria against antibiotics.* Proc Natl Acad Sci U S A, 2010. **107**(8): p. 3776-81.
50. Lane, M.C., et al., *Expression of flagella is coincident with uropathogenic Escherichia coli ascension to the upper urinary tract.* Proc Natl Acad Sci U S A, 2007. **104**(42): p. 16669-74.
51. Overhage, J., et al., *Swarming of Pseudomonas aeruginosa is a complex adaptation leading to increased production of virulence factors and antibiotic resistance.* J Bacteriol, 2008. **190**(8): p. 2671-9.
52. Talley, N., *Clinical examination: a systematic guide to physical diagnosis.* 2018: Elsevier Australia. 227.
53. CDC. *Inflammatory bowel disease (IBD)*. 2018 03/22/2018; Available from: https://www.cdc.gov/ibd/what-is-IBD.htm#1.
54. Rashvand, S., et al., *Dietary patterns and risk of ulcerative colitis: a case-control study.* J Hum Nutr Diet, 2018. **31**(3): p. 408-412.
55. Andersen, V., et al., *Diet and risk of inflammatory bowel disease.* Dig Liver Dis, 2012. **44**(3): p. 185-94.
56. Mukhopadhya, I., et al., *IBD-what role do Proteobacteria play?* Nat Rev Gastroenterol Hepatol, 2012. **9**(4): p. 219-30.
57. Aroniadis, O.C. and L.J. Brandt, *Fecal microbiota transplantation: past, present and future.* Curr Opin Gastroenterol, 2013. **29**(1): p. 79-84.
58. Russell, R.K. and J. Satsangi, *Does IBD Run in Families?* Inflammatory Bowel Diseases, 2008. **14**: p. S20-S21.
59. Noble, C.L. and I.D.R. Arnott, *What Is the Risk That a Child Will Develop Inflammatory Bowel Disease if 1 or Both Parents Have IBD?* Inflammatory Bowel Diseases, 2008. **14**: p. S22-S23.
60. Siegel, C.A., et al., *Risk of Lymphoma Associated With Combination Anti-Tumor Necrosis Factor and Immunomodulator Therapy for the Treatment of Crohn's Disease: A Meta-Analysis.* Clinical Gastroenterology and Hepatology, 2009. **7**(8): p. 874-881.
61. Nguyen, G.C. and J. Sam, *Rising Prevalence of Venous Thromboembolism and Its Impact on Mortality Among Hospitalized Inflammatory Bowel Disease Patients.* American Journal of Gastroenterology, 2008. **103**(9): p. 2272-2280.
62. Barbeau, J., *Mouse Models of Inflammatory Bowel Disease*, in *CrownBio*. 2019.

63. Pizarro, T.T., et al., *SAMP1/YitFc mouse strain: a spontaneous model of Crohn's disease-like ileitis.* Inflamm Bowel Dis, 2011. **17**(12): p. 2566-84.
64. Kuhn, R., et al., *Interleukin-10-Deficient Mice Develop Chronic Enterocolitis.* Cell, 1993. **75**(2): p. 263-274.
65. Okayasu, I., et al., *A Novel Method in the Induction of Reliable Experimental Acute and Chronic Ulcerative-Colitis in Mice.* Gastroenterology, 1990. **98**(3): p. 694-702.
66. Cooper, H.S., et al., *Clinicopathological Study of Dextran Sulfate Sodium Experimental Murine Colitis.* Laboratory Investigation, 1993. **69**(2): p. 238-249.
67. Webre, D.J., P.M. Wolanin, and J.B. Stock, *Bacterial chemotaxis.* Current Biology, 2003. **13**(2): p. R47-R49.
68. Josenhans, C. and S. Suerbaum, *The role of motility as a virulence factor in bacteria.* International Journal of Medical Microbiology, 2002. **291**(8): p. 605-614.
69. Darnton, N.C., et al., *Dynamics of Bacterial Swarming.* Biophysical Journal, 2010. **98**(10): p. 2082-2090.
70. Morgenstein, R.M., B. Szostek, and P.N. Rather, *Regulation of gene expression during swarmer cell differentiation in Proteus mirabilis.* Fems Microbiology Reviews, 2010. **34**(5): p. 753-763.
71. Michaels, B. and L.S. Tisa, *Swarming motility by Photorhabdus temperata is influenced by environmental conditions and uses the same flagella as that used in swimming motility.* Canadian Journal of Microbiology, 2011. **57**(3): p. 196-203.
72. Hall, A.N., et al., *SwrD (YlzI) Promotes Swarming in Bacillus subtilis by Increasing Power to Flagellar Motors.* Journal of Bacteriology, 2018. **200**(2).
73. Partridge, J.D., et al., *Escherichia coli Remodels the Chemotaxis Pathway for Swarming.* Mbio, 2019. **10**(2).
74. Chen, W., et al. *Bacterial Swarmers exhibit a Protective Response to Intestinal Stress*. 2020; Available from: https://www.biorxiv.org/content/10.1101/759886v3.
75. Wioland, H., E. Lushi, and R.E. Goldstein, *Directed collective motion of bacteria under channel confinement.* New Journal of Physics, 2016. **18**.
76. Wioland, H., et al., *Ferromagnetic and antiferromagnetic order in bacterial vortex lattices.* Nature Physics, 2016. **12**(4): p. 341-U177.
77. Theillard, M., R. Alonso-Matilla, and D. Saintillan, *Geometric control of active collective motion.* Soft Matter, 2017. **13**(2): p. 363-375.
78. Wioland, H., et al., *Confinement Stabilizes a Bacterial Suspension into a Spiral Vortex.* Physical Review Letters, 2013. **110**(26).
79. Lushi, E., H. Wioland, and R.E. Goldstein, *Fluid flows created by swimming bacteria drive self-organization in confined suspensions.* Proceedings of the National Academy of Sciences of the United States of America, 2014. **111**(27): p. 9733-9738.
80. Beppu, K., et al., *Geometry-driven collective ordering of bacterial vortices.* Soft Matter, 2017. **13**(29): p. 5038-5043.
81. Nishiguchi, D., et al., *Publisher Correction: Engineering bacterial vortex lattice via direct laser lithography.* Nat Commun, 2018. **9**(1): p. 4932.
82. Araujo, G., et al., *Orbiting of Flagellated Bacteria within a Thin Fluid Film around Micrometer-Sized Particles.* Biophysical Journal, 2019. **117**(2): p. 346-354.
83. Doostmohammadi, A., et al., *Stabilization of active matter by flow-vortex lattices and defect ordering.* Nature Communications, 2016. **7**.
84. Hamby, A.E., et al., *Swimming bacteria power microspin cycles.* Science Advances, 2018. **4**(12).

85. Grossmann, R., et al., *Pattern formation in active particle systems due to competing alignment interactions.* European Physical Journal-Special Topics, 2015. **224**(7): p. 1325-1347.
86. Grossmann, R., et al., *Vortex Arrays and Mesoscale Turbulence of Self-Propelled Particles.* Physical Review Letters, 2014. **113**(25).
87. Darnton, N., et al., *Moving fluid with bacterial carpets.* Biophysical Journal, 2004. **86**(3): p. 1863-1870.
88. Ester, M.K., H. Sander, J. Xu, X. *A Density-Based Algorithm for Discovering Clusters in Large Spatial Database with Noise*. in *Proceedings of the Second International Conference on Knowledge Discovery and Data Mining*. 1996. AAAI Press.
89. Turner, L., et al., *Visualization of Flagella during Bacterial Swarming.* Journal of Bacteriology, 2010. **192**(13): p. 3259-3267.
90. DiLuzio, W.R., et al., *Escherichia coli swim on the right-hand side.* Nature, 2005. **435**(7046): p. 1271-4.
91. Tsang, A.C.H. and E. Kanso, *Circularly confined microswimmers exhibit multiple global patterns.* Physical Review E, 2015. **91**(4).
92. Li, Y., et al., *Noncontact Cohesive Swimming of Bacteria in Two-Dimensional Liquid Films.* Physical Review Letters, 2017. **119**(1).
93. Armitage, J.P., D.G. Smith, and R.J. Rowbury, *Alternation in the cell envolope composition of Proteus Mirabilis during the development of swarmer cells. Biochimica et Biophisica Acta*, 1979. **584**(1979): p. 389-397.
94. Tremblay, J. and E. Deziel, *Gene expression in Pseudomonas aeruginosa swarming motility.* Bmc Genomics, 2010. **11**.
95. Wang, Q.F., et al., *Gene expression patterns during swarming in Salmonella typhimurium: genes specific to surface growth and putative new motility and pathogenicity genes.* Molecular Microbiology, 2004. **52**(1): p. 169-187.
96. Daniels, R., J. Vanderleyden, and J. Michiels, *Quorum sensing and swarming migration in bacteria.* Fems Microbiology Reviews, 2004. **28**(3): p. 261-289.
97. Arikawa, K. and Y. Nishikawa, *Interleukin-8 induction due to diffusely adherent Escherichia coli possessing Afa/Dr genes depends on flagella and epithelial Toll-like receptor 5.* Microbiol Immunol, 2010. **54**(9): p. 491-501.
98. Stanton, T.B. and D.C. Savage, *Motility as a factor in bowel colonization by Roseburia cecicola, an obligately anaerobic bacterium from the mouse caecum.* J Gen Microbiol, 1984. **130**(1): p. 173-83.
99. Rooks, M.G., et al., *Gut microbiome composition and function in experimental colitis during active disease and treatment-induced remission.* ISME J, 2014. **8**(7): p. 1403-17.
100. Erben, U., et al., *A guide to histomorphological evaluation of intestinal inflammation in mouse models.* Int J Clin Exp Pathol, 2014. **7**(8): p. 4557-76.
101. Tran, H.Q., et al., *Flagellin-elicited adaptive immunity suppresses flagellated microbiota and vaccinates against chronic inflammatory diseases.* Nat Commun, 2019. **10**(1): p. 5650.
102. Okada, T., et al., *IL-8 and LYPD8 expression levels are associated with the inflammatory response in the colon of patients with ulcerative colitis.* Biomed Rep, 2020. **12**(4): p. 193-198.
103. Chassaing, B., et al., *Dextran sulfate sodium (DSS)-induced colitis in mice.* Curr Protoc Immunol, 2014. **104**: p. Unit 15 25.
104. Cullender, T.C., et al., *Innate and adaptive immunity interact to quench microbiome flagellar motility in the gut.* Cell Host Microbe, 2013. **14**(5): p. 571-81.

105. Chassaing, B., R.E. Ley, and A.T. Gewirtz, *Intestinal epithelial cell toll-like receptor 5 regulates the intestinal microbiota to prevent low-grade inflammation and metabolic syndrome in mice.* Gastroenterology, 2014. **147**(6): p. 1363-77 e17.
106. Hsu, C.C., R. Okumura, and K. Takeda, *Human LYPD8 protein inhibits motility of flagellated bacteria.* Inflamm Regen, 2017. **37**: p. 23.
107. Barak, J.D., et al., *Previously uncharacterized Salmonella enterica genes required for swarming play a role in seedling colonization.* Microbiology, 2009. **155**(Pt 11): p. 3701-9.
108. Finkelshtein, A., et al., *Bacterial Swarms Recruit Cargo Bacteria To Pave the Way in Toxic Environments.* mBio, 2015. **6**(3).
109. Allison, C., et al., *The role of swarm cell differentiation and multicellular migration in the uropathogenicity of Proteus mirabilis.* J Infect Dis, 1994. **169**(5): p. 1155-8.
110. Yang, Y. and C. Jobin, *Microbial imbalance and intestinal pathologies: connections and contributions.* Dis Model Mech, 2014. **7**(10): p. 1131-42.
111. Morales-Soto, N., et al., *Preparation, imaging, and quantification of bacterial surface motility assays.* J Vis Exp, 2015(98).
112. Jass, J.R., *Hyperplastic-like polyps as precursors of microsatellite-unstable colorectal cancer.* Am J Clin Pathol., 2003. **119**(6): p. 773-5.
113. Perse, M. and A. Cerar, *Dextran sodium sulphate colitis mouse model: traps and tricks.* J Biomed Biotechnol, 2012. **2012**: p. 718617.
114. Suzuki, K., et al., *Pivotal Role of Carbohydrate Sulfotransferase 15 in Fibrosis and Mucosal Healing in Mouse Colitis.* PLoS One, 2016. **11**(7): p. e0158967.
115. Volk, J.K., et al., *The Nlrp6 inflammasome is not required for baseline colonic inner mucus layer formation or function.* J Exp Med, 2019. **216**(11): p. 2602-2618.
116. Lagkouvardos, I., et al., *Sequence and cultivation study of Muribaculaceae reveals novel species, host preference, and functional potential of this yet undescribed family.* Microbiome, 2019. **7**(1): p. 28.
117. Sasaki, Y., et al., *Endoscopic quantification of mucosal surface roughness for grading severity of ulcerative colitis.* Digestive Endoscopy, 2008. **20**(2): p. 67-72.
118. Kearns, D.B. and R. Losick, *Cell population heterogeneity during growth of Bacillus subtilis.* Genes Dev, 2005. **19**(24): p. 3083-94.
119. Walter, V., C. Syldatk, and R. Hausmann, *Screening Concepts for the Isolation of Biosurfactant Producing Microorganisms.* Biosurfactants, 2010. **672**: p. 1-13.
120. Bodour, A.A. and R.M. Miller-Maier, *Application of a modified drop-collapse technique for surfactant quantitation and screening of biosurfactant-producing microorganisms.* Journal of Microbiological Methods, 1998. **32**(3): p. 273-280.
121. Dilmohamud, B.A., et al., *Surface tension and related thermodynamic parameters of alcohols using the Traube stalagmometer.* European Journal of Physics, 2005. **26**(6): p. 1079-1084.
122. Venkatesh, M., et al., *Symbiotic bacterial metabolites regulate gastrointestinal barrier function via the xenobiotic sensor PXR and Toll-like receptor 4.* Immunity, 2014. **41**(2): p. 296-310.
123. McCafferty, J., et al., *Stochastic changes over time and not founder effects drive cage effects in microbial community assembly in a mouse model.* ISME J, 2013. **7**(11): p. 2116-25.
124. Datta, S., N. Costantino, and D.L. Court, *A set of recombineering plasmids for gram-negative bacteria.* Gene, 2006. **379**: p. 109-15.
125. Lau, P.C., et al., *PCR ligation mutagenesis in transformable streptococci: application and efficiency.* J Microbiol Methods, 2002. **49**(2): p. 193-205.

126. Wiles, T.J., et al., *Combining quantitative genetic footprinting and trait enrichment analysis to identify fitness determinants of a bacterial pathogen.* PLoS Genet, 2013. **9**(8): p. e1003716.
127. Singh, V., et al., *Proneness of TLR5 deficient mice to develop colitis is microbiota dependent.* Gut Microbes, 2015. **6**(4): p. 279-83.
128. Walters, W., et al., *Improved Bacterial 16S rRNA Gene (V4 and V4-5) and Fungal Internal Transcribed Spacer Marker Gene Primers for Microbial Community Surveys.* mSystems, 2015. **1**(1).
129. Edgar, R.C., *Search and clustering orders of magnitude faster than BLAST.* Bioinformatics, 2010. **26**(19): p. 2460-1.
130. Caporaso, J.G., et al., *QIIME allows analysis of high-throughput community sequencing data.* Nat Methods, 2010. **7**(5): p. 335-6.
131. Caporaso, J.G., et al., *Global patterns of 16S rRNA diversity at a depth of millions of sequences per sample.* Proc Natl Acad Sci U S A, 2011. **108 Suppl 1**: p. 4516-22.
132. Edgar, R.C., *UPARSE: highly accurate OTU sequences from microbial amplicon reads.* Nat Methods, 2013. **10**(10): p. 996-8.
133. DeSantis, T.Z., et al., *Greengenes, a chimera-checked 16S rRNA gene database and workbench compatible with ARB.* Appl Environ Microbiol, 2006. **72**(7): p. 5069-72.
134. Selvam, R., et al., *Effect of Bacillus subtilis PB6, a natural probiotic on colon mucosal inflammation and plasma cytokines levels in inflammatory bowel disease.* Indian J Biochem Biophys, 2009. **46**(1): p. 79-85.
135. Colgan, S.P. and C.T. Taylor, *Hypoxia: an alarm signal during intestinal inflammation.* Nat Rev Gastroenterol Hepatol, 2010. **7**(5): p. 281-7.
136. Jeckel, H., et al., *Learning the space-time phase diagram of bacterial swarm expansion.* Proceedings of the National Academy of Sciences of the United States of America, 2019. **116**(5): p. 1489-1494.
137. Costanzo, A., et al., *Transport of self-propelling bacteria in micro-channel flow.* Journal of Physics: Condensed Matter, 2012. **24**(6): p. 065101.
138. Saintillan, D. and M.J. Shelley, *Orientational order and instabilities in suspensions of self-locomoting rods.* Physical review letters 2007. **99**(5): p. 058102.
139. Lushi, E. and C.S. Peskin, *Modeling and simulation of active suspensions containing large numbers of interacting micro-swimmers.* Computers & Structures, 2013. **122**: p. 239-248.
140. Copeland, M.F. and D.B. Weibel, *Bacterial swarming: a model system for studying dynamic self-assembly.* Soft matter, 2009. **5**(6): p. 1174-1187.
141. Wensink, H.H., et al., *Meso-scale turbulence in living fluids.* Proceedings of the National Academy of Sciences of the United States of America, 2012. **109**(36): p. 14308-14313.
142. Wensink, H.H. and H. Lowen, *Emergent states in dense systems of active rods: from swarming to turbulence.* Journal of Physics-Condensed Matter, 2012. **24**(46).
143. Bar, M., et al., *Self-Propelled Rods: Insights and Perspectives for Active Matter.* Annual Review of Condensed Matter Physics, Vol 11, 2020, 2020. **11**: p. 441-466.
144. Baskaran, A. and M.C. Marchetti, *Statistical mechanics and hydrodynamics of bacterial suspensions.* Proceedings of the National Academy of Sciences of the United States of America, 2009. **106**(37): p. 15567-15572.
145. Fauvart, M., et al., *Surface tension gradient control of bacterial swarming in colonies of Pseudomonas aeruginosa.* Soft Matter, 2012. **8**(1): p. 70-76.
146. Ke, W.-J., et al., *Water surface tension modulates the swarming mechanics of Bacillus subtilis.* Frontiers in microbiology, 2015. **6**: p. 1017.

147. Guadayol, Ò., et al., *Microrheology reveals microscale viscosity gradients in planktonic systems.* bioRxiv, 2020: p. 2020.04.09.033464.
148. Kearns, D.B. and R. Losick, *Swarming motility in undomesticated Bacillus subtilis.* Mol Microbiol, 2003. **49**(3): p. 581-90.
149. Kearns, D.B., et al., *Genes governing swarming in Bacillus subtilis and evidence for a phase variation mechanism controlling surface motility.* Mol Microbiol, 2004. **52**(2): p. 357-69.
150. Pradel, E., et al., *Detection and avoidance of a natural product from the pathogenic bacterium Serratia marcescens by Caenorhabditis elegans.* Proc Natl Acad Sci U S A, 2007. **104**(7): p. 2295-300.